THE
PHYSICAL REVIEW
A Journal of Experimental and Theoretical Physics Established by E. L. Nichols in 1893
VOL. 60, NO. 9 NOVEMBER 1, 1941 SECOND SERIES

Artificial Radioactive Isotopes of Thallium, Lead, and Bismuth

KASIMIR FAJANS AND ADOLF F. VOIGT*
Department of Chemistry, University of Michigan, Ann Arbor, Michigan
(Received September 12, 1941)

The radioelements produced by deuteron and neutron bombardment of thallium and lead have been investigated. The cloud chamber was used to observe the sign of the particles and the energies were determined from absorption measurements. A low intensity 65-min. lead isotope is formed by the deuteron bombardment of Tl; it emits gamma-rays and electrons of 1.00-Mev energy. The properties of two radioelements reported in a preliminary note have been more thoroughly studied. The long-lived thallium isotope produced by deuteron and neutron bombardment of Tl has a half-life of 3.5 ± 0.5 years; it emits negative beta-particles with a maximum energy of 0.87 Mev. The provisional assignment is to Tl^{206}. The 52-hour Pb isotope from the deuteron bombardment of Tl emits gamma-rays (450 kev), conversion electrons (370 kev), and x-rays (95 kev). Its assignment is uncertain. Two activities first obtained by others from the deuteron bombardment of Pb have been studied. The half-life of the 3-hour Pb was measured as 3.32 ± 0.03 hours and its beta-ray energy as 0.70 Mev. The 6.4-day Bi was found to emit gamma-rays of 1.1 Mev and electrons of 0.86 Mev. The excitation functions for these two activities were measured; that for the 6.4-day Bi indicates that a *d-n* reaction is responsible for its production. The recently reported 10-min. positron activity in Pb and 18-hour Bi activity could not be confirmed.

INTRODUCTION

IN a previous publication[1] we reported part of our study of the activities produced by bombarding thallium with slow and fast neutrons and with deuterons. The present publication reports the continuation of this study and its extension to the activities produced from lead. In the latter work uranium lead with an isotopic composition different from ordinary lead was used in the assignment of mass numbers to the activities. (See the following paper.)

I. SUMMARY OF PREVIOUS INVESTIGATIONS

The early work on thallium was summarized in reference 1 and was concerned with the activation of thallium by slow and fast neutrons to give a 4–5-min. thallium isotope which was assigned by Heyn[2] to Tl^{204}. Low intensities of other activities (50 min. and 97 min.) had also been mentioned.

Deuteron bombardment of lead had been found by Thornton and Cork[3] to give a 3-hour activity which they identified as lead and assigned to Pb^{209}, assuming that its observed beta-decay would lead to stable Bi^{209}. Other lead periods which had been reported were an 80-min. period obtained by DeVries and Diemer[4] from the fast neutron activation of lead and a 1.6-min. period produced by x-ray irradiation by Waldman and Collins.[5]

* Horace H. Rackham Pre-doctoral Fellow, 1940–41.
[1] K. Fajans and A. F. Voigt, Phys. Rev. **58**, 177 (1940).
[2] F. A. Heyn, Nature **139**, 842 (1937).
[3] R. L. Thornton and J. M. Cork, Phys. Rev. **51**, 383 (1937).
[4] H. DeVries and G. Diemer, Physica **6**, 599 (1939).
[5] B. Waldman and G. B. Collins, Phys. Rev. **57**, 338 (1940).

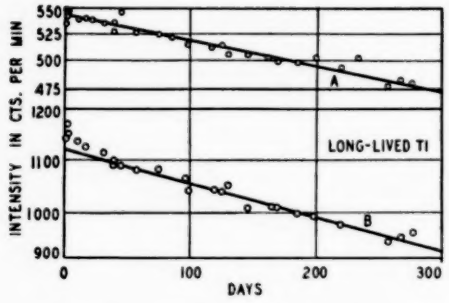

FIG. 1. Decay curves of the long-lived Tl.

In our previous paper[1] we reported a comparison of the artificial 4–5-min. period with AcC″, Tl^{207}. The half-life of the former was measured as 4.23 ± 0.03 min. and the latter as 4.76 ± 0.05 min. The 4.23-min. period was produced in high intensities by the deuteron bombardment of thallium and was identified chemically as Tl. The range of the negative beta-particles which it emits was found to be 0.75 ± 0.05 g/cm², which leads to an energy of 1.65 Mev if the Feather formula is used. It does not emit gamma-rays.

Prolonged slow neutron activation did not give the 97-min. period previously reported but did yield a low intensity of a new long period which was found in greater intensity from the deuteron bombardment of thallium. Its half-life appeared to be between 1 and 2 years and it was provisionally assigned to Tl^{206}.

An activity of 52 hours half-life was produced by the deuteron bombardment of Tl. It was identified chemically as lead and found to emit electrons and gamma-rays.

Since that time Bretscher and Cook[6] reported the production of a 4.6-min. Tl activity by the fast neutron activation of lead. They concluded it to be AcC″, Tl^{207}, by comparing its half-life with those of AcC″ from actinium, 4.7 min., and of the slow neutron-induced Tl activity, 4.1 min.

A thorough study of the activities produced in Tl and in Pb was made by Krishnan and Nahum[7] who mention our previous publication in a note added in proof. They reported 4.4 ± 0.1 min. as the half-life of Tl^{204}, and their absorption measurements led to a range of 0.8 g/cm² of aluminum for the beta-particles. They found fast neutron activation of thallium to give a 13-day period which is also produced by the action of deuterons on mercury, and they assigned it to Tl^{202}.

They reported two lead isotopes produced by the deuteron bombardment of Tl. One was a 54-hour activity emitting gamma-rays, electrons and x-rays, which is obviously identical with our 52-hour period. The other was a 10.25-min. positron activity.

From the deuteron bombardment of lead they observed three periods: the 3-hour lead isotope, a 6.35-day Bi activity emitting gamma-rays, electrons and x-rays, and a weak 18-hour activity found in the Bi fraction.

II. Experimental Methods

1. Production and measurement of the radioactivity

The activities were obtained on the cyclotron of the Physics Department of this University which has been producing a beam current of 5–15 μa of 9–10-Mev deuterons. The measuring instruments were two Lauritsen quartz fiber electroscopes, equipped with cubical ionization chambers which have been used for some time in this laboratory and recently were made of cast aluminum as designed by Mr. A. S. Micelli. They are 8 cm on an outside edge, are provided with thin aluminum windows on the top and bottom, and have glass receptacles filled with anhydrous magnesium perchlorate as a drying agent. These electroscopes were used mostly for the work with short periods while several bubble-type Geiger-Mueller tubes with scaling circuits served for observing the longer periods. Absorption curve measurements were made with both types of instruments.

2. Purification of the material

The extensive purification of the thallium used for the bombardments has been described previously.[1] To obtain lead free from thallium, reagent quality lead nitrate was acidified with HCl, boiled to oxidize any thallium present, and treated with ether to extract it. The lead was precipitated as carbonate, ignited to PbO, and bombarded as such or as PbO_2 obtained by passing chlorine into an alkaline solution of the PbO.

[6] E. Bretscher and L. G. Cook, Nature **146**, 430 (1940).
[7] R. S. Krishnan and E. A. Nahum, Proc. Cambridge Phil. Soc. **36**, 490 (1940).

3. Chemical processes used in the separations

After the bombardment of thallium (as metal or Tl_2O_3) and its dissolution in acid, the following process was generally used to separate the thallium and lead from each other and from any impurities:

(a) precipitation of Pb as $PbSO_4$;
(b) precipitation of Hg, etc., as sulfides in acid solution;
(c) oxidation of thallium to $TlCl_3$, followed by its extraction with ether;
(d) reduction of $TlCl_3$ to TlCl;[8]
(e) precipitation of thallium as TlCl, TlI, or Tl_2CrO_4;
(f) purification of the lead fraction (a) by dissolving it in ammonium acetate and reprecipitating it with sulfuric acid.

Whenever necessary the chemical identities were proved by fractional crystallization (on cooling) of the carriers of the activity, TlCl and PbI_2. The fractions obtained were weighed and measured and the specific activities were compared.

After bombarding and dissolving the PbO or PbO_2, steps (a) and (f) (see above) were used for obtaining the lead isotopes while the bismuth was separated by one of the following reactions:

(a) precipitation as Bi_2S_3 from an acid or ammonium polysulfide solution;
(b) reduction to metal in alkaline solution by sodium stannite or formaldehyde.

For further purification the Bi_2S_3 or Bi were converted to $BiCl_3$, and BiOCl was precipitated by dilution of a slightly acid solution of the latter. For final chemical identification the fractional precipitation of BiOCl on dilution was used.

III. Activities Studied

1. The long period in thallium

Two samples containing relatively high intensities of the long period thallium were obtained by deuteron bombardments of 37 and 100 μah at 9 Mev. Their intensities were 500 and 1100 ct./min., respectively. The half-lives resulting from the curves A and B in Fig. 1 are 4.0 ± 0.5 and 3.1 ± 0.4 years, the average value is 3.5 ± 0.5 years.

The chemical identification as thallium was made as described above. The specific activity of three TlCl fractions agreed within 5 percent.

Cloud-chamber photographs show the beta-radiation to be negative and absorption measurements indicate the absence of gamma-rays. The absorption curve of the beta-rays of the thallium and of RaE were measured on the same instrument, and the range for thallium was obtained by using the comparison method of Feather.[9] The range found (see Fig. 2) was 0.31 ± 0.03 g/cm^2 of aluminum, which leads to an energy of 0.87 ± 0.05 Mev, if the Feather formula is used, $R=0.543E-0.160$.

Periods of the same order of magnitude but of low intensity were obtained by slow neutron activation (6 ct./min.) and Cd-filtered fast neutrons (1–2 ct./min.).

Thus fast as well as slow neutron bombardment apparently produces both thallium periods, the 4 min. (see Sec. I) and the 3 yr. The two possibilities for their assignment are Tl^{204} and Tl^{206}.[10] One would expect that the isotope 204

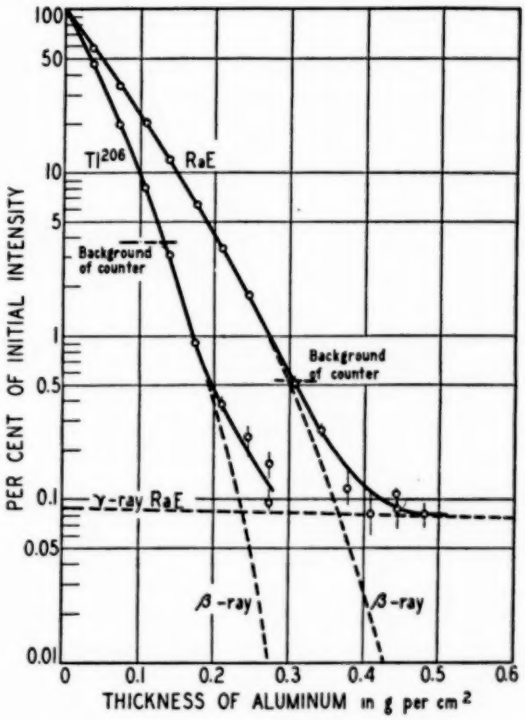

FIG. 2. Absorption curves of the long-lived Tl and RaE.

[8] If a more rapid separation was desired, steps (c) and (d) were omitted.

[9] N. Feather, Proc. Camb. Phil. Soc. **34**, 599 (1938).

[10] The possibility of isomerism has not been overlooked, but is improbable, because of the type of activities, both being beta-emitters with no gamma-rays.

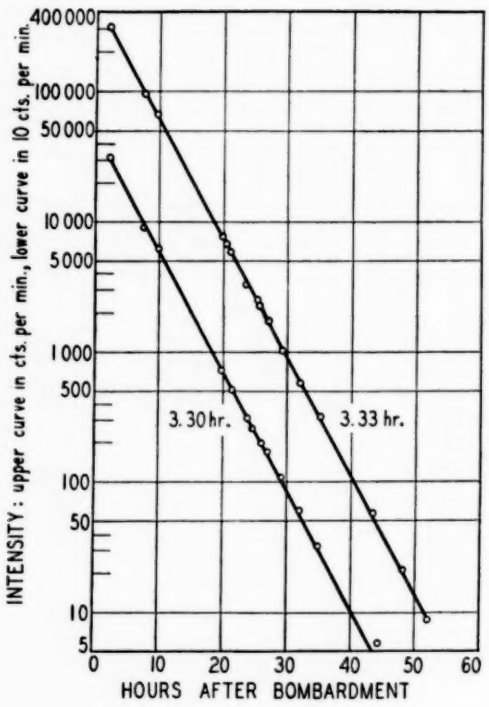

FIG. 3. Decay curves of Pb^{209}.

would be produced in good yields from 203 by slow neutrons and from 205 by fast, while 206 would only be produced by slow neutrons from 205. However, as cadmium filtration does not remove all of the slow neutrons, it is not surprising that some of both activities are found in bombardments with Cd-filtered neutrons, one of these being produced by the slow neutrons not removed by the cadmium. More intense bombardments under controlled conditions will be necessary before a decision can be made. At present it seems best to leave the assignment of the 4-min. period to Tl^{204} and tentatively assign the 3-year period to Tl^{206}.

2. The thirteen-day thallium

We observed this period from fast neutron bombardments of thallium, one of the methods used by Krishnan and Nahum[7] and identified it chemically as thallium by the usual reactions and fractionation process. The average value for the half-life is 11.8 ± 1.2 days, obtained from five rather weak samples.

3. The four-minute thallium

Our work on this activity was reported in reference 1 and is summarized above.

4. Attempts to produce thallium from lead

Lead oxide was given short deuteron bombardments and Tl was separated by the extraction process. The only activity in the thallium was a very weak 10–15-min. period. The intensity was too low for any study to prove the identity of the active material.

5. The fifty-two hour lead

This isotope, produced by the deuteron bombardment of Tl has been studied in more detail than reported previously. In addition to the chemical reactions listed above it was precipitated as PbI_2, $PbCrO_4$, $PbCl_2$, PbS, and PbO_2. The fractional crystallization as PbI_2 gave three samples whose specific activity agreed within 2 percent. Our value for the half-life is 52 ± 0.5 hr.

Absorption measurements of the gamma-radiation in copper and in lead show two distinct radiations, with the following absorption coefficients and energies:

	Mass Abs. Coef.	Energy	Average
Pb	0.30–0.36 cm^2/g	430–475 kev	
	0.93–1.5	(200–250)	
			450±25 kev
Cu	0.077–0.087	425–475	
	0.51–0.57	92–98	

(The conversion was made from tables in the *International Critical Tables* and curves given by Heitler.[11])

Since the energy of the K x-rays from Tl or Pb is about 90 kev, the result for the softer of these two radiations in copper identify it as this x-radiation. The values determined for the energy of this radiation from the data in lead are meaningless because of the discontinuity in the absorption coefficient-energy curve.

The range of the beta-particles in aluminum was found to be 0.110 ± 0.005 g/cm^2, which, according to a curve given in Rasetti,[12] leads to an energy of 370 kev. Our former value of 500 kev was determined from less accurate measurements and on the basis of the Feather formula which does not apply to energies less than 700 kev.

These data are in complete accord with the picture of the primary activity as a gamma-ray,

[11] W. Heitler, *The Quantum Theory of Radiation* (The Clarendon Press, Oxford, 1936) p. 216.
[12] F. Rasetti, *Elements of Nuclear Physics* (Prentice-Hall, New York, 1936), p. 68.

partially internally converted to give the observed electrons of 370-kev energy which is less than that of the gamma-rays (450 kev) by approximately 90 kev, the binding energy of the K electrons in lead or thallium.

In our previous publication we suggested that this activity was due to a metastable state of either Pb^{204} or Pb^{206}, produced from Tl^{203} or Tl^{205} by the usual d-n reaction, and decaying to the corresponding stable isotope with the emission of the observed gamma-ray. Krishnan and Nahum reported the production of this activity by the slow and fast neutron activation of lead tetraethyl and also found its excitation threshold to be about 7 Mev. These observations led them to the conclusion that the activity is Pb^{205} produced from Tl^{205} by a d-$2n$ reaction and decaying to Tl^{205} by K electron capture. As the discussion of excitation functions (see Sec. IV) seems to indicate that d-$2n$ processes are improbable for heavy elements at these energies, the question is still open.

6. The three-hour lead

A number of determinations of the half-life of this isotope on electroscope and Geiger counter gives the value 3.32 ± 0.03 hr., in considerable disagreement with Krishnan and Nahum's value of 2.75 ± 0.05 hr. In one case our sample was followed for 17 half-lives without showing any other period (see Fig. 3), justifying the conclusion that this is the only long period produced by the deuteron bombardment of lead. Separations were completed in 20 min. so that a short period (less than 5 min.) could be produced and escape detection.

Our value for the range of the beta-particles was 0.22 g/cm² of Al, checking the same value in the experiments of Krishnan and Nahum. The energy corresponding to this range is 700 kev by the Feather formula. The assignment is discussed in the following paper.

7. The one-hour lead

Krishnan and Nahum described a 10-min. positron activity as a lead isotope produced by the deuteron bombardment of a thallium preparation. In order to check this we bombarded pure Tl_2O_3 with a current of 10 μa of 9-Mev deuterons for periods of 5 min. to 1 hour. In each case the separation was made immediately and measurements were begun 15 to 20 min. after bombardment. The results were always the same; there was no trace of a 10-min. period. However, a new weak 65 ± 5-min. period was found in addition to the 52-hour activity (see Fig. 4).

The 65-min. period was identified as lead in the usual way and in particular by a fractional crystallization of PbI_2. Three fractions showed the same ratio of the 1-hour to 52-hour periods within the experimental error. Extrapolated to the end of bombardment these ratios are: 0.36, 0.37, 0.33, agreeing within the uncertainty of ±0.02 for each. The relatively high error is due to the low intensity of the short period compared with that of the longer one. The ratio for infinite bombardment is 1/150 showing that the probability of production of the 65-min. period is much less than that of the 52-hour.

Cloud-chamber observation of the lead precipitate shortly after the bombardment of thallium with deuterons showed only negative tracks. Absorption measurements show gamma- as well as beta-activity, the former being about 17 percent of the total radiation as measured on the Geiger counter.

The absorption curve in Al shows the range of the electrons to be 0.38 ± 0.03 g/cm² correspond-

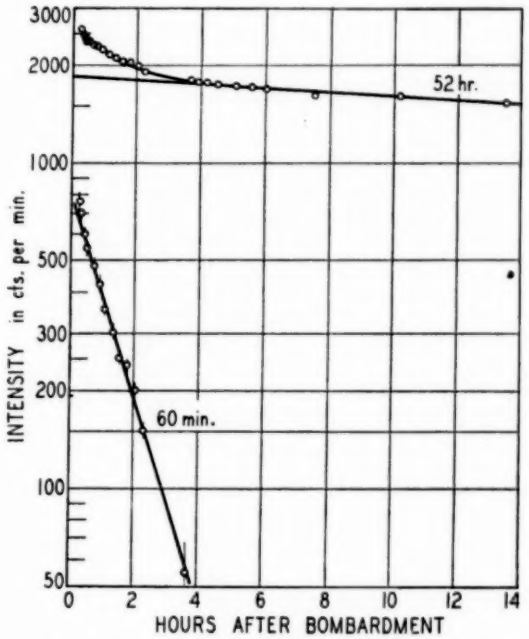

FIG. 4. Decay curves of one hour and 52-hour lead activities.

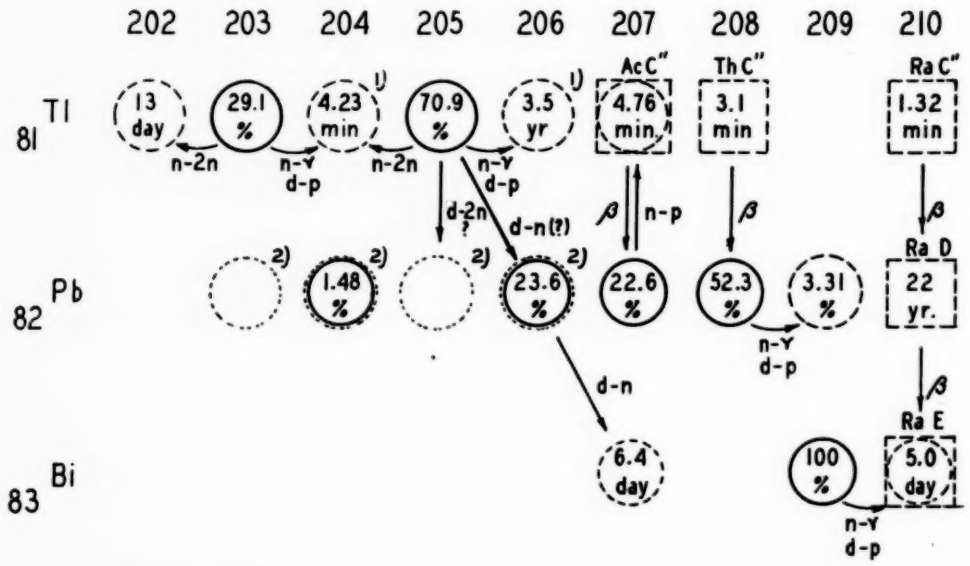

FIG. 5. Isotopes of Tl, Pb, and Bi. Solid circles indicate stable isotopes. Broken squares indicate natural radioactive isotopes. Broken circles indicate artificial radioactive isotopes. Dotted circles indicate uncertain assignments. (1) Assignment possibly reversed. (2) Assignment of 1-hour and 52-hour Pb isotopes is not certain. Pb^{209} has a period of 3.31 hours.

ing to a maximum energy of 1.00 ± 0.05 Mev (Feather). Rough measurements in lead show the energy of the gamma-ray to be of the order of magnitude of a million electron volts. The electron activity may result from the partial internal conversion of this gamma-ray, in which case the energy of the gamma-ray would be 1.1 Mev (see paragraph 5).

The assignment of this activity is still less certain than that of the more intense 52-hour activity. It may be a metastable state of Pb^{204} or Pb^{206} or it may be Pb^{203}, decaying by K capture to Tl^{203}. The latter would require a d-$2n$ reaction for its production, the probability of which is discussed in Section IV.

8. The six-day bismuth

This period was produced by bombarding lead with deuterons and has been identified as bismuth by the method described above. Several determinations of its half-life give the value 6.4 ± 0.1 days in agreement with the value of 6.35 days obtained by Krishnan and Nahum. The range of its beta-rays was measured as 0.30 ± 0.02 g/cm^2 of Al, which leads to an energy of 0.85 ± 0.04 Mev. The absorption coefficient of its gamma-rays in lead was found to be 0.066 ± 0.006 cm^2/g which corresponds to an energy of 1.1 ± 0.1 Mev. If we assume that this isotope emits a gamma-ray which is partially internally converted to give the electrons, we would expect the gamma-ray energy to be 0.95 ± 0.05 Mev. The observed value (1.1) agrees poorly but within the experimental error. The primary decay process is probably K electron capture leading to a stable Pb isotope.

The assignment of this isotope is discussed in the following paper.

The curves show no indication for the weak 18-hour activity found in the bismuth separation by Krishnan and Nahum.

9. Summary

The various stable isotopes and radioactive isotopes, both natural and induced are shown in Fig. 5.

IV. Excitation Functions

The excitation functions of the 3-hour lead and 6-day bismuth isotopes were measured by bombarding a stack of 6 lead foils with deuterons and following the decay of each. The foils were made by rolling reagent quality lead metal to the required thickness, 0.01 to 0.02 mm. They were measured without chemical separation and the 3-hour and 6-day activities were extrapolated to

beginning time for comparison. The thicknesses were evaluated by weighing the measured part of the foils (squares 12 mm on an edge) and determining the area with a comparator. The specific activities are plotted in Fig. 6 against the beam energy. The original beam energy was taken as 9.7 Mev from its range in air, 64 cm (corrected to 760 mm and 15°C). The data of Mano[13] were used to calculate the energy loss of the deuteron beam in Pb. The resulting energy of the beam, calculated for the median thickness of each foil, is used in the curves.

The 3-hour lead, produced by a *d-p* reaction, has an excitation curve similar to those for other *d-p* processes in heavy elements.

In the case of the 6-day Bi a decision is desired as to whether it is produced by a *d-n* or a *d-2n* process. The production threshold is at or above 7 Mev. The threshold for the *d-n* process increases greatly with increasing atomic number. For the lightest elements (Li, Be) it is 0.4 Mev, for those of medium atomic weight it is a few Mev, while for several heavy elements thresholds near 7 Mev have been observed (Hg^{198} from Au^{197}, Po^{210} from Bi^{209}).[14–16]

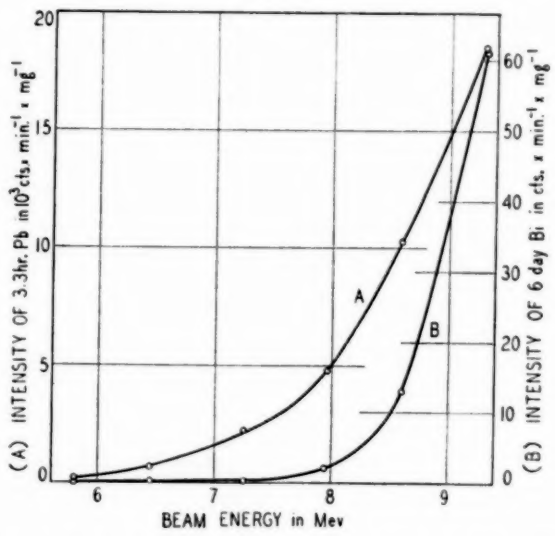

FIG. 6. Excitation curves of the 3-hour Pb and 6-day Bi.

On the other hand, one excitation curve for a *d-2n* process in the lighter elements (Zn^{63} from Cu^{63})[17] shows a threshold energy of 9 Mev. It is logical to assume that the threshold for *d-2n* processes will also increase with increasing atomic number. For the heaviest elements it would thus be distinctly higher than the value of 7 Mev observed for the Bi activity. The threshold and the shape of the excitation function for Bi resemble so closely those of Hg and Po that it seems probable to assume the same process. As the activity is produced from Pb^{206} (see the following paper) the reaction would be Pb^{206}, *d-n*, Bi^{207}.

This also affects the assignment of the 52-hour lead period. Its threshold has been given by Krishnan and Nahum[7] as about 7 Mev also. Again, this makes a *d-n* process probable and the assignment of the 52-hour activity to a metastable state of Pb^{204} or Pb^{206} more likely than to Pb^{205}. A similar situation may exist with respect to the 65-min. period but the threshold energy of that activity is not known.*

The investigation received helpful support by grants from the Horace H. Rackham Trust Fund.

[13] G. Mano, J. de phys. et rad. **5**, 628 (1934).

[14] R. S. Krishnan, Proc. Camb. Phil. Soc. **37**, 186 (1941).

[15] D. G. Hurst, R. Latham, and W. B. Lewis, Proc. Roy. Soc. **A174**, 126 (1940).

[16] H. A. Bethe, Rev. Mod. Phys. **9**, 200 (1937) has concluded on theoretical grounds that the *d-2n* process will become probable at 7 Mev for heavy elements.

[17] R. S. Livingston and B. T. Wright, Phys. Rev. **56**, 656 (1940).

* *Note added in proof.*—The results given in the new paper by R. Sherr, K. T. Bainbridge, and H. H. Anderson, Phys. Rev. **60**, 473 (1941) may influence the discussion in Section IV. They consider it probable that the 25-hour mercury isotope is Hg^{197} rather than Hg^{198}, and, therefore, that its production from Au^{197} is a *d-2n* rather than a *d-n* process.

The Use of Uranium Lead in the Assignment of Artificial Radioactive Isotopes

KASIMIR FAJANS AND ADOLF F. VOIGT
Department of Chemistry, University of Michigan, Ann Arbor, Michigan

(Received September 12, 1941)

Uranium lead and ordinary lead were bombarded with deuterons under the same conditions in order to establish from which of the stable lead isotopes the 3.3-hour Pb and 6.4-day Bi activities are produced. The intensities of the resulting radioelements were compared with the abundances of the isotopes. The 3.3-hour lead was found to be produced from Pb^{208} and the reaction must be Pb^{208}, *d-p*, Pb^{209}. The 6.4-day Bi is produced from Pb^{206}. Its assignment depends on the type of reaction; the more probable one is Pb^{206}, *d-n*, Bi^{207}.

IN order to assign mass numbers to the 3-hour lead and the 6-day bismuth isotopes studied in the preceding paper[1] we compared their intensities as produced in ordinary lead and in lead obtained from uraninite from Morogoro, Africa.[2] The two samples of lead were bombarded with deuterons under the same conditions and the ratios of the intensities of each of the two periods were calculated. These ratios should correspond to the ratios of percent abundances for the particular stable isotopes of lead from which the activity is produced. Table I gives the percent abundances and the ratios derived from them.

Since the uranium lead was obtained by chemical separation from uraninite, it contains the lead isotope, radium D, which decays to Pb^{206} by the following processes:

$$\text{RaD} \xrightarrow{\beta} \text{RaE} \xrightarrow{\beta} \text{RaF} \xrightarrow{\alpha} \text{RaG}$$
$$Pb^{210}\ 22\ \text{yr.}\ Bi^{210}\ 5\ \text{days}\ Po^{210}\ 140\ \text{days}\ Pb^{206}.$$

After the bombardment a chemical separation of the lead and bismuth was made. Since the RaD was in equilibrium with its daughter products, a separation of bismuth from the lead takes along any RaE present and leaves the RaD with the lead. From this the RaE grows with its 5-day recovery period.

It was necessary, then, to remove the RaE from the lead shortly before bombardment, since its presence would mask the 6.4-day Bi. The pre-separation was made by dissolving the uranium lead chloride in hot water, adding $BiCl_3$, and reducing with alkaline formaldehyde. The metallic bismuth was filtered off and the lead in the filtrate was oxidized to PbO_2 with chlorine.

Known weights of this PbO_2 and ordinary PbO_2 were bombarded, the energy of the beam, 9.5 Mev, and the total bombardment, 1.5 μah, being the same in both cases. The PbO_2 was dissolved in HCl and a known amount of $BiCl_3$ was added as carrier. Both elements were separated by the methods described in the preceding paper. The weights and activities of the resulting $PbSO_4$ and BiOCl were determined. The weight of BiOCl was compared with the original amount of Bi added giving the percent recovered.

The lead fraction from the uranium lead (measured on the Geiger-Mueller counter) showed the decay of the 3-hour period, followed by an increase due to the recovery of RaE (see Fig. 1). The beta-radiation from RaD is extremely soft and only a very small fraction of the particles are counted under the experimental conditions. The total natural activity can be expressed by the formula $A=E(1-e^{-\lambda t})+D$, in which E is the limiting value of the recovering activity, RaE, λ its decay constant, and D is a constant activity. Values for E and D calculated

TABLE I. *Isotopic composition of the uranium lead and ordinary lead.*

LEAD	204	206	207	208	REF.
Morogoro	0.0%	93.1%	6.9%	0.0%	Aston[1]
Morogoro	0.001	94.20	5.63	0.17±0.02	Nier[2]
Ordinary	1.48	23.59	22.64	52.29	Nier[3]
Ratio	0.0007	3.99	0.249	0.00325	Nier

[1] K. Fajans and A. F. Voigt, Phys. Rev. **60**, 619 (1941).
[2] O. Hönigschmid and S. Horowitz, Monats. f. Chem. **36**, 355 (1915). I am indebted to Professor Hönigschmid for this preparation. K. F.

[1] F. W. Aston, Proc. Roy. Soc. **A140**, 535 (1933).
[2] A. O. Nier, Phys. Rev. **55**, 153 (1939).
[3] A. O. Nier, J. Am. Chem. Soc. **60**, 1571 (1938).

from the growth curve *A*, Fig. 1 (followed for 70 days), were used for numerical extrapolation (curve *B*). Subtraction from the total curve (*C*), gives the decay of the 3-hour activity (*D*).

The Bi activity was corrected (25–50 ct./min. in the different experiments) for the growth of the RaE during the interval of about an hour between its separation from the lead and the end of the bombardment. The intensities of all of the samples were extrapolated to the end of bombardment.

Two independent comparisons of the normal and uranium lead were made. They are not comparable with each other due to a different position of the beam on the target. In experiment 1 the weight of Bi was not determined, and in 2a, the activity of the lead could not be evaluated accurately, due to an interfering short period impurity. For these reasons these two parts have been rejected. The results are shown in Table II.

The intensities of the two periods produced in the various samples were corrected for the different amounts bombarded and recovered and gave the ratios, which are listed in Table III with the nearest ratio expected from the isotopic abundances (see Table I).

As shown in Table I, there is a great difference in the magnitude of the ratios expected, so that an agreement in order of magnitude is all that is necessary for establishing the isotopes from

TABLE II. *Weight and activity of bombarded samples.*

Exp.	Lead Used	Weight Bombd.	Wt. of Pb Measured	Activity of Pb	Percent Bi Recovered	Activity of Bi
1	Ord.	0.0375 g	0.0341g	4.3×10^5 ct./min.		409 ct./min.
	U		0.0130	5.7×10^2		
	Ord.	0.0365	0.0354	5.3×10^5	70	660
2	a *U*	0.0365			69	2.64×10^3
	b *U*	0.0385	0.0316	2.1×10^3	67	2.70×10^3

TABLE III. *Comparison of activity and abundance ratios.*

Period	Exp.	Activity Ratio U Pb/Ord. Pb	Abundance Ratio U Pb/Ord. Pb	Expected for Production from
3-hr. Pb	1	0.0035	0.0033 ± 0.0003	208
	2b	0.0045		
6-day Bi	2a	4.07	3.99	206
	2b	4.04		

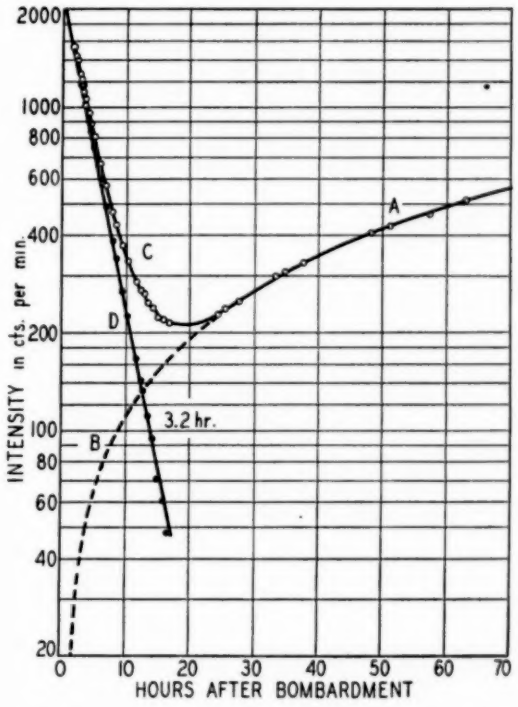

FIG. 1. Decay of Pb^{209} and growth of RaE after bombardment of uranium lead.

which the activities are produced. The two values for lead in Table III agree sufficiently well with the value expected to make certain that the 3-hour lead is produced from Pb^{208}. The process must, therefore, be Pb^{208}, *d-p*, Pb^{209} as proposed by Thornton and Cork.[3] The two values for bismuth leave no doubt that the 6.4-day bismuth is produced from Pb^{206}. Since the excitation function of this activity seems to be that for a *d-n* reaction (see the preceding paper), the 6.4-day Bi can be assigned, at least provisionally, to Bi^{207}.

The radioactive samples described in this and the foregoing paper were obtained from the cyclotron of the Physics Department. We wish to express our appreciation to Professor J. M. Cork for his interest and to the other members of the cyclotron group for conducting the bombardments. The investigations were made possible by grants from the Horace H. Rackham Trust Fund.

[3] R. L. Thornton and J. M. Cork, Phys. Rev. **51**, 383 (1937).

The Scattering of Protons by Protons from 200 to 300 kev

G. L. RAGAN,* W. R. KANNE,** AND R. F. TASCHEK‡
University of Wisconsin, Madison, Wisconsin

(Received September 2, 1941)

Proton-proton scattering between 200 and 300 kev has been studied as a function of energy and of angle. The results are in good agreement with Breit's calculations based on a square well proton-proton interaction potential of e^2/mc^2 radius and 10.500 Mev depth. The scattering chamber was isolated from the accelerating tube by a differential pumping system. Scattered protons were detected by Geiger-Klemperer proportional counters filled with purified hydrogen. Two separate counters connected to similar amplifier-recorder circuits detected simultaneously protons scattered at different angles from the beam, and the ratio of scattering at these angles was calculated directly. Tests of the performance of the counters are given. Two different scattering chambers yielded similar results.

INTRODUCTION

EXPERIMENTS performed in 1936 by Tuve, Heydenburg, and Hafstad[1] on protons of 600- to 900-kev energy scattered by hydrogen gave results differing greatly from that predicted by Mott's formula which is based on a repulsive Coulomb field between protons. A mathematical analysis by Breit, Condon, and Present[2] showed that these data were best explained by assuming the presence of an attractive nuclear force between protons at small separations. These analyses indicated that a minimum in the 45° scattering should occur in the neighborhood of 400 kev, because of the interference between the repulsive Coulomb scattering and the attractive nuclear force scattering. In 1937 Hafstad, Heydenburg, and Tuve,[3] using protons of 200 to 600 kev, found proof of the existence of this minimum.

Accurate scattering data enable one to determine the width, r_0, and the depth, D, of the square potential well representing the interaction between protons. The high energy data[4, 5] analyzed by Breit, Thaxton, and Eisenbud[6] (hereafter referred to as BTE) indicate good agreement with a well of radius e^2/mc^2 and depth 10.500 Mev. A well of $0.75e^2/mc^2$ radius and 19.6905-Mev depth gives the same scattering at 2200-kev energy (see Fig. 7 of BTE), so that either well may be considered as fitting the data at the highest voltages investigated. However, the theoretical scattering curve for the 19.6905-Mev well deviates from the experimental points at lower voltages.

The desirability of obtaining accurate data in the low energy region was pointed out by BTE, pp. 1057–1060. On either side of the above-mentioned minimum the scattering is particularly sensitive to the choice of well parameters, hence experiments at about 300 kev and at about 500 kev are particularly good for determining these. The principal object of the experiments reported in this paper is to obtain data at energies below that at which the scattering minimum occurs, of sufficient accuracy to enable a clear choice to be made between the two wells mentioned above.

SCATTERING CHAMBERS

Two different scattering chambers were used. The first was one having fixed openings at 15° intervals into which counters could be waxed. These openings were in the form of accurately aligned tubes; the defining slits and holes of the counters were centered in tubes which slipped

* Now at Massachusetts Institute of Technology.
** Now at Illinois Institute of Technology.
‡ Now at Oldbury Electro-Chemical Company, Niagara Falls, New York.
[1] M. A. Tuve, N. P. Heydenburg, and L. R. Hafstad, Phys. Rev. **50**, 806 (1936).
[2] G. Breit, E. U. Condon, and R. D. Present, Phys. Rev. **50**, 825 (1936).
[3] L. R. Hafstad, N. P. Heydenburg, and M. A. Tuve, Phys. Rev. **53**, 239 (1938).
[4] R. G. Herb, D. W. Kerst, D. B. Parkinson, and G. J. Plain, Phys. Rev. **55**, 998 (1939).
[5] N. P. Heydenburg, L. R. Hafstad, and M. A. Tuve, Phys. Rev. **56**, 1078 (1939).
[6] G. Breit, H. M. Thaxton, and L. Eisenbud, Phys. Rev. **55**, 1018 (1939).

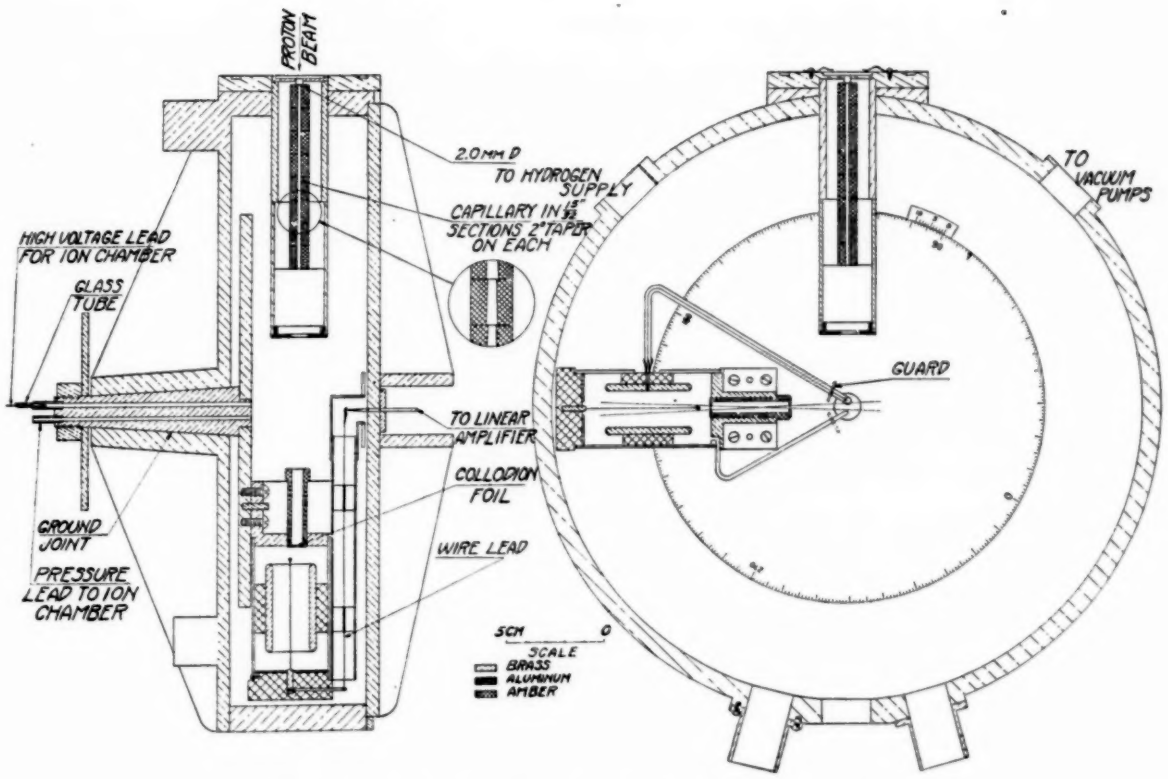

FIG. 1. Scattering chamber, referred to as the second chamber.

snugly into these. This was the same apparatus shown in Fig. 3 of an earlier paper[7] from this laboratory, with the exception of the counting apparatus. Only four of the 15°-interval tubes are shown there; actually there were openings at 15°, 30°, 45°, 60°, 75°, and 105°, both right and left of the beam. Four counters were used at angles 15° left, 30° left, 15° right, and 45° right in taking the hydrogen data. Two similar pulse amplifiers were used, enabling us to count simultaneously at two angles. The openings of the defining systems were made of such size that comparable counting rates occurred at various angles.

The second scattering chamber was more versatile than the first one. It has only two openings of the aligned-tube type; these were at 15°, right and left, and into them two monitoring counters were fitted. These were ordinarily connected in parallel to the same amplifying circuit in order to reduce errors due to possible fluctuations of beam position. A third counter, with larger defining apertures was mounted inside the scattering chamber on a graduated disk which could be rotated by means of a ground joint. At angles smaller than 35°, the rotating counter obstructed the monitor on its own side of the beam, so only the one on the opposite side of the beam was used. Correspondingly, the beam itself struck the body of the counter at angles below 22°. No effect attributable to this was observed when the scattering chamber was evacuated. Two views of the complete chamber are given in Fig. 1. Apiezon grease *N* was used on the ground joint. The top plate was waxed on with Picein wax; the two monitor counters were also waxed in with Picein into the two aligned tubes shown at 15° in Fig. 1. The body of the chamber and the top plate were turned from brass castings. The guard shown near the center of the chamber occupied the dashed position when the counter was on the right side of the chamber. It was useful at smaller angles to protect the defining slit system of the rotating counter from slit scatter-

[7] W. R. Kanne, R. F. Taschek, and G. L. Ragan, Phys. Rev. **58**, 693 (1940).

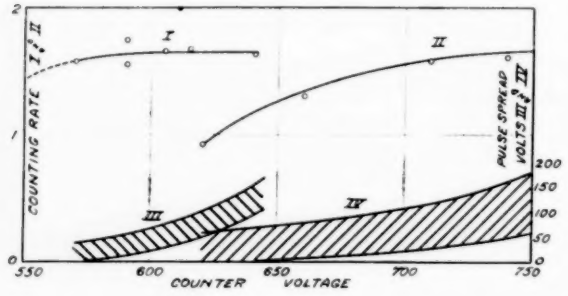

FIG. 2. Proportional counter plateaus and corresponding pulse spreads. Pulse spreads were visually estimated on oscilloscope on output of linear amplifier. These data were taken at 250 kv with protons scattered at 45° in hydrogen. The counter contained hydrogen at 25 mm of mercury pressure for curves I and III, and 44-mm pressure for curves II and IV.

ing from the collimating capillary system; this guard, as well as the general design of the apparatus, was similar to that of Herb and collaborators.[4] Along with the diaphragm shown about halfway between the exit end of the collimating capillary and the center of the chamber, it gave adequate protection against slit scattering.

COUNTERS

There are several difficulties which arise in the low energy region which are not met with in the higher energy range. The most important of these is that the ionization-collecting counter used at higher energies will not detect a proton of these low energies because of insufficient ionization per proton. Our first problem, then, was to find a reliable detector for protons of 100 to 150 kev, since these are the energies of protons scattered at 45° from a beam of 200 to 300 kev. In their experiments in this region, Hafstad, Heydenburg and Tuve[3] used Geiger point counters. These they found to be sensitive, but not quantitatively reliable. We first tried using gross ionization current measured with an Edelmann string electrometer, as described in another paper[7] from this laboratory. This method, however, was not sufficiently sensitive nor quantitative for this problem.

The counters finally adopted were of the Geiger-Klemperer proportional-counter type. Figure 1 includes two views of one of our counters. The rest of our counters were essentially the same, being of the same construction as shown by Brubaker and Pollard,[8] but about twice as long and half as large in diameter as theirs. The defining slit and hole were so placed that the protons detected traveled the entire length of the counter, roughly parallel to the center wire. The wire was connected to the first stage of a five-stage pulse amplifier with reduced gain (three stages would probably have sufficed). The cylinder surrounding the wire was maintained at a constant potential of some 600 to 900 volts negative. The counter was separated from the scattering chamber by a thin foil of collodion, of perhaps 20-kev stopping power; it was filled with purified hydrogen at presures of 3 to 4 cm of mercury. Brubaker and Pollard found hydrogen to be one of the best gases tried in this type of counter. A further advantage was that any leakage from the counters into the scattering chamber did not contaminate the chamber; this is important as these extremely thin collodion foils always leaked a little.

These counters gave good voltage plateaus, as indicated in Fig. 2. The two counter pressures illustrated are extremes, most of our data having been taken at pressures of 30 to 40 mm of mercury. The pulse size was visually estimated on a cathode-ray oscilloscope connected to the output of the amplifier. It was always found that if the output pulses were greater than 50 volts and less than 120 volts the counters were operating in the plateau region. This afforded a convenient means of setting counter voltages. It will be noticed that the pulse distribution as well as the plateau was better in the case of the 25-mm curve. This was true only for low proton energies, and may probably be given the following explanation. Let us assume a reasonable range of energies to be present in the protons entering the counter, this spread being due to straggling in the collodion foil, variation in thickness of foil passed through due to curvature of the foil under gas pressure, variations in loss of energy in the gas of the scattering chamber, etc. If the gas pressure in the counter is low enough so that all the protons have residual ranges greater than the counter length, then the differences in pulse size will presumably be due to variations in specific ionization alone. However, if the gas

[8] G. Brubaker and E. Pollard, Rev. Sci. Inst. **8**, 254 (1937).

pressure is high enough that a considerable number of the protons are stopped in the counter, then the variation in total ionization over these residual ranges will enter. On the other hand, too low a counter pressure gave poor plateaus for protons of any energy used. Pressures of about 30 to 40 mm of mercury seemed to be quite satisfactory in all respects.

As a further check on the performance of the counters, the scattering of protons in purified helium at 105° and 60° was observed with the first chamber by counting simultaneously at these angles with two separate counters. The same two counters were used as were used at 45° and 30° in the hydrogen work with the first chamber. The energies of the protons scattered at these angles in helium are 52.5 percent and 77.0 percent of the beam energy, which is almost the same as the 50.0 percent and 75.0 percent for 45° and 30° in hydrogen. Figure 3 shows the results. Vertical lines on the points indicate their statistical reliability. The horizontal line at 15.15 $\times 10^{-2}$ is the value of the scattering ratio given by Rutherford's formula which is probably valid under these conditions. Experiments at the Carnegie Institution of Washington[9] on proton-helium scattering show an anomaly at 1 Mev which increases with both energy and angle, and indicates that too much faith should not be placed in this assumption. However, the fact that our proton-helium scattering ratio agrees so well with the Rutherford formula at 300 kev, where it is expected that our counters should be quite reliable, seems to argue against the presence of any appreciable anomaly under the conditions of our experiment. The fact that the observed ratios are less than the Rutherford value below 300 kv is just what is to be expected on the basis of our observations of the counter behavior. At 200 kv and below it was obvious from oscilloscopic observations of the pulses that the spread in pulse size was excessive, and that a considerable percentage of them were not large enough to be recorded by the recording circuit. This situation gradually improves with increasing beam energy, so that the efficiency of the counters should approach unity at higher energies. Thus it seems quite safe to assume (1) that there is no detectable scattering anomaly at 105° for a beam energy of 300 kev and (2) that the low values observed for the 105°/60° ratio are caused by reduced efficiency of the counters. On the basis of these assumptions, the proton-helium scattering ratio curve was used to determine the efficiency of the counters as a function of proton energy. These efficiencies have been used in making corrections to the 45°/30° data in hydrogen given in Fig. 8, taken with the first scattering chamber.

A new counter was constructed for use as the rotating counter in the second scattering chamber, and a separate determination of its efficiency was made. It was convenient to use the results of the 250-kev angular distribution data (Fig. 10) for this purpose. According to the laws of conservation of energy and momentum, in the collision of identical particles equal numbers of particles per unit target volume are scattered into equal angular ranges symmetrical with respect to 45°. The energy of a particle scattered at a small angle is great and the efficiency of the counter is unity. The scattering yield may then be used to predict an expected Mott ratio for the angle symmetrical with respect to 45°. The Mott ratio observed divided by that expected at an angle above 45° gives directly the efficiency of the counter for an incoming particle of the energy corresponding to that angle. The energy of a scattered proton is given by the beam energy multiplied by the square of the cosine of the scattering angle. Figure 4 gives the efficiency of

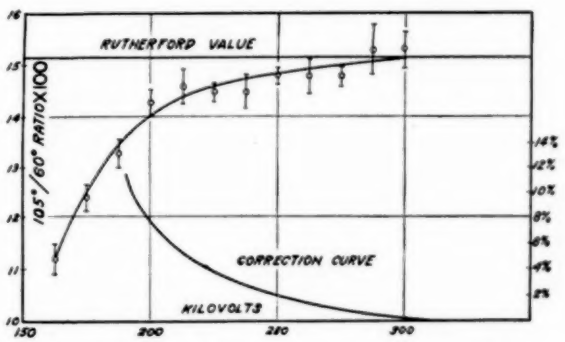

FIG. 3. Counter efficiency correction curve applying to 45°/30° ratio data of first chamber, Fig. 8. The experimental points give the ratio of 105° to 60° scattering of protons in helium. The lower curve and right hand ordinate scale give the efficiency correction. The abscissa refers to accelerating tube voltage.

[9] N. P. Heydenburg and R. B. Roberts, Phys. Rev. **56**, 1092 (1939); N. P. Heydenburg and N. F. Ramsey, Jr., Phys. Rev. **60**, 42 (1941).

the rotating counter as a function of the energy of incident protons.

Other Apparatus and Techniques

The essential features of the transformer-rectifier high voltage apparatus have been described by Haworth, King, Zahn, and Heydenburg.[10] An approximate calibration of the voltmeter has indicated no disagreement with the original calibration discussed in reference 10, which has been used in this work. The high voltage ripple was 1 percent r.m.s.

The proton beam entered the second chamber through a $3\frac{3}{4}$-inch capillary tube of 2 mm diameter; it was made up of eight sections, each tapered 2° to prevent any of the beam striking the wall of the capillary and being scattered with reduced energy into the chamber along with the true beam. The first chamber had a similar 3-inch capillary of six sections. The proton beam did not pass through any foil in entering the chamber. There was a continual flow of hydrogen into the chamber and through the capillary, thereby maintaining pressures up to 1 or 2 mm of mercury. This pressure was measured by a manometer containing low vapor pressure diffusion pump oil. A differential pumping system then removed the gas, isolating the scattering chamber from the vacuum maintained in the accelerating tube. This pumping apparatus and capillary are described more fully in reference 7. In some early trials using thin aluminum foils to isolate the chamber we found by magnetic analysis that much energy straggling was introduced by passing the beam through such a foil. This difficulty is, of course, of little moment at the beam energies used by others in the high energy region. The fact that fresh gas was continually being supplied and contamination swept out was also advantageous.

Rather than trying to measure the actual beam current (0.1 to 0.2 microampere came through the differential pumping channels and capillary) we adopted the procedure of counting scattered protons simultaneously at two different angles. This gave directly the ratio of the scattering at these two angles, provided the geometry of the counters was known. Or, one angle could be used simply for a monitor, and the other counter could be set at different positions; this gave for each angle the count relative to that at the monitor position. These methods have the following desirable features. (1) They eliminate the need for current measurement. Such a measurement would be exceedingly difficult to make accurately since capture and loss of electrons by protons of the beam would be appreciable in passing through a foil into a Faraday cage, or even in passing through the gas of the chamber itself. (2) Accurate pressure measurement and control are unnecessary, since pressure changes affect both counters similarly. (3) A certain amount of voltage fluctuation is compensated for; for instance, the ratio of the counts at a given pair of angles would remain constant at all energies for Rutherford scattering.

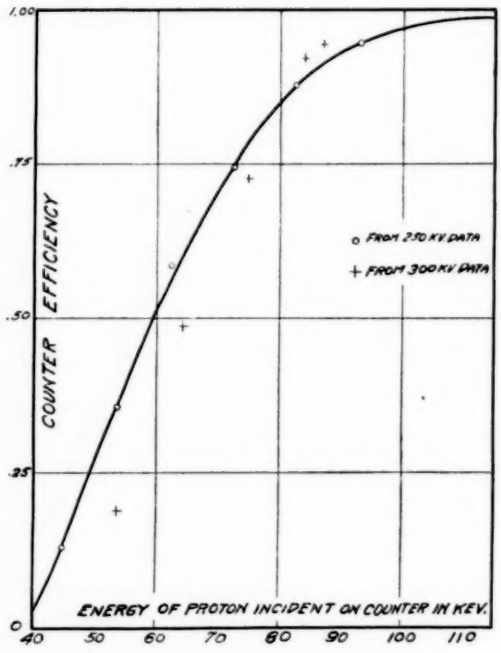

FIG. 4. Efficiency of rotating counter in second scattering chamber. The 250-ky data are the more reliable and are used as the basis for the correction.

To assure that the proton beam accurately intersected the axis of the scattering chamber, the chamber was shifted until the proton-beam spot fell near the center of a quartz plate at the end of the scattering chamber. Since it was necessary for the beam to traverse the 2-mm capillary of the differential pumping system with as little loss of current as possible, leveling screws

[10] L. J. Haworth, L. D. P. King, C. T. Zahn, and N. P. Heydenburg, Rev. Sci. Inst. **8**, 486 (1937).

moving the chamber in and perpendicular to its plane were next used to adjust the chamber to the position where maximum current was obtained in a Faraday cage at the end of the (evacuated) scattering chamber. This procedure was followed with both chambers.

To further center the beam in the second chamber, the rotating counter was set at 45° where the scattering varied slowly with angle, and the chamber was adjusted until the ratio of the scattering into the left monitor to the scattering into the 45° counter was equal to the same ratio for the right monitor. The slightly different geometrical apertures of the two monitor counters were of course allowed for.

To determine the exact zero of the divided circle, the ratio of the scattering at 250 kev at angles 35°, 36°, 37.5° and 39° to that at 15° was taken with the rotating counter first on one side of the beam, then at the corresponding angles on the other side. These data were plotted separately, each set being accurately linear and quite parallel but differing from the other by an angular displacement of 0.8°. It was then assumed that the zero of the scale was off by 0.4° and all the data shown were taken at the correct angles.

Observations have been taken in the angular range 15° to 90° to determine whether any large amount of slit scattering was present with the scattering chamber evacuated. Too few pulses from the monitors were observed on the oscilloscope to allow counting, but quite a few pulses from the rotating counter were observed for angles below about 25°. Since there was gas leakage from the counters which were at a pressure of 45 mm of mercury, and since the geometry factor for the rotating counter was about ninety times that of either of the monitors, the number of pulses at small angles was no more than was to be expected on the basis of scattering from residual gas in the chamber. These observations were made at both 250 kv and 300 kv, with the number of pulses observed with the rotating counter at small angles being appreciably less at the higher voltage. There is, of course, the possibility that there still are slit scattering effects in the proton-proton scattering data due to the spreading of the beam when gas is in the chamber, but the effect of this spreading cannot easily be estimated, and can hardly be large.

The counting circuit was so arranged that the two recording circuits and a clock were turned on and off simultaneously. The time was, of course, not directly needed in the calculations, but gave a useful check of counting rates. During the taking of the data frequent checks were made on the character of pulses and background by observation with a cathode-ray oscilloscope which could be switched from one counting circuit to another. With each change in energy or angle the counter voltages had to be re-set, since the size of pulse was proportional to the ionization produced by the proton. As mentioned above, when discussing counters, the proper voltage was easily and reliably determined by setting for pulses in the range of 50 to 120 volts at the amplifier output. During the course of a run the pressure in the counters slowly decreased due to leakage through the foils; this also necessitated counter voltage adjustment several times an hour.

Before starting a run the counters were filled with fresh hydrogen, purified by passage through a palladium tube. Then this same hydrogen source was used to furnish the gas for the scattering chamber; as mentioned above, this gas was continuously admitted and pumped out through the capillary. Liquid air was supplied to a trap which had large diameter connections with the scattering chamber.

Reduction of the Data

Since the data were taken as the ratio of the scattering at two angles, it was necessary to know the relative geometrical factors involved in the counters being used. Table I gives the various dimensions of all the counters used in the data reported herein. The notation is that of BTE, reference 6.

At the beginning and end of each run, and sometimes in between, a check was made of the contamination in the following way. The beam voltage was set at 100 or 150 kv, and the 45° counter voltage so adjusted that the protons scattered from hydrogen, having lost half their energy in the collision, were not detected, while those scattered from heavier contaminant atoms, having lost little energy, gave large enough pulses to be counted reliably. Thus the 45° counter registered only the scattering due to contaminants. When counting was done at the same time

at an angle of either 15° or 30°, no separation of these two scattered groups occurred, since little energy was lost in either type of collision. From a comparison of the contaminant scattering (45°) with contaminant plus hydrogen scattering (15° or 30°), the amount of contamination present was calculated. Since our data seemed from the outset to be in approximate agreement with the calculations of BTE for an interaction well of e^2/mc^2 radius and 10.500-Mev depth, the contamination corrections were made by assuming these calculations for the hydrogen scattering and the Rutherford law for contaminant scattering. The amount of contamination present is conveniently expressed in terms of the equivalent air pressure (in units of 10^{-4} mm of mercury per mm of mercury of hydrogen pressure in the scattering chamber) which would give the observed scattering, and is called A/p. Simultaneous counting of course only gives the ratio of contamination to hydrogen. Because of the anomaly, the proton-proton scattering intensity in these experiments is very low, causing this correction to be of considerable importance. The variation of the contamination correction with angle is shown in Figs. 5, 6, and 7.

Another important correction, referred to as the geometry correction, is due to the non-linear variation of scattering with angle. Since the defining slit system for the counters necessarily admits scattering from a finite range of angles, this non-linearity causes the scattering observed to be too great. Corrections for this effect were made on the basis of Eq. (7.2) of BTE, again under the assumption that the scattering follows the calculations for the 10.500-Mev well. Had the 19.6905-Mev well been assumed, the corrected ratio for 45°/30° at 300 kev would have been raised by approximately 3 percent, while at other angles and lower energies the difference between the results with the two wells would be much less. The corrections calculated from Eq. (7.2) of BTE agreed extremely well with earlier calculations made as follows. The hole of the counter defining-system was divided into several zones parallel to the defining slit. Then the area under the theoretical scattering curve between the limits defined by the slit was found for the average angle corresponding to each zone. These curve-areas were weighted according to the corresponding zone-area, and averaged. Comparison of this averaged area with that which would have been obtained had the angular variation been linear gave the desired correction. The variation of the geometrical correction with angle is included in Figs. 5–7.

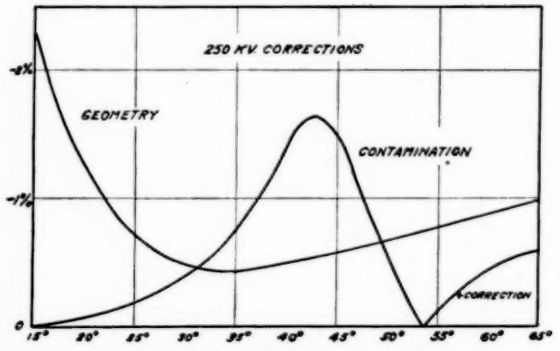

FIG. 5. Geometry and contamination correction curves for the 250-kv data, Fig. 10, and Table III. The contamination correction is for units of A/p, the equivalent air contamination in 10^{-4} mm of mercury per mm of mercury of hydrogen pressure in the scattering chamber.

It should be recalled that an efficiency correction, described in the section on counters, was applied to the energy variation data. Also, the 300-kv angular distribution data (Fig. 11) were corrected for pick-ups from sparks on the assumption that each spark caused one extra pulse. The inaccuracy of this correction when the counting rate is low indicates that the deviation at 45° may originate in this way.

TABLE I. *Data on counter slit systems. All dimensions are given in millimeters. The notation is that of* BTE, *p. 1026. The geometrical constant of a counter slit system is given by* $2\pi ba^2/R_0h$; *numbers proportional to the various values of this expression are given in the last two columns.*

First or Second Apparatus	Angle	Slit Width "2b"	Hole Diam. "2a"	Hole to Slit "h"	Hole to Center "R_0"	Relative Geometry Factor	
First	45°H_2 105°He	4.042	3.080	40.0	155	36.10	
First	30°H_2 60°He	1.964	1.840	40.0	155	6.250	
First	15°	1.007	1.028	40.0	155	1.000	
First	15°	1.024	1.018	40.0	155	1.000	
Second	15°*R*	0.106	1.028	40.0	192	0.0852	1.083
Second	15°*L*	0.100	1.018	40.0	192	0.0787	1.000
Second	Rotates	0.868	2.009	40.0	70	7.30	92.8

DISCUSSION OF RESULTS

The results of the experiments with the first scattering chamber are summarized in Table II and Figs. 8 and 9. In this table total counts

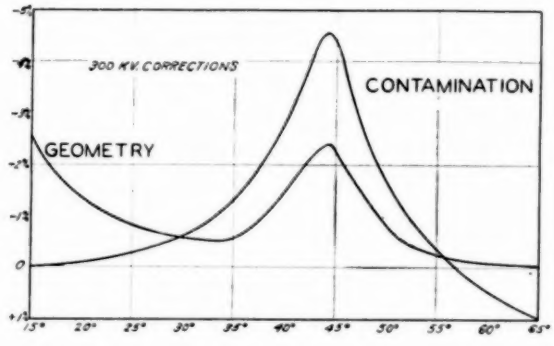

FIG. 6. Geometry and contamination corrections for the 300-kv data, Fig. 11 and Table IV. The contamination corrections are for units of A/p.

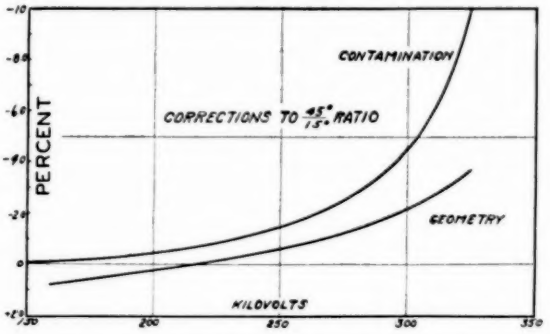

FIG. 7. Geometry and contamination correction curves for the 45°/15° ratio data, Fig. 12 and Table V. The contamination correction is for units of A/p.

representing numerous runs are given. Particular emphasis was placed on the 45°/30° data. These data were broken down into six groups as follows: three ranges of scattering pressure were chosen—5 to 10 mm of oil (density 0.89), 10 to 15 mm, and 15 to 20 mm; in each of these, two subgroups were made by counter pressure, one for pressures below 35 mm of mercury and one for higher pressures. Plotting these points revealed no systematic trend of the data with either counter pressure or scattering pressure variations. The lack of an effect with changing scattering pressure seems to eliminate the possibility of any appreciable errors due to multiple scattering in the data obtained with the first scattering chamber. The data taken at 320 kv are included, though it should be pointed out that the sparking of the outfit, which was not corrected for in this point, the small number of counts, and the geometry and contamination corrections of about 30 percent cast doubt upon the reliability of this point.

Angular distribution data taken with the sec-

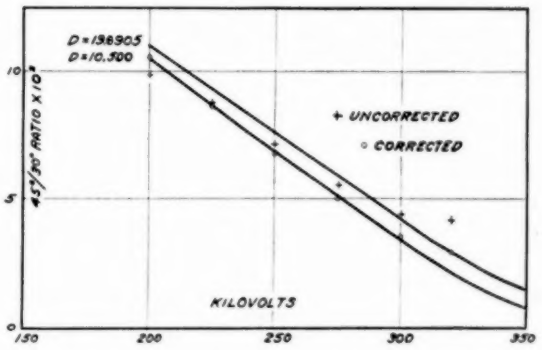

FIG. 8. Proton-proton scattering, first chamber data. The ratio of 45° scattering to 30° scattering multiplied by 100 is plotted as a function of voltage along with the corresponding theoretical curves (solid lines) for $r_0=\frac{3}{4}e^2/mc^2$, $D=19.6905$ Mev and $r_0=e^2/mc^2$, $D=10.500$ Mev.

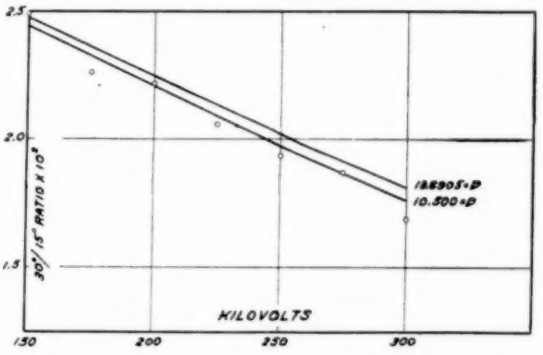

FIG. 9. Proton-proton scattering, first chamber data. The ratio of 30° scattering to 15° scattering multiplied by 100 is plotted as a function of voltage, along with the corresponding theoretical curves (solid lines) for $r_0=\frac{3}{4}e^2/mc^2$, $D=19.6905$ Mev, and also $r_0=e^2/mc^2$, $D=10.500$ Mev.

ond scattering chamber for the range from 15° to 65° have been obtained for incident proton energies of 249.5 kev and of 298.3 kev. These data have been expressed in the form of a ratio P/P_M of observed scattering to the scattering expected from Mott's formula, because the scattering at low angles is of a different order of magnitude than that at 45°. The values of P/P_M

TABLE II. *Proton-proton scattering results, first apparatus.*

Variation with energy, 45° to 30° ratio						
Energy, kev	200	225	250	275	300	320
Total counts at 45°	29,044	78,284	31,272	12,604	4,864	420
Total counts at 30°	50,960	155,104	75,104	39,248	19,152	1,728
Uncorrected ratio, %	9.88	8.74	7.21	5.56	4.40	4.21
Corrected ratio, %	10.53	8.65	6.80	5.00	3.58	2.99

Variation with energy, 30° to 15° ratio							
Energy, kev	150	175	200	225	250	275	300
Total counts at 30°	12,760	5,028	4,448	15,612	6,668	5,040	4,680
Total counts at 15°	82,048	35,456	31,680	120,096	54,544	42,448	43,472
Uncorrected ratio, %	2.49	2.27	2.25	2.08	1.96	1.90	1.72
Corrected ratio, %	2.49	2.26	2.24	2.06	1.94	1.87	1.69

TABLE III. *Angular variation of P/P_M at 249.5 kev. θ, angle; C, counter and scaling circuit used; N_P, actual number of protons counted; p, hydrogen pressure in scattering chamber in mm of oil; A/p, ratio of equivalent air pressure in units of 10^{-4} mm of mercury giving observed contamination, to chamber pressure in mm of mercury;* Corr, *sum of geometry and contamination corrections in percent; R, observed scattering ratio, including geometrical factor, multiplied by 10^4; $(P/P_M)u$, uncorrected ratio to Mott; $(P/P_M)c$, ratio to Mott with geometry and contamination corrections. The "A" counter is the monitor at 15°, "B" is the rotating counter.*

θ	C	N_P	p	A/p	Corr	R	$(P/P_M)u$	$(P/P_M)c$
15°	A4	776						
	B16	71,100	9.5	2.52	−2.3	10,710	0.952	0.929
345°	A4	840						
	B16	72,600	9.5	2.52	−2.3	9,360		
20°	A4	2,544						
	B16	46,500	11.2	2.64	−1.45	2,140	0.876	0.865
340°	A4	2,500						
	B16	48,850	10.6	2.64	−1.45	2,120		
22.5°	A4	3,628						
	B16	36,020	12.3	1.69	−1.19	1,162	0.845	0.836
337.5°	A4	3,276						
	B16	34,200	12.3	1.69	−1.19	1,130		
25°	A4	1,468						
	B16	7,610	7.2	4.0	−1.50	607		
25°	A4	3,312						
	B16	16,910	11.4	2.5	−1.20	598	0.781	0.769
335°	A4	1,672						
	B16	9,060	7.1	4.0	−1.50	587		
335°	A4	2,400						
	B16	13,200	11.2	2.5	−1.20	596		
27.5°	A4	1,544						
	B16	4,530	7.2	4.0	−1.68	343		
27.5°	A4	2,868						
	B16	8,565	11.2	2.5	−1.26	337	0.734	0.723
332.5°	A4	1,568						
	B16	4,965	7.2	4.0	−1.68	342.5		
332.5°	A4	3,516						
	B16	10,920	11.1	2.5	−1.26	337		
30°	A4	1,880						
	B16	3,360	7.2	3.95	−2.08	209		
30°	A4	3,516						
	B16	6,080	10.2	3.0	−1.70	202	0.681	0.674
330°	A4	3,444						
	B16	6,320	10.1	3.0	−1.70	199		
330°	A4	1,848						
	B16	3,441	7.2	3.95	−2.08	201.7		
32.5°	A4	2,512						
	B16	2,674	7.2	3.95	−2.51	124.3	0.624	0.606
327.5°	A4	2,024						
	B16	2,207	7.2	3.95	−2.51	118.1		
35°	A4	6,098						
	B16	3,600	11.2	2.0	−1.97	69.2		
35°	A16	5,165						
	B4	1,604	7.0	3.95	−3.47	69.6	0.524	0.506
325°	A16	4,148						
	B4	1,428	7.2	3.95	−3.47	77.3		
325°	A16	5,860						
	B4	3,516	11.2	2.0	−1.97	65.0		
37.5°	A16	7,655						
	B4	1,424	7.1	4.20	−4.75	41.75	0.421	0.401
322.5°	A16	7,945						
	B4	1,412	7.1	4.20	−4.75	39.87		
40°	A16	11,200						
	B4	1,328	7.1	3.95	−6.03	26.53	0.348	0.335
320°	A16	16,770						
	B4	1,848	23.5	1.13	−2.08	24.75		
42.5°	A16	16,490						
	B4	1,296	7.0	3.95	−7.04	17.65		
42.5°	A16	24,590						
	B4	1,924	21.4	1.10	−2.34	17.51	0.286	0.275
317.5°	A16	29,100						
	B4	2,252	21.2	1.40	−2.84	17.31		
317.5°	A16	18,040						
	B4	1,300	6.7	3.0	−5.46	16.20		
45°	A16	22,030						
	B4	1,312	7.1	3.40	−5.7	13.33		
45°	A16	33,200						
	B4	2,152	22.3	0.90	−1.96	13.82	0.266	0.256
315°	A16	24,410						
	B4	1,616	22.8	1.16	−2.36	14.83		
315°	A16	12,910						
	B4	804	6.8	3.90	−6.45	13.63		
47.5°	A16	23,410						
	B4	1,420	9.0	2.2	−2.85	13.61		
47.5°	A16	31,580						
	B4	1,864	21.5	1.00	−1.65	13.23	0.280	0.272
312.5°	A16	28,210						
	B4	1,848	20.9	1.30	−1.95	14.68		
312.5°	A16	20,920						
	B4	1,288	9.3	6.7	−7.35	13.80		
50°	A16	19,300						
	B4	1,452	9.3	2.3	−1.94	16.91	0.341	0.334
310°	A16	17,160						
	B4	1,416	8.9	2.8	−2.21	18.51		
52.5°	A16	14,280						
	B4	1,412	9.3	2.4	−1.05	22.1	0.397	0.395
307.5°	A16	12,860						
	B4	1,332	9.0	2.7	−1.09	23.2		
55°	A16	11,760						
	B4	1,492	9.3	2.5	−0.48	29.0	0.452	0.449
305°	A16	16,370						
	B4	2,200	9.0	2.5	−0.48	30.10		
57.5°	A16	9,350						
	B4	1,444	7.0	3.3	−0.070	33.63	0.451	0.451
302.5°	A16	8,452						
	B4	1,360	6.8	3.3	−0.070	37.82		
60°	A16	11,080						
	B4	1,900	9.1	2.5	+0.25	38.23	0.395	0.396
300°	A16	10,130						
		1,788	9.2	2.5	+0.25	39.31		
62.5°	A16	11,620						
	B4	1,540	7.1	3.3	+0.86	30.82	0.269	0.267
297.5°	A16	9,020						
	B4	1,360	6.8	3.3	+0.86	33.93		
65°	A16	9,220						
	B4	872	9.2	2.5	+0.52	21.15	0.106	0.104
295°	A16	14,960						
	B4	980	7.1	3.3	+1.00	14.05		

were calculated from:

$$(P/P_M)_\theta = [(P/P_M)_{15°}\mathfrak{M}(15°)\cot 15°/ \mathfrak{M}(\theta)\cot\theta]S(\theta)/S(15°), \quad (1)$$

where $S(\theta)/S(15°)$ is the observed ratio of the number of protons scattered into the rotating counter at the angle θ to the number of protons scattered into the monitor at the angle 15° during the same time interval, divided by a constant factor due to the geometry of the counter apertures. The quantity in brackets is calculated from the tables of $\mathfrak{M}$ in BTE and $(P/P_M)_{15°}$ is the Mott ratio[11] for 15°, calculated from the assumed well parameters $r_0 = e^2/mc^2$ and $D = 10.5$ Mev. These values were taken from unpublished tables furnished us by Professor Breit. If the

[11] The symbols P/P_M and $\mathfrak{R}$ are both used by BTE to represent the Mott ratio.

TABLE IV. *Angular variation of P/P_M at 298 kev. Notation is same as for Table III.*

θ	C	N_P	p	A/p	Corr	R	$(P/P_M)_U$	$(P/P_M)_C$
15°	A4	1,228						
	B16	105,296	21.1	1.2	−2.3	10,020	0.881	0.861
345°	A4	1,236						
	B16	103,296	22.5	1.0	−2.3	9,060		
20°	A4	2,972						
	B16	41,568	21.1	1.10	−1.67	1,950		
340°	A4	3,384						
	B16	64,048	21.2	1.10	−1.67	2,050	0.822	0.808
20°	A4	4,648						
	B16	84,192	23.3	1.00	−1.65	2,120		
20°	A4	3,484						
	B16	64,304	21.7	1.45	−2.33	2,158		
340°	A4	3,176						
	B16	53,872	21.7	1.45	−2.33	1,839		
25°	A4	4,188						
	B16	21,760	23.8	0.99	−1.35	609		
25°	A4	5,708						
	B16	26,960	21.3	1.7	−1.91	554	0.748	0.737
335°	A4	4,440						
	B16	23,632	21.3	1.30	−1.34	576		
25°	A4	4,788						
	B16	24,656	21.1	1.25	−1.11	603		
30°	A4	5,340						
	B16	8,400	10.0	3.49	−2.34	183.2		
330°	A4	4,700						
	B16	7,712	9.5	3.49	−2.34	174.0	0.583	0.570
330°	A4	4,740						
	B16	7,872	21.2	0.85	−1.07	178.7		
30°	A4	7,856						
	B16	12,112	20.0	1.20	−1.26	165.0		
32.5°	A4	4,832						
	B16	4,624	20.8	1.60	−1.80	110.5		
32.5°	A4	4,220						
	B16	3,888	17.1	~1.40	−1.65	106.9	0.516	0.507
327.5°	A4	4,880						
	B16	4,400	19.3	1.10	−1.42	97.0		
35°	A16	6,976						
	B4	1,796	10.4	3.49	−4.44	57.2		
35°	A16	6,752						
	B4	3,244	20.1	1.55	−2.48	56.0	0.401	0.390
325°	A16	6,912						
	B4	3,432	20.2	1.00	−1.75	53.5		
37.5°	A16	15,168						
	B4	2,240	21.8	1.30	−3.45	33.0		
37.5°	A16	12,432						
	B4	1,852	21.2	1.1	−3.05	33.1	0.328	0.319
37.5°	A16	11,008						
	B4	1,692	16.5	1.30	−3.45	34.3		
322.5°	A16	15,568						
	B4	2,304	21.3	1.0	−2.85	32.8		
322.5°	A16	15,168						
	B4	2,092	19.3	1.0	−2.85	30.7		
40°	A16	23,360						
	B4	1,788	20.6	0.85	−3.68	17.02		
320°	A16	23,200						
	B4	1,792	23.6	0.75	−3.40	16.97	0.225	0.217
42.5°	A16	46,880						
	B4	2,044	22.3	0.90	−5.67	9.53		
317.5°	A16	41,408						
	B4	1,752	23.3	0.775	−5.17	9.21	0.151	0.142
45°	A16	24,496						
	B4	820	20	1.30	−7.92	7.26		
45°	A16	23,760						
	B4	728	19.5	1.10	−7.04	6.69		
45°	A16	43,712						
	B4	1,480	21.4	1.40	−8.36	7.47		
315°	A16	36,272						
	B4	1,096	15	0.94	−6.33	5.23	0.128	0.118
315°	A16	19,264						
	B4	700	19	1.30	−7.92	7.87		
315°	A16	47,664						
	B4	1,420	20.1	1.5	−8.81	7.06		
47.5°	A16	27,168						
	B4	868	23.0	0.45	−2.76	6.94		
47.5°	A16	24,864						
	B4	876	21.5	1.20	−4.82	7.72		
312.5°	A16	51,888						
	B4	2,068	22.5	0.80	−3.72	8.74	0.154	0.148
50°	A16	35,392						
	B4	1,760	22.3	0.60	−1.78	11.49		
310°	A16	39,088						
	B4	2,016	22.0	0.83	−2.17	11.35	0.214	0.210
52.5°	A16	23,824						
	P4	1,680	18.0	1.20	−1.48	15.68		
307.5°	A16	18,428						
	B4	1,896	19.8	1.25	−1.52	22.70	0.298	0.294
307.5°	A16	20,980						
	B4	1,644	21.4	1.45	−1.70	17.55		
55°	A16	20,096						
	B4	2,088	21.2	1.50	−0.680	23.20		
55°	A16	20,992						
	B4	2,100	21.0	0.70	−0.400	22.21		
305°	A16	17,040						
	B4	2,016	22.0	0.89	−0.470	26.30	0.364	0.363
57.5°	A16	11,344	20.6	1.50	+0.05	41.0		
	B4	2,088						
302.5°	A16	10,400						
	B4	1,836	20.5	1.40	+0.05	39.3	0.494	0.494
60°	A16	9,744						
	B4	1,544	21.0	1.20	+0.41	35.4		
60°	A16	7,974						
	B4	2,032	21.5	1.80	+0.68	56.8		
300°	A16	9,504						
	B4	1,844	20.4	1.30	+0.45	43.2	0.424	0.427
300°	A16	16,384						
	B4	2,600	21.8	1.35	+0.485	35.5		
65°	A16	13,968						
	B4	1,620	17.3	1.20	+1.20	25.65		
295°	A16	20,736						
	B4	1,608	18.5	1.13	+1.13	17.30	0.136	0.138
65°	A16	12,880						
	B4	1,440	21.9	1.65	+1.65	24.65		
295°	A16	22,384						
	B4	2,492	21.7	1.65	+1.65	24.65		

corresponding value for the 19.6905-Mev well had been used at 250 kev, for instance, the values of the Mott ratio calculated from our data would only have been 0.42 percent higher throughout at this energy.

Tables III and IV list the angular distribution data obtained for incident proton energies of 249.5 and 298.3 kev. Data were taken at corresponding angles on opposite sides of the beam and averaged. Each run is separately tabulated since these were often taken under different conditions of contamination and pressure in the scattering chamber. The letters A and B refer to the fixed and rotating counters, respectively, while the numbers 4 and 16 refer to the factor of the scaling circuit used in each case. It will be seen that in both tables the 15° data have the fewest protons on A. This is due to the fact that the scattering at 15° is so large that the intensity of the proton beam must be greatly reduced if a reasonable number of protons is to be observed on the rotating counter, which has a very large aperture. This, however, makes the number of protons entering the monitor counter quite small.

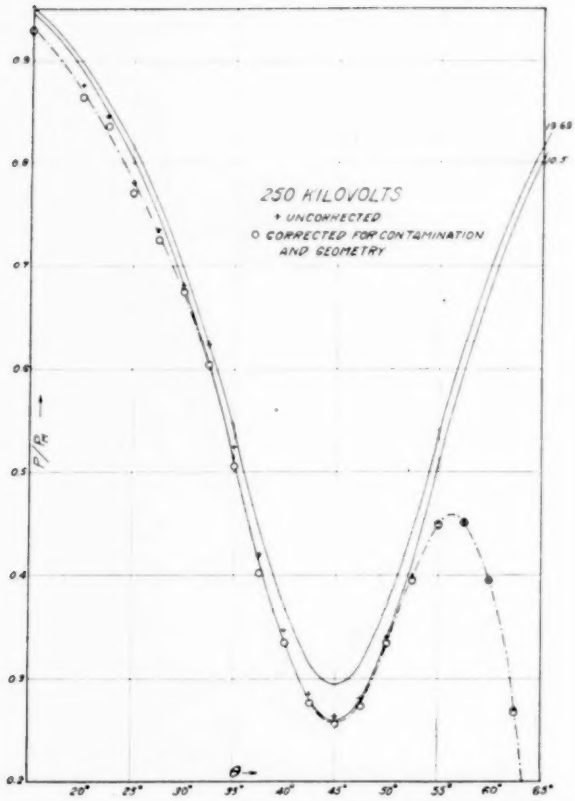

FIG. 10. Proton-proton scattering at 250 kv, second chamber data, plotted as ratio to Mott scattering along with theoretical curves (solid lines) for $r_0=\frac{3}{4}e^2/mc^2$, $D=19.6905$ Mev (upper curve) and $r_0=e^2/mc^2$, $D=10.500$ Mev (lower curve). The dashed curve is experimental for a proton energy of 249.5 kev at the scattering volume; its value at the higher angles yields the efficiency correction curve, Fig. 4.

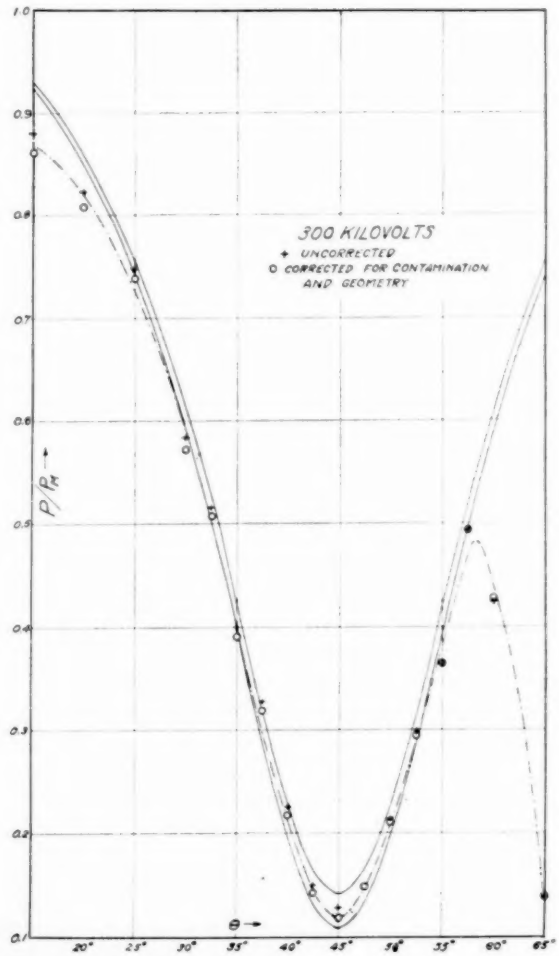

FIG. 11. Proton-proton scattering at 300 kv, second chamber data, plotted as ratio to Mott scattering along with theoretical curves (solid lines) for $r_0=\frac{3}{4}e^2/mc^2$, $D=19.6905$ Mev, and $r_0=e^2/mc^2$, $D=10.500$ Mev. The dashed curve is experimental, for a proton energy of 298.3 kev at the scattering volume.

These data are again presented in Figs. 10 and 11, while Figs. 5 and 6 show the corresponding correction curves. The experimental voltages are slightly lower than those for the theoretical curves. This would be of greatest importance at 45°, where the theoretical curve for 298.3 kev (the experimental value) would be 2 percent higher and account for part of the discrepancy.

In Table V are listed the data on the energy variation of P/P_M for 45°, shown also in Fig. 12. Figures 4 and 7 show the corrections for these data. The angle 45° was chosen because, as is seen, the anomaly is large and the choice between potential wells is here most easily made. Because of the stopping power of the gas in the scattering chamber, the energy of the protons when scattered was less than the energy given by the accelerating voltage. Livingston and Bethe's[12] curves for the stopping cross section of protons in air, together with the relative stopping power of hydrogen were used to correct for this. The total path length of the protons in hydrogen at the oil manometer pressure was assumed to be 12 cm. This corresponds to assuming that one-half of the length of the differential pumping system capillary has hydrogen at manometer pressure in it. The corrections amount to 3.46 kev/mm of mercury at 175 kev and 2.86 kev/mm of mercury at 325 kev. In taking the data, it was attempted to set the accelerating voltage higher by the correct amount, but since this was

[12] M. S. Livingston and H. A. Bethe, Rev. Mod. Phys. **9**, 245 (1937).

not always successful, the energies at the scattering volume were individually calculated.

It may be seen that at 15°, Eq. (1) should reduce to the identity $(P/P_M)_{15°}=(P/P_M)_{15°}$. However, the 15° points in the angular distributions, Figs. 10 and 11, do not fall on the proper theoretical curves. This is a manifestation of error in the small angle data. There were a number of experimental difficulties encountered at small angles which may have caused error. (1) It was possible to monitor only on one side of the beam. (2) The beam struck the body of the counter. This caused no increase in scattering when the chamber was evacuated, but the possible effect of the presence of the gas is unknown. (3) Because of the difference in the geometries of the monitors and the rotating counter, very small beam currents had to be used. As seen in the tables, the statistical accuracy of the counting rate in the monitor counters is poor. Also, it is possible that the necessary changes in the probe and focusing voltages may have introduced a slight shift in beam direction and changed the intensity distribution within the beam itself. (4) The geometry correction is largest at small angles. (5) An error in the geometrical factor for the counters would be most noticeable at small angles. (6) No corrections have been made for finite beam width. These are estimated in BTE, p. 1040, are largest at small angles, and increase the P/P_M ratio. (7) No corrections have been made for multiple scattering effects. (8) The divided circle and vernier may have been inaccurate.

In order to try to find which of these sources of error existed, data were taken as a function of scattering chamber pressure. A smaller slit was used on the rotating counter to reduce its counting rate. A minimum of about 5 percent in the scattering yield at 20° for both 250 kv and 300 kv was observed at about 12 mm of oil pressure. The values at oil pressures below 8 mm approach the theoretical yield within 1 percent, but the statistical accuracy of the low pressure data is not that good. However, some of our scattering data were taken in the pressure range which we subsequently found to be a minimum. An effect seems to be present at 15°, but it is of smaller magnitude and the statistical accuracy of the points is not good, so that no conclusions can be drawn for this angle. No pressure effect was found at 35°.

Our apparatus was of course not designed to measure a pressure effect, and no account has been taken of this effect in either the tabulated data or the curves. Attempts to interpret it, however, have suggested a number of factors which may be valuable in criticizing our data. It is interesting that the greatest effect of pressure variation occurred near the transition between laminary and molecular flow of the gas leaving the capillary. A pressure effect would of course suggest multiple scattering, which would be more likely to reduce our P/P_M ratios than to increase them. The 15° monitoring counter, whose yield goes into the denominator of the fraction P/P_M, would be expected to receive the greatest multiple scattering effect. Finally, there is an important difference between the two scattering chambers used in these experiments. In the first chamber the two counters involved were the same distance from the scattering volume, but

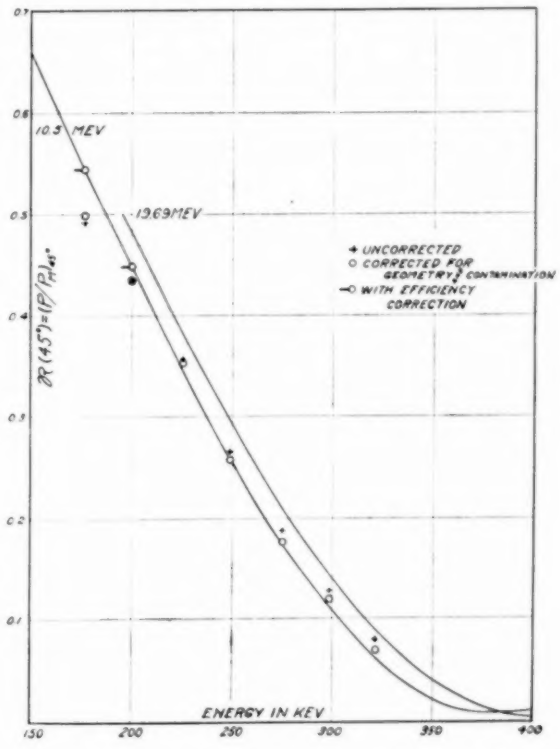

FIG. 12. Proton-proton scattering at 45°, second chamber data, plotted as ratio to Mott scattering along with theoretical curves (solid lines) for $r_0=\frac{3}{4}e^2/mc^2$, $D=19.6905$ Mev, and $r_0=e^2/mc^2$, $D=10.500$ Mev.

TABLE V. *Energy variation of* $(P/P_M)_{45°}$. *Notation is same as for Table III except: E, proton energy in kev;* $(P/P_M)e$, *ratio to Mott with geometry, contamination and efficiency corrections.*

E	C	N_P	θ	p	A/p	Corr	R	$(P/P_M)u$	$(P/P_M)c$	$(P/P_M)e$
	A16	22,080								
	B4	2,400	45.0°	23.0	0.82	+0.062	24.38	0.495	0.498	0.544
176.5	A16	25,504								
	B4	2,912	315.0°		0.83		25.5			
	A16	19,328								
	B4	1,952	45.0°	22.4	0.80	−0.30	22.5	0.435	0.434	0.448
200.2	A16	19,968								
	B4	2,000	315.0°	22.5	0.80		22.62			
	A16	25,184								
	B4	2,072	45.0°	23.0	0.95	−1.022	18.42	0.357	0.353	0.353
225.9	A16	26,640								
	B4	2,204	315.0°	23.0			18.52			
	A16	22,048								
	B4	1,312	45.0°	7.1	3.4	−5.7	13.33	0.251		
	A16	33,200								
	B4	2,052	45.0°	22.3	0.90	−1.96	13.82	0.261	0.256	0.256
249.5	A16	20,656								
	B4	1,288	315.0°	7.1	3.9	−6.45	13.96	0.263		
	A16	24,448								
	B4	1,616	315.0°	23.2	1.16	−2.36	14.83	0.279		
	A16	34,768								
	B4	1,624	45.0°	21.8	2.0	−6.35	10.45	0.193	0.177	0.177
275.3	A16	43,648								
	B4	1,924	315.0°	21.5	1.50	−4.98	9.88	0.183		
	A16	24,496								
	B4	820	45.0°	20.0	1.30	−7.92	7.26			
	A16	23,760								
	B4	728	45.0°	19.5	1.10	−7.04	6.69			
	A16	43,712								
	B4	1,480	45.0°	21.4	1.40	−8.36	7.47	0.128	0.118	0.118
298.3	A16	36,272								
	B4	1,096	315.0°	15.0	0.94	−6.33	5.23			
	A16	19,264								
	B4	700	315.0°	19.0	1.30	−7.92	7.87			
	A16	47,664								
	B4	1,420	315.0°	20.1	1.50	−8.81	7.06			
	A16	42,928								
	B4	888	45.0°	24.0	1.13	−13.9	4.42	0.081	0.0703	0.0703
321.4	A16	38,672								
	B4	832	315.0°	24.0	1.13		4.62			

in the second chamber they are at quite different distances. It would seem that any pressure effect that may exist at 15° should find its origin in this difference of distances, and it may be that multiple scattering could thus affect the monitor and rotating counters differently.

Unfortunately, time limitations prevented a more thorough investigation of this source of error. Nevertheless, other experimental errors, particularly in the divided circle, statistics, the geometrical factor, and pick-up from sparks at the higher voltages, can account for the deviations between the experimental data and the theoretical scattering curves for a potential well of e^2/mc^2 radius and 10.500-Mev depth. All of the data, taken as a function of energy with two different scattering chambers, and also as a function of angle are in consistent agreement with calculations based on this interaction potential well.

The authors are greatly indebted to Professor G. Breit for encouraging discussions of many aspects of this problem and for the use of the tabulated theoretical results. They have also benefitted by discussions with Professor R. G. Herb. They wish to express their gratitude to Mr. J. P. Foerst for his kind cooperation and the accurate construction of the scattering chambers, and to the Wisconsin Alumni Research Foundation for financial support.

The Spark Spectrum of Europium, Eu II

HENRY NORRIS RUSSELL, WALTER ALBERTSON, AND DOROTHY N. DAVIS
University Observatory, Princeton University, Princeton, New Jersey and Massachusetts Institute of Technology, Cambridge, Massachusetts

(Received June 30, 1941)

Structure of the spectrum. The strongest lines of Eu II arise from transitions based on the ground-level of Eu III, $f^7\ {}^8S°$. The lowest terms are $f^7s\ {}^9S°$, $^7S°$. Next come $f^7d\ {}^9D°$, $^7D°$. Numerous levels, combining with these terms, arise from f^6s^2, f^6sd, and f^8. The number of levels identified is 156; of lines classified, 467. All the stronger lines are included. *Unclassified lines.* About 2000 lines remain unclassified. They probably arise from transitions between levels based upon higher limits in the f^7 configuration of Eu III. *Ionization potential.* Series of three consecutive $^9S°$ and $^7S°$ terms give the value 11.21 volts. *Zeeman effect.* Patterns for 459 lines, measured at the Massachusetts Institute of Technology, with a field of 87,850 gauss, are tabulated. The g values for 118 levels have been determined. Those for the low levels agree with theory; the higher levels are much perturbed. Patterns for a few lines of Eu I and Eu III are given. The latter confirm that the ground state is $^8S°$.

THE second spectrum of europium consists of a simple portion, containing the strongest lines and recognizable series, and a much more extensive complex portion. An analysis of the former by one of us[1] is here somewhat extended and a part of the complex portion interpreted.

I. OBSERVATIONS

(1) The wave-lengths and intensities are taken from King's accurate and comprehensive list[2] which extends from 2109 to 10165A. These measures were made on arc and furnace spectra. After eliminating lines shown to belong to Eu I by the analysis of this spectrum[3] or by temperature class, there remain 2681 lines. Of these 1861 were recorded as enhanced in the spark, and can be definitely assigned to Eu II. We are greatly indebted to Dr. King for re-examining a number of critical cases. For wave-lengths greater than about 4000A most of the lines recorded by King as of temperature class V probably belong to Eu I; short of 3000A almost all should be attributed to Eu II, as the lines of Eu I must here be few and faint.

"Lines of a rich spectrum which is quite absent from the arc, and probably belongs to Eu III" were omitted from King's list. It is probable that some high excitation lines of Eu II are among them. Many of the lines show hyperfine structure, and King's measures are therefore usually given only to 0.01A.

The strongest lines of Eu II are of very great intensity in the arc, and strong in the furnace, so that they are placed in the rather rare temperature class II E. The great bulk of the lines, however, are of class VE.

(2) Observations of the Zeeman effect obtained with the Bitter magnet[4] of the Massachusetts Institute of Technology with a field of 87,850 gauss have been generously placed at our disposal by Professor Harrison. These extend from λ2317 to λ7426 and include all the stronger lines and a great number of faint ones. They were measured upon Harrison's automatic measuring engine.[5] The film-records which it produces are equally notable for the accuracy of the measures and the convenience of their discussion. The permanent record is a great advantage, since any line may be re-examined without replacing a plate in the measuring engine.

The limit of resolution, for lines of favorable intensity (in the usual units) is less than $0.2a$ at λ2500 and less than $0.1a$ in the visible. Some of the patterns in the red are very wide: that for λ7217 extends over 13.3A.

The observed patterns for 460 lines are tabulated in abbreviated form in Table X. Without their aid, the complex part of the spectrum could hardly have been interpreted.

[1] W. Albertson, Phys. Rev. **45**, 499 (1934).
[2] A. S. King, Astrophys. J. **89**, 377 (1939).
[3] H. N. Russell and A. S. King, Astrophys. J. **90**, 155 (1939).
[4] G. R. Harrison and F. Bitter, Phys. Rev. **57**, 15 (1940).
[5] G. R. Harrison, J. Opt. Soc. Am. **25**, 169 (1935).

II. Structure of the Spectrum

(3) The simple part of the spectrum has as limit the ground-level $4f^7\ {}^8S°$ of Eu III, which is undoubtedly very much the lowest. Addition of a $6s$ electron gives the ground-terms of Eu II, $a^9S°$, $a^7S°$; of $5d$, $a^9D°$, $a^7D°$; of $6p$, z^9P, z^7P; of $7s$, $e^9S°$, $e^7S°$; of $6d$, $e^9D°$, $e^7D°$; and of $8s$, $f^9S°$, $f^7S°$. The last four terms are new. Combinations between these terms account for 72 lines—four percent of the whole number but almost all the strongest ones. Additional series members have not been found. (See Section 9.)

(4) The strongest remaining lines lie between 3100 and 2600A. A few of them show absorption in the furnace at high temperatures. These lines arise from transitions between the ground-levels $a^9S°$, $a^7S°$ and a host of even levels, which combine also with $a^9D°$ (some strongly) and more weakly with $a^7D°$. Values of the Zeeman parameter g have been found for most of these levels. All but a few of these exceed 1.5. There are many higher levels, combining with $a^7D°$, whose combinations with the ground-levels lie beyond the limit of observation. A few high odd levels have been identified by combinations with z^9P, z^7P.

(5) Many fairly strong lines remain unclassified. Most of these are between 4200 and 3000A. There are many resolved Zeeman patterns which indicate that a great many levels with different g values are involved. Most of the latter are less than 1.5. No progress has been made in analyzing this group. Its general nature may however be interpreted, with some confidence, as arising from the transition $4f^7 6s - 4f^7 6p$ with other limits than ${}^8S°$. The next lowest terms of f^7 should be ${}^6(PDFGHI)°$. By analogy with the d^5 configurations in Cr and Mn we should expect these terms to lie at least 25,000 cm^{-1} higher than $f^7\ {}^8S°$, and to have narrow separations.

Table I. *Levels of* Eu II.

Config.	Terms	Electron-Jump to f^7s	Electron-Jump to f^7d
f^8	${}^7F$	$((f-s))$	$f-d$
f^6s^2	${}^7F$	$((s-f))$	$((s-f,\ s-d))$
f^6sd	${}^{9,7,5}(PDFGH)$	$d-f$	$(d-f,\ s-d)$
f^6d^2	${}^{9,7,5}(SPDFGHI,\ DFG)$ ${}^7(PDFGHIK,\ PDFGH,\ F)$	$(d-f,\ d-s)$	$d-f$

Addition of an s electron gives ${}^{7,5}(PDFGHI)°$—twelve terms, with 64 component levels—and of a p electron, a triad of terms for each of these—in all 36 terms, and 408 levels. These should be 50,000 cm^{-1} or more above the ground-level. The transition $f^7s - f^7p$ (considering these groups of levels only) should give rise to thousands of lines lying mainly in the near ultraviolet. Most of the mass of unclassified lines in this region probably originate thus. There are two ways of breaking into such a complex of lines—with the aid of frequency differences and g values. The first demands that a large proportion of the faint satellite lines in the multiplets shall be recorded; and there are not enough lines in the present list to make it probable that this is the case. Highly precise g values are available for many lines; but when these were arranged in order of magnitude, there were very few of the concentrations near particular values which would occur if many lines from a single level were involved, and searches with the frequency differences shown by the few encouraging cases proved fruitless. Past experience has shown[6] that attempts at analysis in such a case are very unpromising.

(6) The levels combining with $a^9S°$, $a^7S°$, which lie between 30,000 and 45,000, cannot belong to f^7p but may come from configurations with six or eight f electrons. Both f^6 and f^8 give one term much lower than any others. From these we obtain the values given in Table I.

The electron jumps involved in transitions to the low levels are given on the right. The double jumps in parentheses should give fainter lines than the single $d-f$ jump, while those in double parentheses are very improbable. Hence f^6s^2 (though probably the lowest of the configurations) may be excluded here. The very strong combinations with $a^9S°$ are probably nonets from f^6sd.

The relative levels of f^6s^2, f^6sd, and f^6d^2 may be estimated by interpolation between La and Lu. The lowest levels in each configuration are:

La II $6s^2\ {}^1S°$ 7394; $5d6s\ {}^1D_2$ 1394; $5d^2\ {}^3F_2$ 0

Lu II $f^{14}6s^2\ {}^1S_0$ 0; $f^{14}5d6s\ {}^3D_1$ 11796;

$f^{14}5d^2\ {}^5F_2$ 29406.

This indicates that f^6sd should be a few thousand wave numbers lower than f^6d^2 in

[6] W. Albertson, Phys. Rev. **52**, 644 (1937).

TABLE II. *High even levels of* Eu II.

TERM	OBS.	g THEOR.	COMBINATIONS $a^9S^\circ_4$	$a^7S^\circ_3$	$a^9D^\circ_6$	$a^9D^\circ_5$	$a^9D^\circ_4$	$a^9D^\circ_3$	$a^9D^\circ_2$	$a^7D^\circ_5$	$a^7D^\circ_4$	$a^7D^\circ_3$	$a^7D^\circ_2$	$a^7D^\circ_1$
y^9P_5	1.749	1.800	800		60	8	8			1	*m*			
y^9P_4	1.895	1.950	1200	600		100	60	15		10	—	1		
y^9P_3	2.037	2.250	1000	600			20	30	40		3	6	*m*	
x^9P_5	1.715	1.800	250		400	50	12			*m*	*m*			
x^9P_4	1.889	1.950	200	200		300	100	40		3	—	—		
x^9P_3	2.163	2.250	300	300			100	150	100		3	*m*	1	
y^7P_4	1.746	1.750	4	300		20	—	80		15	6	3		
y^7P_3	1.922	1.917	10	250			10	—	80		8	6	2	
y^7P_2	2.188	2.333		600				—	35			3	6	6
z^9D_6	1.687:	1.667			5	8				—				
z^9D_5	1.710	1.733	300		8	2	8			—	—			
z^9D_4	1.824	1.850	200	—		10	10	5		—	—	—		
z^9D_3	2.002	2.083	100	20			—	3	8		—	—	—	
z^9D_2	2.511	2.667		20				—	*m*			—	—	—
z^7F_6	1.485	1.500			—	—				150				
z^7F_5	1.460	1.500	*v*		—	—	—			50	125			
z^7F_4	1.466	1.500	*v*	*v*		—	—	—		4	80	80		
z^7F_3	1.460	1.500	*v*	*v*			—	—	—		6	30	30	
z^7F_2	1.451	1.500		*v*				—	—			8	40	15
z^7F_1	1.494	1.500							—				10	20
z^7F_0	%	%												12
y^9D_6	1.621	1.667			20	8								
y^9D_5	1.569	1.733	—		8	8	12							
y^9D_4	1.672	1.850	—	12		15	—	15						
y^9D_3	1.974	2.083	—	40			12	—	20					
y^9D_2	....	2.667		40				3	6					

v denotes that a line is in the vacuum region, *m* that it is masked, — that it is absent.

Eu II, and the unobservable f^6s^2 still lower. The relative positions of the f^6sd terms may be estimated from those of f^6d in Sm II[7] of which the lowest is a^8H, followed by a^8D, a^8G, b^8G, and a^8P.

(7) Among the observed levels, the intensities and g values clearly define two ^9P terms and one ^7P. A ^9D term includes the lowest levels, another lies higher, and a ^7F accounts for some very strong lines near λ2500. The g values and multiplet intensities for those terms are given in Table II. The high level of a^7D° tends to reduce the intensities of its combinations in the arc.

The first five terms give good multiplets, and the assignments appear secure; the last is more doubtful. There is evidence of perturbation in the g values. From the intensities and positions (Table II) y^9P and x^9D clearly belong to f^6sd, and x^9P to f^6d^2—likewise probably y^7P. The higher term z^7F may come from f^6d^2 or f^8. The latter seems more probable, on account of the isolation and great strength of the multiplet. Among the high odd levels not belonging to series, part of a $^7F^\circ$ term (e^7F°) is identified by g values, and a term e^7D has been tentatively

[7] W. Albertson, Astrophys. J. **84**, 26 (1936).

TABLE III. *Stronger lines of* Eu II.

INTENSITY	>1000	1000 TO 500	500 TO 250	250 TO 125	125 TO 80
No. of lines	23	11	19	23	54
No. classified	23	11	19	23	46

TABLE IV. *Values of* n^* *in Rydberg formula.*

ELECTRON	TERM	n^*	TERM	n^*
6*s*	$a^9S^\circ_4$	2.1997	$a^7S^\circ_3$	2.2202
7*s*	$e^7S^\circ_4$	3.2488	$e^7S^\circ_3$	3.2692
8*s*	$f^7S^\circ_4$	4.2662	$f^7S^\circ_3$	4.2873
6*p*	z^9P_5	2.6099	z^7P_4	2.6214
	z^9P_3	2.5607	z^7P_2	2.6300
5*d*	$a^9D^\circ_6$	2.3485	$a^7D^\circ_5$	2.4376
	$a^9D^\circ_2$	2.3309	$a^7D^\circ_1$	2.4456
6*d*	$e^9D^\circ_6$	3.4846	$e^7D^\circ_5$	3.5698
	$e^9D^\circ_2$	3.4706	$e^7D^\circ_1$	3.5719

TABLE V. *Probable error of one determination of g.*

TERMS	N	n	r_0
$a^9S°$, $a^7S°$	2	42	±0.0057
$a^9D°$	5	30	±0.0065
High even terms	23	65	±0.0066
z^9P, z^7P	6	47	±0.0060
High odd terms	8	22	±0.0063
$a^7D°$, z^7F	9	20	±0.0057
All	53	226	±0.0062

adopted. These may come from f^6sp, which gives two $^7F°$ terms, or f^6dp, which gives six. The corresponding transitions involve the jumps $f-p$, $p-s$ and $f-d$. Both are possible, but the latter is more probable.

(8) The remaining 70 even and 13 odd levels are indicated by numbers in the tables and tentative term-designations are given for some of them. The g values confirm a few of these definitely, but are indecisive for the rest, owing to "g sharing" due to perturbations.

The higher even levels must come mainly from f^6sd and f^6d^2—which would account for many more than have been observed. Some levels from f^7p with higher limits may however be included. The analysis of the spectrum is still far from complete—only 467 lines out of 2681 having been classified. Almost all the strongest lines are however included, as is shown by Table III.

Considerable progress has also been made in identifying electron-configurations. Levels arising from f^7s, f^7p, f^7d, f^6sd and f^6d^2 have been found with certainty, and f^8 and f^6dp very probably.

III. SERIES AND IONIZATION POTENTIAL

(9) A Rydberg formula, applied to $a^9S°$, $e^9S°$, $a^7S°$, $e^7S°$, gives an ionization potential of 11.4 volts.[8] A better approximation may be obtained by estimating the coefficient β in the Ritz formula

$$T=R/n^{*2}, \quad n^*=n-\alpha+\beta T,$$

where T is the term value. When accurate limits and values of n^* are available, we have from the first two terms of a series

$$\beta=\frac{n^*_1-n^*_2+1}{T_1-T_2}.$$

[8] W. Albertson, Phys. Rev. **45**, 499 (1934).

For singly-ionized atoms we have for the s electron:

ELEMENT	Be II	Mg II	Ca II	Zn II	Sr II	Cd II	Ba II	Hg II	Ra II
n_1	2	3	4	4	5	5	6	6	7
$\beta\times10^6$	−0.08	−0.39	−0.63	−0.54	−0.88	−0.88	−1.22	−1.12	−1.46
$0-C$	−0.02	−0.05	−0.01	+0.08	+0.02	+0.02	−0.04	+0.06	0.00

The empirical formula $\beta=10^{-6}\ (0.50-0.28n_1)$ represents these values surprisingly well.

For Eu II, $n_1=6$. Assuming $\beta=-1.18\times10^{-6}$ we find that both the $^9S°$ and $^7S°$ terms indicate a limit close to 90,420. The next series member $8s\ ^9S°$ should then be 24,000 below this, or at the level 66,420. A short search revealed the term $f^9S°$ at 66598.00 with three good combinations. When the limit is adjusted until the $6s-7s$, $7s-8s$ intervals give the same value of β, it is found that $\beta=-0.997\times10^{-6}$ giving a limit 90,716 ($f^7\ ^8S°$ in Eu III) and an ionization potential of *11.21 volts*.

With this limit we find the values of n^* given in Table IV. The large change in n^* for the D terms occurs in the other spectra.

Estimating n^* for the next series members, $8s\ ^7S°$ has been located—provisionally, since its strongest combination is masked by a heavy line. The $6d\ ^9D°$ term should be near 69,000, and $6d\ ^7D°$ about 70,000, but no combinations with z^9P, z^7P have been identified. The same is true for $7p\ ^9P$ (57,000), $7p\ ^7P$ (58,000), $5f\ ^9F$ and ^7F (near 60,000). There are numerous septet levels in this region, but no multiplets have been identified.

IV. ZEEMAN EFFECT. DETERMINATION OF g VALUES

(10) The number of fully resolved Zeeman patterns is large, for two reasons. The field is high; and the important terms have large multiplicities and small values of L, so that the g values are large and widely spaced. When all the components are recorded, the values of J and g for both levels involved are determined by well-known relations. The range of intensity among the σ-components when $J=\pm1$, or the π-components when $J=0$, is great, and the fainter ones are often missed; but the π-components in the first case, and the σ's in the second, are more alike, and can be counted, giving the values of J. The strongest lines are over-exposed; but, fortunately, the σ-components came through faintly

along with the π's, and vice versa—just sufficiently to be measurable when the others are burned out. For faint lines the total number of components, and the J values, may be uncertain. The values of g_1 and g_2 given below (Table VII) may in such cases require correction by an integral multiple of g_1-g_2 (which is always accurately determined if any part of the pattern is resolved).

In so rich a spectrum, the patterns of neighboring lines too often overlap. Separating these tangles into their constituents requires patience, and also skill learned by experience, and many insoluble puzzles remain.

For unresolved patterns, the automatic measuring engine is peculiarly valuable. It records the maximum of the profile of a complex blend—while ordinary measures may approximate to the center of gravity of the confused mass. If A is the position of this maximum in the usual units, then, if $J_1=J_2$, $A_\sigma=\frac{1}{2}(g_1+g_2)$, $A_\pi=J(g_1-g_2)$ so that both g values can be found when J is known. This is often contributed by the analysis of the spectrum; and sometimes, though the separate components cannot be measured, their presence and number are indicated by small waves on the recorded profile.

When $J_1=J_2+1$, $A_\sigma=J_1g_1-J_2g_2$, $A_\pi=0$ and the J's and one g must be found from the analysis. The middle of the unresolved σ-blend should correspond to g; but, as the faint edge may not be recorded, this gives only a rough estimate—which, however, is often of value in showing whether a given line may involve a level of known g.

The ground-level $a^9S^\circ_4$ is involved in 19 resolved patterns, which give g values ranging from 1.965 to 2.004 with a mean of 1.984. The probable error r of a single determination comes out ±0.0063 and of the mean ±0.0014. For $a^7S^\circ_3$ there are 23 resolved lines, giving $g=1.981\pm0.0011$, $r=\pm0.0051$.

The results for other groups of levels are summarized in Table V, where N is the number of levels included, and n the number of resolved lines. The weight of each level is $n-N$. Each resolved line gives two g values so that there are 113 of them. The independent determinations of r are in remarkably good agreement.

(11) Comparing the observed and theoretical values for the low terms, we have Table VI. The observed values are systematically too small. This may arise from an error in the calibration constant, which was determined from the observed patterns of a small number of lines of other elements which appeared on the plates. Multiplication by 1.0086 makes the observed sum equal to the theoretical, and gives the corrected values in column 4. The residuals for the corrected values afford conclusive evidence of the reality of this correction. They are but little greater than their probable errors, except for z^9P_4, z^7P_4, z^9P_3, z^7P_3, which share their g values, preserving the sums.

For the higher terms this g sharing is much greater, and term designations must be correspondingly nebulous.

(12) The observed Zeeman patterns of 459 lines are given in Table VII. Classified lines are marked by an asterisk preceding the wave-length. The third column gives the number of π-components measured on the films, counting the central line (if present) and the components on one side only, and the fourth the positions, of the

TABLE VI. *Observed and theoretical g values.*

TERM	OBS.	THEOR.	CORR.	RES.	P.E.
$a^9S^\circ_4$	1.984	2.000	2.001	+0.001	±0.0014
$a^7S^\circ_3$	1.981	2.000	1.998	− .002	.0013
$e^9S^\circ_4$	1.985	2.000	2.002	+ .002	.0027
$e^7S^\circ_3$	1.974	2.000	1.991	− .009	.0043
Sum	7.924	8.000	7.992		
$a^9D^\circ_6$	1.659	1.667	1.673	+ .006	± .0035
$a^9D^\circ_5$	1.726	1.733	1.741	+ .008	.0020
$a^9D^\circ_4$	1.842	1.850	1.858	+ .008	.0023
$a^9D^\circ_3$	2.062	2.083	2.080	− .003	.0017
$a^9D^\circ_2$	2.641	2.667	2.664	− .003	.0021
Sum	9.930	10.000	10.016		
$a^7D^\circ_5$	1.592	1.600	1.606	+ .006	± .0062
$a^7D^\circ_4$	1.628	1.650	1.642	− .008	.0044
$a^7D^\circ_3$	1.728	1.750	1.743	− .007	.0044
$a^7D^\circ_2$	1.981	2.000	1.998	− .002	.0036
$a^7D^\circ_1$	2.972	3.000	2.997	− .003	.0036
Sum	9.901	10.000	9.986		
z^9P_5	1.789	1.800	1.804	+ .004	± .0018
z^9P_4	1.877	1.950	1.893	− .057	.0016
z^9P_3	2.195	2.250	2.214	− .036	.0016
z^7P_4	1.801	1.750	1.816	+ .056	.0015
z^7P_3	1.943	1.917	1.960	+ .043	.0021
z^7P_2	2.312	2.333	2.332	− .001	.0025
Sum	11.917	12.000	12.019		

TABLE VII. *Zeeman patterns of* Eu II.

λ	Arc Int.	No. Meas.		π		No. Meas.		σ		J_1	Obs. g_1	J_2	Obs. g_2
*7426.57	1500	4	0	358	725	5	755	1113	1480	4	1836	3	2195
*7370.22	2500	6	0	153	304	8	1119	1271	1423	5	1727	4	1879
*7301.17	2500	3	124	260	390	6	2070	2180	2329	3	2070	3	2200
*7217.55	1500	3	0	452	895	4	1297	1748	2200	3	2197	2	2646
*7194.81	1500	1	136	B		1	1856	C		(4)	1873:	(4)	1839
*7077.10	3000	4	0	193	384	6	1289	1480	1683	4	1872	3	2066
*6645.11	8000	6	0	131	264	9	1003	1131	1393	6	1661	5	1794
*6437.64	4000	1	327	B		6	1732:	1797:	1863:	5	1735	5	1799
*6303.41	2000	3	0	132	241	4	1661::	1786:	1908:	5	1785	4	1846
*6173.05	2000	1	0	D		1	1406	A		(5)	(1726)	(4)	1806
*6049.51	2000	1	232	B		1	2732	C		(4)	1850	(4)	1792
*5966.07	1200	5	0	266	526	5	1014	1276	1539	4	1796	3	2054
*5872.98	500	2	...	254	375	5	1940	2067	2201:	3	2070	3	1946
*5818.74	1000	3	0	704	1407	3	535	1232	1940	3	1940	2	2644
4639.40	4	1	...	213		3	1854:	1951:	2040:	2	1950:	2	2043: ?
4637.74	2	1	0	D		1	1305	A					
4612.43	2	1	0	D		1	1406	B					
4591.06	8?	5	0	220	441	3	1087	1332	1530	5	1750:	4	1970:
*4585.68	8	4	0	298	560	2	m	1057:	1360:	(4)	(1628)	(3)	1908:
4581.62	5	4	0	222	446	6	883	1108	1350	4	1558		1782
4580.23	5	2	...	313:	404	5	1630	1763	1910	3	1767	3	{1630 or 1904
4567.68	1	1	0	D		1	1452	C					
4564.93	2	1	047	B		1	1409	C					
4555.59	6	1	0	D		1	1634	C					
4539.69	3	2	0	1052		2	?	900	1957	2	902	1	152
*4539.24	12	1	0	D		1	2080	B		(4)	1985	(3)	(1943)
*4522.59	2000	3	217	424	634	6	1990	2196	2406	3	1985	3	2197
4516.94	4	1	0	D		1	1365:	A?					
4511.53	3	1	032	B		1	1438	C					
*4508.66	10	1	0	D		1	1995:	C		(4)	(1842)	4	2148:
4505.73	2	1	0	D		1	1530	B?					
4502.10	2	4	466	680	952	1	851	C		4	968:	4	0734:
*4488.28	15	5	019:	157	328	8	1622:	1758:	1920:	(5)	(1580)	(4)	1746
*4485.15	100	4	369:	547:	735	8	1813	1997	2160	4	1987	4	1806
4471.64	4	4	0	290	528:	4	1880	2160	2380	4	1596:	3	1326:
*4464.97	200	3	0	329	654	4	1326	1656	1960	3	1984	2	2311
4463.83	3	1	0	D		1	1434	B?					
4461.546	2	5	0	157	316	4	1559:	1709:	1880:	5	1251:	4	{839: 1095:
4453.08	1	1	0	D		1	1667	C					
4451.63	2	4	0	256	515:								
4444.26	4	1	070	B		1	1463	C					
4442.42	3	1	0	D		1	1361	C					
4441.47	15	3	0	106	219	3	1538:	1603:	1722				
*4435.58	3000	3	0	120	242	too strong!				4	1860	(3)	(1981)
4429.76	15	3	0	096	179	7	1090:	1201:	1282	6	801	5	703
4426.42	5	4	0	234	473	6	850	1097	1330	4	613	3	374
4419.66	8	2	0	142	....	4	1380	1490	1651	3	1651	2	1788
4410.47	1	1	0	D		1	1394	B?					
4407.07	15	1	0	D		1	1423	B					
*4405.27	20	5	0	102	204	4	m	1208	1404:	5	1611:	4	1713:
4403.15	6	1	074	B		1	1004	C					
4397.70	8	1	0	D		1	705	C					
4391.37	10	2	154:	282		4	0	138	278:	2	139	2	−002
4389.07	4	4	287:	377:	460	8	1093:	1204	1297	5	1196	5	1105
*4383.17	200	4	0	169	353	6	1266	1434	1620	4	1789	3	1964
4382.05	4	1	0	D		1	1303	C?					
4379.81	5	1	0	D		1	1808	C					
4372.20	8	4	0	105	204	1	1794	B		4	1491:	3	1390:
4369.47	40	1	0	D		1	1460	A					
4368.42	8	2	0	612		2	1210	1828		2	1827	1	2443
4361.57	8	1	175	B		1	1142:	C					
4357.76	5	1	0	D		1	1242:	S					
*4355.09	300	5	0	198	396	6	999	1190	1379	5	1775	4	1971
4352.94	5	1	0	D		1	1474	A?					
4352.24	6	5	0:	141	283	6	1927	2033	m	4?	1818	3?	1707
4351.261	4	4	0	178	360	3	1603:	1759:	1935:	4	1422:	3	1252
4335.45	4	1	0	D		1	1610	C					
4334.75	12	1	104	B		1	1240:	A and B					
4330.61	40	1	0	D		1	1612	A?					
4317.67	8	1	0	D		1	1281:	S, B?					
4300.84	5	6	0	267	540	7	1941	2246	2499	6	1200:	5	940:
4295.44	15	1	0	D		1	1369:	C					
4288.60	2	5	0	213:	424:	5	856	1059	1259	5	1476	4	1684
4283.873	4	3	0	226	452	3	218	448	690:	3	680	2	910
4281.920	8	3	468	706	938	8	528	752	993	4	523	4	{290 or 756
4260.98	5	1	0	D		1	1341	S					
4253.805	20	2	....	311	456	5	1022	1113	1239:	5	1012	5	1114
4247.06	25	5	0	257	508	5	782	1020	1281	5	276	4	28
4238.689	20	2	0	154		2	2150:	2323:		2	2320:	1	2485:
4234.094	8	4	0	121	229	4	1089	1210	1320	4	0974	3	0858
4232.45	12	6	0	095	181	0				6?		5?	
4211.275	10	4	0	378	731	3	1107	1474	1841	4	0740	3	0373
*4205.05	6000	4	0	211	424	6	2200	2396	2577	4	1983	3	2193
4192.62	12	1	0	D		1	1299	S					
4189.751	5	0?				3	784	896	989				
4183.78	4	1	0	D		1	1951	A?					
4176.62	8	3	220:	461	693	5	1413	1643	1867	3	1640	3	1410
4172.80	30	1	420	B		1	1308	C					
4162.14	8	4	0	463	928	5	1193	1652:	2118	4	727	3	262

TABLE VII.—*Continued.*

λ	Arc Int.	No. Meas.		π		No. Meas.		σ		J_1	Obs. g_1	J_2	Obs. g_2
4160.475	12	1	**199**	*B*		1	**698**	*A*					
*4151.52	20	3	120	360	**571**	6	2288	2486	**2755**	4	(1842)	3	2062
4148.40	8	1	**0**	*D*		1	**1270**	*S*					
4147.22	12	5	570:	720:	**860**	7	**996:**	**1150:**	**1292:**	6	1154:	6	{1296 or 1012
4145.233	8	6	**0**	165	339	7	1253	1422	**1596**	6	748	5	579
4141.72	40	3	330	473	**598**	7	1418	**1573**	1723	4	1571	4	{1723 or 1419
4141.02	25	1	**221**	*B*		1	**1940**	*C*					
4136.59	20	2	466	**926**		4	**1820**	**2286**	2768	2	2292	2	1825
*4129.73	5000	1	**402**	*B*		5	1767	**1882**	2004	4	1885	4	2004
4120.77	6	1	**244**	*B*		1	**1358**	*C*					
4119.30	15	1	**0**	*D*		1	**1526**	*B*					
*4112.04	30	1	**066**	*B*		1	**2074**	*C*		3	2062	3	2084
4107.90	10	1	**0**	*D*		1	**1794**	*B*					
*4096.804	40	5	**0**	247:	482:	6	**755**	993	1243	5	1722	4	1964
4092.96	3	1	**0**	*D*		1	**1560**	*S*					
*4086.423	8	2	*m*	1519	**2300**	*m*				3	(2062)	3	1298
*4085.38	40	3	**0**	600	1200:	5	**897**	1472	2065	3	2090	2	2693
4080.77	4	1	**0**	*D*		1	**1118**	*A*					
4076.95	4	4	1044	1421	**1768**	8	**1230**	**1578**	**1935**	5	1583	5	{1938 or 1228
4071.38	10	3	**0**	025	*m*	3	1842	*m*	**2050**	5?	1617:	4?	1507:
4067.132	3	1	**0**	*D*		1	**1393**	*S*					
4066.05	4	2	168:	**280**		4	1510	**1648**	**1791**	2	1791	2	1649
4062.65	15	2	**0**	151	*m*?	3	**1157**	1328	1488	3?	1485	2?	1645
4062.15	15	4	**0**	200	380	4	1172	1362	**1557**	4	995	3	809
4061.566	10	6	**0**	130	262:	7	1420:	1531:	**1677:**	6	1031	5	902
4059.37	15	1	**0**	*D*		1	**1630**	*C*					
4037.149	5	2	*m*	913	**1376**	6	**1418**	1880:	2330	3	1876	3	1419
4031.35	4	6	**0**	328	658	7	1587:	1938	**2260**	6?	625	5?	295
4029.577	4	1	**0**	*D*		1	**1019**	*A*					
4018.39	6	2	**0**	816		3	**830**	1639	2437:	2	1640	1	2452
*4017.58	100	4	**0**	133	284	5	**m**	1045	1208	5	1717:	4	1886:
*4011.69	100	1	**295**	*B*		6	**1874**	**1986**	2095	4	1882	4	1990
3995.98	10	2	890	**1790**		4	**−232**	655	1561	2	662	2	−233
3993.931	15	1	**0**	*D*		1	**1237**	*B*					
3988.24	8	1	**0**	*D*		1	**967:**	*A*					
3975.566	5	2	**0**	307		3	1480:	1781	**2098**	2	1786	1	1476
*3971.98	4000	4	**0**	177	365	6	**1268**	1434	1608	4	1796	3	1976
3968.88	3	4	**0**	176:	340	6	**080**	236:	444	4	442	3	617
3966.59	8	4	461	685	**916**	8	**995**	**1241**	1463:	4	1234	4	1005
*3964.90	60	1	**183**	*D*		1	**1820:**	*C*		(4)	(1842)	4	1888
3960.74	3	2	140:	**301**		4	**1637:**	**1790**	1948	2	1792	2	1642
3959.22	3	3	**0**	378	734:	6	**887:**	1202	1630	3?	1636:	2?	2005:
3957.916	15	1	**157:**	*B*		1	**1579**	*B*?					
3953.43	6	2	**m**	131		1	**2033**	*B*					
3947.60	3	3	**0**	157	312								
3943.97	6	3	**0**	298	605:	4	**m**	1188	1500	3	1489:	2	1779:
*3943.08	40	4	**0**	212:	432:	4	**1370**	1580	1774	4	1987	3	2196
3939.19	8	1	**0**	*D*		1	**1152**	*A*					
3938.248	2	1	**0**	*D*		1	**1437**	*A*					
3930.50	4000	1	**105**	*B*		1	**1953**	*C*		3	1971	3	1936
*3928.87	15	3	**m**	158:	328:	0	*m*	*m*	*m*	(4)	(2062)	3	1900:
3927.95	4	3	**0**	278	559	4	**m**?	640	910	3?	910:	2?	1184:
3922.526	3	5	735	985	**1240**	6	651	**910**	1170:	4	911	4	{ 666 or 1156
*3917.29	60	4	**0**	98:	196:	3	**1228**	*m*	*m*	6	1654	5	1758
3913.72	10	3	**0**	363	725	5	**698**	1055	1430:	3	1427	2	1062
*3907.10	3000	3	**0**	329	657	5	**1324**	1658	1985	3	1985	2	2314
3903.62	3	3	485	1010:	**1448**	5	**1152**	**1638**	2101	3	1630	3	{2109 or 1151
3900.18	10	3	**0**	128	*m*	5	**1238**	1366:	1504	4	1635	3	1767
3899.49	10	1	**0**	*D*		1	**2000**	*A*					
3889.52	6	4	525	796:	**1020**	7	**1319**	**1578**	1825	4	1572	4	1315
3876.07	2	3	319:	486	**642**	6	**1008**	1178	1357	4	1017	4	{ 857 or 1178
3873.11	4	1	**115**			1	**1607**	*C*?					
3863.66	10	1	**0**	*D*		1	**1132**	*B*					
3861.18	80	1	**0**	*D*		1	**1048**	*A*					
3849.62	2	4	**m**	*m*	342	5	1972:	2120:	**2283:**	6	1481:	5	1320:
3849.38	8	3	101:	290:	**455**	1	**1368**	**m**	*m*	3	1368:	3	1524
3848.40	10	3	**0**	181	376:	4	265	459	**646**	3	267	2	077
3848.20	8	1	**080**	*B*		1	**2433:**	*A*					
3846.40	4	1	**0**	*D*		1	**1340**	*S*					
*3844.23	8?	1	**139**	*B*		1	**1737**	*C*		5	1751	5	1723
3842.354	8	1	**107**	*B*		1	**1009**	*C*					
*3838.239	30	5	**0**	377	767	9	**−413**	020:	408	{5 {4	1175 1548	4 3	1555 or 1928
3831.18	8	3	376	760	**1119**	5	**262**	**637**	996	3	634	3	259
3828.93	30	2	160:	**300**		4	**1633**	**1790**	1939	2	1788	2	1636
*3826.68	50	5	**0**	282	561	9	**382**	665:	958	5	1520	4	1800
3825.14	10	1	**0**	*D*		1	**1238**	*C*					
*3819.67	6000	5	**0**	200	401	7	**m**	1186	1390	5	1789	4	1989
3815.495	80	4	**0**	167	332	7	**883**	1044	1260	4	1388	3	1554
3813.07	1	1	**0**	*D*		1	**975**	*B*?					
3805.81	5	3	**0**	794	1580	5	**−094**	704	1470:	3?	1492	2?	2280
3804.27	15	6	**0**	172	345	10?	**471**	640	798	6?	1293	5?	1457
3801.58	8	6	**0**	89	172	7	**780:**	862:	974:	6?	1232	5?	1322
*3799.492	10	2	*m*	728:	**979**	7	1267:	**1520:**	**1796:**	(4)	(1801)	4	1559
*3799.009	100	4	**0**	324	642	6	**857**	1198	1508	4	1835	3	2160
3796.33	8	3	**0**	171	348	4	1072:	1256	**1435**	3	1078	2	901

TABLE VII.—*Continued.*

λ	Arc Int.	No. Meas.		π		No. Meas.		σ		J_1	Obs. g_1	J_2	Obs. g_2
3795.04	20	*1*	**0**	*D*		*1*	**1289**	*C*					
3794.776	5	*4*	**0**	166	368:	*3*	**406**	589	754:	5?	1080::	4?	1250::
*3793.06	25	*2*	*m*	570	**692**	*8*	**1624:**	**1780:**	1898:	(5)	(1726)	5	1588:
*3791.50	30	*1*	**0**	*D*		*1*	**1778**	*B?*		(5)	(1726)	4	1713
*3788.765	30	*2*	*m*	825	**1266**	*6*	1517:	**1935**	2360	3	1941	3	1525
3781.40	50	*3*	**0**	118	*m*	*3*	**802:**	855:	*m*	5	1017:	4	1072:
3780.54	10	*2*	**0**	1164:		*2*	**1825**	634:	*m*	2	634:	1	−542:
3777.613	15	*4*	**0**	861	1706	*6*	**−297**	560	1421	4?	2274:	3?	3131:
3771.147	25	*4*	**0**	377	756	*6*	**380**	743	1136	4	1505	3	1882
3769.33	15	*1*	**0**	*D*		*1*	**1367**	*A* or *B*					
*3765.93	150	*1*	**277**	*B*		*2*	**2076**	**2161:**	*m*	(3)	(2062)	3	2152
*3761.12	300	*5*	**0**	172	340	*9*	**1035**	1204	1378	5	1719	4	1890
3760.33	50	*4?*	597	831:	**1029:**	*8?*	**1502:**	**1706**	1910	4?	1707	4?	1505
3758.54	20	*1*	**0**	*D*		*1*	**1731**	*B*					
*3757.639	30	*3*	**0**	761	1510	*4*	**811**	**1570**	**2311**	2	2313	2	1563
3756.80	4	*1*	**0**	*D*		*1*	**1731**	*B*					
3753.77	6	*1*	**249**	*B*		*1*	**1496**	*C*					
3753.05	30	*1*	**207**	*B*		*1*	**2560**	*C*					
*3744.54	20	*2*	*m*	233:	**532:**	*0?*	*m*	*m*	*m*	(4)	(1842)	4	1709:
*3743.556	100	*3*	**0**	486	969	*5*	**1190**	1670	2153:	3	2154	2	2638
3742.34	15	*1*	**0**	*D*		*1*	**1458**	*A?*					
*3741.31	400	*1*	**0**	*D*		*1*	**1362**	*A*		(6)	(1659)	5	1719
3740.25	20	*4*	366	550:	**743:**	*6*	**1417**	**1630**	**1832**	4	1628	4	{1833: or 1423:
3733.65	25	*6*	478	572	**685**	*12*	**1472**	1600	1703	6	1595	6	1478
*3724.94	4000	*4*	384	584:	**751:**	*8*	**1800**	1988	2171	4	1989	4	1800
3720.72	10	*6?*	**0**	172	357	*2*	**1226:**	1389:	*m*	4?	1902:	3?	2072:
3717.69	80	*4*	427	660	**869**	*7*	1280	**1493**	1713	4	1496	4	{1283 or 1709
3716.937	60	*4*	**0**	234:	471:	*6*	**634**	845	1055	4	1268:	3	1480:
*3714.904	100	*1*	**208**	*B*		*1*	**1853**	*C*		(4)	(1842)	4	1894
*3713.45	125	*1*	**0**	*D*		*1*	**1911**	*A*		(3)	(2062)	2	2137
*3710.870	80	*1*	**0:**	*D?*		*1*	**2022**	*B*		6	1775	(5)	(1726)
3707.42	20	*1*	**0**	*D*		*1*	**1590**	*B*					
3697.94	12	*1*	**0**	*D*		*1*	**1572**	*B*					
3696.42	20	*3*	**0**	234	469	*2*	2249:	**2444**		3?	1996:	2?	1762:
3695.14	3	*1*	**0**	*D*		*1*	**1403**	*A*					
3693.80	20	7	**0**	180	362	*7*	1910	2080	**2273**	7	1203	6	1025
*3688.42	1500	*1*	**0**	*D*		*1*	**2059**	*A*		(4)	(1984)	3	1959
3685.675	6	*3*	**0**	470	950	*6*	1660:	2130:	**2603:**	3	1660:	2	1183:
*3683.267	40	*3*	**0**	165	323	*4*	**1369:**	1538	1716:	(5)	(1726)	4	1890
3679.500	80	*3*	**0**	180	360	*4*	1644	1798	**1992**	3	1626	2	1447
*3678.259	100	*2*	**0**	546		*3*	**1768**	2310	2850	2	2309	1	2852
*3674.634	50	*1*	**0**	*D*		*1*	**1720**	*S*		(5)	(1726)	5	1714
3668.96	5	*1*	**0**	*D*		*1*	**1280:**	*A* and *B*					
3666.77	8	*2*	**0**	376		*3*	874	1262	**1630**	2	1255	1	878
3666.27	15	*1*	**250**	B		*1*	**1193**	*C*					
3658.77	10	*3*	**0**	345	680	*0*	*m*	*m*	*m*				
3648.26	15	*1*	**145**	*B*		*1*	*m*						
*3646.75	35	*1*	458	**m**		*4*	**1729**	**2154**	**2610**	2	2169	2	2624
3645.18	30	*3*	**0**	242	488	*5*	**1840**	2118	2360:	3	2360:	2	2610:
3636.718	10	*4*	**0**	201	398	*5*	1719:	2076	**2457**	4	1345	3	977
*3632.18	80	*3*	262:	679	**1001**	*5*	**1725**	2086	2399	3	1730:	3	2066
3631.79	15	*3*	402	612	**819**	*?*	*m*	*m*	*m*	4		4	
*3629.80	40	*1*	**0**	*D*		*1*	**1798**	*C*		4	(1801)	4	1795
3627.41	25	*1*	**138**	*B*		*1*	**1076**	*C*					
*3622.54	150	*1*	**0**	*D*		*1*	**1080:**	*A*					
3621.890	50	*4*	**0**	241	494	*5*	779:	992	**1236**	4	495	3	742
*3616.152	100	*5*	**0**	294	591	*8*	**300**	595	900	5	1502	4	1804
3612.19	20	*3*	**0**	425	864	*3*	1541	1972	**2410**	3?	1544	2?	1110
*3611.357	25	*3*	**0**	940	1793	*5*	**−134**	805:	1780	3	1734	2	2644
*3606.70	80	*3*	**0**	301	606	*4*	2046	2366	**2680**	3	2054	2	1744
*3603.20	200	*4*	812	1197	**1609**	*8*	**1441**	**1835**	2230	4	1834	4	1434
3596.85	20	*1*	**0**	*m*	*m*	*6*	**462**	603	755	4?	908	3?	1058
3591.312	20	1	**0**	*S*		*1*	**1603**	*S*					
3590.146	15	*5*	**0**	155	302	*7*	1220	1371	**1527**	5	908	4	755
3587.14	4	*4*	**0**	255	521	*5?*	**0?**	234	499	4?	755	3?	1013
3573.92	10	*2*	**0**	133	*m?*	*2*	**910**	1047	*m*	3?	1181:	2?	1316:
3570.10	40	*1*	**0**	*D*		*1*	**1031**	*A*					
*3562.174	20	*4*	**0**	309	585	*3*	**1493**	1770	2068	3	2070	2	2363
*3552.516	100	*1*	**594**	*B*		*5*	**1606**	1727	1853	5	1725	5	1608
3549.71	20	*1*	**0**	*D*		*1*	**1405**	*B?*					
3549.6	8	*0*	**m**			*1*	**1390**	*C?*					
3543.85	60	*1*	**0**	*D*		*1*	**1160**	*A*					
3543.11	6	*2*	184	**353**		*5*	947:	1140:	1332:	2?	1327:	2?	1444:
*3542.152	80	*2*	284	**569**		*4*	**2380:**	**2644**	2901	2	2642	2	2364
*3538.08	40	*4*	1082:	1483	**1847**	*8*	1413	**1782**	2160	5	1783	5	1413
3537.74	15	*1*	**0**	*D*		*1*	**1092**	*B*					
3534.12	20	*1*	**189**	*B*		*1*	**1258**	*C*		4?	1282	4?	1234
3531.79	15	*1*	**123**	*B*		*1*	**1312**	*C*		4?	1328	4?	1296
*3531.151	60	*5*	875	1168	**1450**	*10*	1213	**1507**	**1787**	5	1791	5	1501
3527.87	30	*5*	**0**	235	500	*6*	**250**	497:	724	5	1202	4	1439
3526.648	8	*5*	**0**	296	617	*6*	**327**	588	879	5	1482:	4	1779:
*3521.09	100	*3*	**0**	134	260	*3*	**1001**	**1106:**	*m*	6	1655	5	1786
3520.14	8	*1*	**0**	*D*		*1*	**1390:**	*A*					
3518.482	25	*1*	**0**	*D*		*1*	**779**	*A*					
3511.163	10	*1*	**0**	*D*		*1*	**1077**	*B*					
*3511.03	60	*1*	**574**	*B*		*6*	1551:	**1653**	1762	6	1659	6	1756
*3508.852	20	*1*	**0**	*D*		*1*	**1621**	*A*		5	1726	4	1746
*3505.30	20	*3*	**0**	538	1079	*5*	**907**	1437	1979	3	1973	2	2511
3497.65	5	*4*	**0**	836	1630:	*4*	1526	2325	**3177**	3?	1518	2?	690
3495.13	15	*6*	**0**	231	442	*10*	**060**	305	534	6	1201	5	1426

TABLE VII.—*Continued.*

λ	Arc Int.	No. Meas.		π		No. Meas.		σ		J_1	Obs. g_1	J_2	Obs. g_2
3491.11	12	4?	0	322	641	5	748	1079	1390	4?	1715	3?	2037
3489.25	25	5	0	222	444	9	729	953	1182	5	1596:	4	1810:
*3488.301	30	2	0	262		3	2130	2624	3150	2	2635	1	3155
3485.16	15	3	0	212	437	6	751	965	1189	4	1393	3	1176
3481.62	30	4	0	399	799	6	424	815	1213	4	1614	3	2014
*3476.604	30	5	0	384	709	6	117	471	833	5	1532	4	1884
3474.50	15	5	0	403	806	7	−197:	197:	621	5	1422	4	1824
3469.28	30	1	0	D		1	828	B					
3466.86	20	4	0	642	1270	6	−539	105	725	4	1374	3	2010
*3461.38	80	3	0	715	1440	5	491	1200	1922	3	1920	2	2637
*3457.56	30	3?	0	432	810	?	m	m	m	?		?	
3453.474	50	4	0	210	437	5	1299	1510	1730	4	1084	3	868
3446.37	20	1	0	D		1	1458	A					
*3445.176	30	1	0	D		1	2155	B		(3)	(2062)	2	2016
*3440.999	80	4	0	312	592	7	850	1129	1450	4	1753	3	2053
*3440.820	30	2	0	652		3	1740	2375	3002	(2)	(2312)	1	2962
3435.72	30	1	0	D		1	1430	B					
3435.05	40	1	0	D		1	1165	A					
*3427.757	15	1	943	B		4	1860	2318	2762	2	2310	2	1844
*3425.022	80	1	156	B		1	1639	C		6	1652	6	1626
3423.09	60	1	0	D		1	1273	C?					
*3421.68	25	4	0	154	324	0	m	m	m	(3)	(1943)	2	2094
3421.231	12	1	0	D		1	1091?	B					
3419.845	25	5	0	208	412	5	597:	805	990	5	1427	4	1635
T3418.809	(8)	3	259	521	805	5	573	702	836:	3	1734	3	1472
3417.42	10	1	273	B		1	1374	C		4?	1340	4?	1408
3416.73	60	1	0	S		1	1413:	A					
3412.72	60	5	0	192	391	7	585?	777:	974:	5	1168:	4	1350:
3406.14	25	6	0	453	860	?	m	m	m				
3405.43	15	1	605	S		2	344	964		1	347	1	961
*3396.58	200	5	0	156	320	9	1034	1189	1349	5	1662	4	1819
*3391.989	100	4	0	368	738	4	505	980	1338	4	1704	3	2074
3390.783	80	1	0	D		1	939	A					
3373.22	25	1	150	B		1	1286:	C?					
3370.52	8	1	296	B		1	1277:	C					
*3369.055	200	5	0	124	284	4	1203	A		6	1639	(5)	(1726)
*3367.635	40	3	291	623	946	6	1717:	2041:	2343	(3)	(2062)	3	{2374 or 1750
3355.42	20	1	0	D		1	1328	A					
*3338.75	80	5	0	321:	672	6	0	375	722	5	1447	4	1805
3338.49	30	1	142	B		1	1217	C?					
3336.51	15	1	0	D		1	1368	S					
3333.66	10	1	0	D		1	967	S					
3331.21	15	3	0	459	887	5	197	644	1122	3	1088	2	1538
3328.05	15	1	418	B		5	905	1062	1206	3?	1209:	3?	1059:
3325.97	30	1	0	D		1	1327	B					
*3321.857	100	1	0	D		1	1647	C?		(6)	(1659)	5	1661:
*3313.33	400	1	182	B		1	1840	C		4	1862:	4	1818:
*3308.02	200	6	0	463	915	8	−529	−109	456	5	1414	4	1875
3304.497	50	3	373	598	735:	6	1546	1735	1924	4	1732	4	{1540 or 1924
*3301.95	150	5	0	373	730	mess				5	1517	(4)	(1877)
3298.30	25	1	0	D		1	1447	A and B					
*3277.78	600	3	0	429	875	4	1453	1815	2205	(3)	(2195)	2	2631:
3269.39	5	1	0	D		1	1282	A					
*3266.39	200	4	0	374	735	5	764:	1093:	1442	4	1815	3	2176
3265.69	10	1	0	D		1	1335	A					
3263.48	6	5	0	340	655:	8	1650	1992	2300	5	1075:	4	{ 755: or 1395:
3262.59	10	1	0	D		1	1042	A					
3259.38	3	1	199	B		1	1390:	C?		6?	1406:	6?	1374:
3258.68	20	1	640	B		1	1525	C		9?	1561	9?	1489
3251.44	20	1	0:	D		1	1094	A					
3235.81	4	1	0	D		1	1269	A					
3232.315	20	6	0	186	366	6	550	738:	940	6?	1544	5?	1743
*3221.694	30	3	0	282	567	4	1172	1452	1740	3	1738	2	1455
3207.31	20	4	0	291	604	6	326	667	1000	4	1288	3	1598
3187.03	6	4?	0	190	368	?	m	m	m	?		?	
3179.23	4	1	101	B		1	1553	C?					
*3173.607	100	1	0	D		1	1929	S		(4)	(1984)	3	2002
3172.89	4	1	0	D		1	1412	B					
*3171.942	50	4	482	614:	802:	7	1424	1590	1755	5	1588	5	{1428 or 1748
3170.964	10	1	0	D		1	1390	A?					
*3170.409	50	1	0	D		1	1784	B		(4)	(1628)	3	1576
3166.49	25	1	0	D		1	1680	B					
3149.88	60	5	0	194	397	5	1112?	1312	1523	5	1914:	4	2113:
3149.41	5	1	0	D		1	1037	S					
*3144.207	15	2	567:	1301		4	650	1327	1975?	2	1974	2	1319
3140.356	15	3	319	657	974	6	1548	1881	2200	3	1877	3	1553
3130.73	80	4	0	139	m	8	713	820	966	5	1238	4	1373
3117.99	15	1	0	D		1	1860	B					
*3113.02	30	1	0	D		1	2069	B		(3)	(1728)	2	1558
*3097.45	100	3	0	286	m	4	1978	2270	2595:	3	1979	2	1690
*3077.358	200	4	342	504	652	8	1828	1982	2140	4	1824	4	1987
3076.069	30	1	478	B		5	1447:	1580:	1691:	4	1683:	4	1564:
3070.46	6	3	0	155	300	4	1152	1328:	1472:	4	1624	3	1777
*3069.110	50	5	0	416	843	6	222	602	1048	5	1461	4	1881
*3054.94	600	1	162	B		1	2018	C		(3)	2045	3	1991
*3042.53	4	3	0	374	774	3	0?	487:	860	?		?	
3035.38	10	3	0	388	814	4	2011:	2429	2840:	3	2031	2	1627
3025.503	12	3	0	679	1354	4	261	936	1611	3	1617	2	2294

TABLE VII.—*Continued.*

λ	Arc Int.	No. Meas.		π		No. Meas.		σ		J_1	Obs. g_1	J_2	Obs. g_2
3017.974	12	3	0	188	358	3	765	943	1108:	3?	1132	2?	1317
3012.385	40	1	0	D		1	1596	B					
*3010.496	4	3	0	253	502	4	1029	1285	1537	3	1536	2	1788
3009.54	12	4	0	145	296	4	785	871	1021	4?	1317	3?	1465
*3006.26	80	3	315	635	959	6	1665	1988	2291	3	1982	3	1665
*3004.80	20	3	0	665	1322	2	647	1291:		3	1981	(2)	(2641)
2998.14	10	1	041	B		1	1260:	C					
*2995.221	50	1	0	S		1	1930	S		4	1968	(3)	(1981)
*2991.33	300	5	0	272	545	9	630	896	1162	5	1710	4	1982
2990.68	3	1	0	S		1	1948:	C					
2986.92	12	4	0	243	495	5	355	m	827	5?	1340	4?	1594
2978.950	20	1	0	D		1	1810	B					
2973.42	5	6?	0	m	572:	6	2508	2750	3026:	5?	2025:	4?	1784:
*2966.52	10	2	0	884		3	1104	1990	2848	2	1990	1	2874
2963.76	4	1	0	D		1	1297	B?					
*2960.21	300	1	0	D		1	1991	A		(3)	(1981)	3	2001
*2959.47	80	4	820	1254	1690:	7	1588	1998	2438	4	2004	4	1585
2956.15	6	3	0	181	373	4	880	m	1251	5?	1613	4?	1796
*2952.68	600	1	0	D		1	1734	C?		4	1909:	(3)	(1981)
*2949.12	25	3	510:	1110:	1658:	6?	932	1480	2008:	(3)	(1981)	3	1434
2948.68	6	3	0	207	395	4	668	867	1069	3	1069	2	1270
*2947.29	100	4	0	314	622	5	2309	2616	2933	4	1993	3	1681
*2940.82	15	4	0	399	801	7	470	847:	1271	4	1672	3	2071
2939.50	6	4	450	684	890	5	1253:	1487:	m	4	1710	4	1483
2932.53	12	1	0	D		1	1316	A or B					
*2925.04	600	1	0	D		1	2080	B		4	2006	(3)	(1981)
2922.56	4	1	0	D		1	1067	A					
*2917.439	30	4	0	398	786	5	412	812	1136	4	1591	3	1984
*2906.68	1000	1	0	D		1	1819	A		(4)	(1984)	3	2026
2904.96	3	2	624	1243		?	m	m	m	2		2	
*2893.83	300	4	0	680	1380	6	2671	3347	4030	4	1992	3	1315
*2887.85	60	4	772	1160	1539	8	1600	1989	2375	4	1990	4	1603
2878.25	4	1	117	B		1	1657:	C					
*2876.06	60	4	0	506	999	7	−024:	459	952	4	1474	3	1983
2874.86	4	3	m	182	383	7	1714:	1908:	2079:	5?	1360:	4?	1179:
*2871.57	12	5	0	236:	454	6	685	909	1132:	5	1589	4	1815
2869.05	3	3	248	465	683	0				3		3	
2867.18	2	2	m	515	734	0				3		3	
*2864.42	20	1	124	B		1	1642	C		6	1663	6	1621
*2862.57	500	4	0	321	640	7	2312	2640	2940	4	1991	3	1673
*2859.67	300	3	193:	363	518	6	1993	2160	2340	3	2166	3	1993
2852.05	15	1	288	B		1	1587	C					
2850.40	3	1	0	S		1	1334	S					
*2843.96	60	3	553	1110	1668	6	1423	1982	2537	3	1983	3	1428
2841.36	2	1	0	D		1	1641	B					
2840.14	4	1	0	D		1	1058	A					
*2833.26	125	4	0	515	1037	7	−055	430	948	4	1461	3	1975
*2829.30	125	3	0	170	365	5	1646	1810	1980	3	1985	2	2165
*2828.72	500	4	0	283	565	6	842:	1124	1408	4	1692	3	1975
2827.26	30	5	0	421	847	3	−134	271	713	5	1543	4	1963
*2820.78	800	1	0	D		1	1918	A		(4)	(1984)	3	2028
*2816.18	500	3	261	509	749	6	1738	1982	2232	3	1987	3	1733
*2813.94	1200	1	357	B		1	1900:	C		(4)	(1984)	4	1895
2813.083	40	1	0	S		1	1985	S					
*2811.75	200	1	0	D		1	1712	A		4	1904	(3)	(1981)
*2802.84	600	3	0	230	459	5	1530	1753	1978	3	1979	2	2206
*2781.93	400	3	756:	1179	1601	5	1214:	m	m	4	1986	4	1591
*2781.89		3	264	514	762	6	1733	1986	2239	3	1987	3	1734
*2752.17	150	4	0	658	1300	6	−700	−051	597	4	1322	3	1972
*2747.286	100	4	0	555	1077	6	m	355:	870	4	1437	3	1982
*2744.26	200	4	1012	1514	2039:	8	965	1463	1979	4	1979	4	1470
*2740.62	200	3	0	382	765	5	1228	1603	1990	3	1984	2	2364
2730.93	5	1	117	B		1	1572	C					
*2729.44	300	3	245:	563	844	6	1425	1705	1979	3	1703	3	1983
*2729.33	300	3	(0)	150	334		m	m	m	(4)	(1984)	3	2176:
*2727.78	800	3	0	242	m	7	m	m	1261	5	1739	4	1969
*2716.98	400	3	254	508	751	6	1244	1479	1731	3	1725	3	1975
*2705.28	150	4	1031	1560	2073	8	1468	1984	2500	4	1982	4	1465
*2701.90	400	5	0	393	790	7	067:	m	746	5	1567	4	1971
*2701.14	250	4	587	874	1147	8	1697:	1988	2273:	4	1990	4	1702
2695.60	5	1	0	S		1	1820	S					
*2692.03	250	1	147	B		1	1957	C		(3)	1972	3	1923
*2685.66	200	1	324	B		1	1929	C		(4)	(1984)	4	1904
*2678.29	200	4	0	414	824	6	319	736	1146	4	1566	3	1980
*2668.34	300	4	0	219	438	6	1059:	1290	1518	4	1739	3	1960
*2658.41	20	3	0	248	476:	0				(4)	(1984)	3	1742
2653.613	40	4	0	1038	2060	4	1130	2172	3095	4	950	3	1990
*2641.27	250	4	0	262	524	8	680	925	1189	5	1712	4	1973
*2638.77	400	4	0	279	562	7	845	1117	1400	4	1685	3	1965
*2635.50	60	5	0	528	1062	6	−650	−133	402	5	1460	4	1990
*2626.776	25	2	..	1670	2185		m	m	m	(4)	(1984)	4	1436
2604.608	40	3	0	194	338	4	1993	2266	2380	3	2008	2	1831
*2600.26	10	2	863	1787		4	237	1110	2018	2	1997	2	1115
*2592.61	10	2	915	1770		2	1083	2000	m	2	1994	2	1090
*2585.76	12	1	0	S		1	2965	S		1	2965	0	0/0
*2581.86	30	3	0	547	1043	5	413	930	1460	3	1464	2	1984
*2577.56	20	3	0	403	791	0	m			5	1586:	(4)	(1984)
*2577.14	150	1	0	D		1	1010	A		6	1485	(5)	(1580)
*2574.76	30	3	300	564	827	6	1185	1457	1737	3	1731	3	1455
*2568.53	20	1	1463			2	1497	2978		1	1502	1	2974
*2568.17	80	4	0	258	524	6	681	936	1203	4	1464	3	1724
*2564.17	125	4	0	166	340	6	807	947	1117	5	1455	4	1623

TABLE VII.—*Continued.*

λ	Arc Int.	No. Meas.		π		No. Meas.		σ		J_1	Obs. g_1	J_2	Obs. g_2
*2563.48	10	2	0	500		3	1498:	1962:	2420:	2	1966:	1	1486:
*2559.18	80	3	263:	448:	660	8	1304	1467	1631	4	1469	4	1633
*2557.54	25	3	360	721	1080	6	1025	1374	1730	3	1738	3	1381
*2554.781	50	1	571	B		1	1580	C		5	1580	5	1466
*2547.243	15	2	0	1522		3	0	1449	2980	2	1451	1	2977
*2542.262	40	2	560	1077		4	910	1448	2003	2	1993	2	1451
2538.52	4	1	0	D		1	1907	B?					
2531.79	8	4	0	425	842	3	493	940	1406	4	1774	3	2197
*2513.76	5	1	0	D		1	1884	S		4	1957	(3)	(1981)
*2499.391	50	2	m	993	1448	4	1028	1498	2005	3	1505	3	1988
*2490.46	10	3	0	264:	496:	1	1260	A		3	1736	(2)	(1981)
*2454.944	60	1	0	S		1	1990:	S		(3)	(1981)	2	1976
*2407.492	40	1	0	S		1	1984	S		(3)	(1981)	3	1987
*2398.916	10	2	473	964		4	1012	1499	1991	2	1994	2	1503
*2390.43	8	1	1479			1	1437	2962		1	1486	1	2965

three strongest of them (others being omitted for economy's sake) in units of 0.001*a*. The strongest component is in heavy type. The letters *B* and *D* denote unresolved patterns strongest at the outer edges or at the center.[9] Components too faint to be recorded are indicated by dots ···, those masked by other lines by *m*. The fifth and sixth columns give similar data for the σ-components—giving the number of components observed on one side of the center, i.e., in the σ+ or σ− group, whichever is the better observed. Unresolved patterns strongest on the inner edge, the outer edge, or at the center are denoted[9] by *A*, *B* and *C*, sharp components by *S*.

The last four columns give the values of *J* and *g* for the two terms involved in each line. For completely resolved patterns, these are derived from the data for the individual line: otherwise, the values of *J* and *g*, or both, found for one term in other ways are used to find *g* for the other. Such assumed values are given in parentheses. Doubtful values are marked by colons. In some cases where the *g* values are ambiguous by a multiple of Δ*g*, two values are given. These *g* values have not been corrected for the scale-factor discussed in Section 11. "*T*" precedes lines taken from Albertson's list.

V. TABLES

(13) *Energy levels.* The levels finally accepted as real are found in Table VIII, which gives the designation, the adopted value, and the mean value of *g*, with the number of lines on which this is based. The whole number of energy levels is 156; of *g* values, 118.

It may be noted that, though $e^9D^\circ_3$ is well defined by four good combinations, all four lines are so blended on the Zeeman plates that no *g* value could be found; and that two of the three combinations of $f^7D^\circ_3$ fall on strong lines shown by Zeeman effect and term analysis to belong elsewhere. The position of the level in the middle of a narrow multiplet is the reason for its inclusion. The level 125_7 depends on a single strong line λ3622.54. The combination $a^9D^\circ_6 - f^6d^2\ ^9F_7$ should give a strong line in this vicinity checked by no other combinations. The observed *g* value is 1.576 and the theoretical 1.571,—strongly supporting this identification.

(14) *Unclassified lines.* Table IX gives particulars regarding those lines of Eu II of intensity 50 or more which have not been classified. The Zeeman patterns and *g* values show that most of these must belong to the undecipherable part of the spectrum described in Section 5.

(15) *Lines of* Eu I. The arc in a magnetic field (as is well known) shows only the strongest lines of neutral atoms of low ionization potential. A few of the strongest lines of Eu I are measured upon the films, with the results given in Table X. The theoretical *g* values are 2.000 for ^8S and 1.778, 1.937, 2.286 for the components of ^8P. The correction found in Section 11 will produce an almost exact agreement.

(16) *Lines of* Eu III. Dr. King has kindly communicated by letter a list of the strongest lines of the high excitation spectrum, in the region covered by our Zeeman data. Patterns have been observed for seven of these. Two are completely resolved, and show that both lines

[9] W. F. Meggers and H. N. Russell, J. Research Nat. Bur. Stand. **17**, 131 (1936).

TABLE VIII. *Levels in* Eu II.

DESIGNATION		LEVEL	g	No.
	$a^9S^\circ_4$	*0.00*	1.984	19
	$a^7S^\circ_3$	*1669.21*	1.981	23
	$a^9D^\circ_2$	*9925.00*	2.641	7
	3	*10081.65*	2.062	8
	4	*10312.82*	1.842	5
	5	*10643.48*	1.726	7
	6	*11128.22*	1.659	2
	$a^7D^\circ_5$	*16860.72*	1.592	4
	4	*17004.06*	1.628	2
	3	*17140.87*	1.728	2
	2	*17247.67*	1.981	3
	1	*17324.66*	2.972	3
	$z^9P^\circ_3$	23774.28	2.195	7
	4	24207.86	1.877	10
	5	26172.83	1.789	8
	$z^7P^\circ_4$	26838.50	1.801	13
	3	27104.07	1.943	5
	2	27256.35	2.312	4
	$z^9D^\circ_2$	30189.31	2.511	1
	3	31500.82	2.002	1
	4	32486.10	1.824	1
	5	33420.20	1.710	1
	6	34764.97	1.687:	1
101_4		33779.95	1.565	1
102_3		33919.70	1.681	1
103_2		33944.49	1.690	1
	$y^9P^\circ_2$	34393.57	2.037	5
	4	35527.02	1.898	5
	5	36648.95	1.749	2
104_3	$z^9H^\circ_3$?	34546.10	1.307	2
105_4		34617.73	1.603	1
106_2	$z^9G^\circ_2$?	34923.43	1.669	2
107_4		35045.98	1.966	2
108_3	$z^9F^\circ_3$?	35440.88	2.004	2
109_2		35567.74	1.434	1
	$z^7D^\circ_2$	35846.96	1.931	1
	3	37167.90	1.733	1
	4	37010.70	1.702	4
110_4	$z^9F^\circ_4$?	35935.81	1.591	2
111_4	$z^9H^\circ_4$?	36428.89	1.472	2
	$x^9P^\circ_2$	36628.00	2.163	5
	4	37223.78	1.892	6
	5	37849.34	1.715	3
112_3		36821.20	1.428	1
113_4	$z^9G^\circ_4$?	36954.00	1.463	2
114_5	$z^9F^\circ_5$?	37000.00	1.578	2
115_2		37003.23	2.151	2
	$y^7P^\circ_2$	37336.83	2.196	2
	3	38804.98	1.916	2
	4	39134.72	1.746	4
116_4		37583.63	1.775	1
117_3		37605.51	1.735	4
$118_{3,4}$		37622.87		
119_2		37799.89	1.744	1
120_5	$z^9G^\circ_5$?	37932.19	1.460	1
121_4		37993.64	1.322	3
122_4		38058.03	1.436	3
	$x^7P^\circ_2$	38146.44	2.364	3
	3	38463.66	1.716	1
	4	39554.43	1.694	3
123_3		38295.89	1.703	1
124_1	$^9F_1$	38582.08	3.155	1
125_7	$^9F_7$	38725.32	1.576:	1
126_5		38784.47	1.601	2
127_4		38995.52	1.566	3
128_2		39099.43	2.016	1
129_6		39601.80	1.756	1
130_3		39767.55	1.750 or 2.374	2
131_6		40316.92	1.632	2
132_4		40870.72	1.892	1
133_6		41099.11		
134_5		41223.24	1.661	1
135_4		41438.13	1.694:	1
136_4		41666.81	1.505	1
137_4		41714.84		
138_2		42391.03	1.935	1
	y^9D_2	42438.56		
	3	43193.46	1.987	1
	4	44075.84	1.672	1
	5	45126.78	1.602	2
	6	46029.14	1.621	1
139_4		42710.14		
$140_{3,4}$		42939.45		
$141_{4,5}$		43461.07		
142_5		43643.12	1.645:	1
143_5		44947.15		
144_4		46032.03	1.418: :	1
145_4		46584.45		
146_2		48171.51	1.455	1
$147_{1,2}$		48180.68		
148_5		48378.03	1.748 or 1.428	1
149_2		48522.28		
150_3		48536.61	1.576	1
151_4		48872.85		
152_3		48910.95		
$153_{4,5}$		49003.10		
154_2		49043.00	1.319	2
	$e^9S^\circ_4$	*49128.03*	1.985	5
155_2		49254.68	1.558	1
156_3		49480.46		
	$e^7S^\circ_3$	*49646.62*	1.974	2
157_2		49720.89		
158_1	$^7D_1$	50947.46	2.874	1
	$e^7F^\circ_5$	*52983.40*	1.526	2
	4	*53160.34*	1.552	2
	3	*53490.44*	1.525	1
	2	*53861.26*	1.563	1
1^0_4		*53783.01*	1.875:	1
	$e^9D^\circ_2$	*54273.98*	2.620:	1
	3	*54320.69*	1.912	1
	4	*54380.30*	1.807	4
	5	*54484.27*	1.507	3
	6	*54565.04*	1.655	1
	$e^7D^\circ_5$	*54428.76*	1.414	1
	4	*54295.03*		
	3	*54589.10*		
	2	*54490.63*		1
	1	*54435.41*	2.852	1
$2^0_{3,4}$		*54600.07*		
3^0_3		*55156.18*		
4^0_2		*55193.08*		
5^0_2		*55559.02*		
	$x^7F^\circ_6$	55651.82	1.490	1
	5	55991.33	1.460	2
	4	56067.39	1.466	2
	3	55967.88	1.460	2
	2	56571.04	1.451	2
	1	56245.61	1.494	2
	0	55986.45	e/0	1
159_2		55693.94	1.115	1
160_2		55807.25	1.090	1
$6^0_{3,4}$		*56158.66*		
161_3		56229.17	1.381	1
	$f^7D^\circ_5$	*56271.40*	1.662	1
	4	*56293.33*	1.649:	1
	3	*56309.21*		
	2	*56321.27*	1.792:	1
	1	*56310.89*	2.962	1
$7^0_{2,3}$		*56421.62*	1.844	1
8^0_2	$^7D^\circ_2$?	*56781.20*	1.454	2
$9^0_{3,4}$		*57127.29*		
10^0_4		*57270.14*		
$11^0_{3,4}$		*57360.07*		
$162_{1,2}$		57363.68		
163_3		57388.87	1.736:	2
$164_{2,3}$		57415.06		
$165_{3,4}$		57634.02		
166_2		58920.64	1.502	1
12^0_3		*59045.49*	2.061	2
167_1		59145.26	1.486	1
168_2		59334.70		
$169_{4,5}$		59343.45		
13^0_3		*59765.77*		
$170_{3,4}$		59995.34		
	$f^9S^\circ_4$	*66598.00*		
	$f^7S^\circ_3$	*66836.16*		

TABLE IX. *Strongest unclassified lines of* Eu II.

λ	Arc Int.	Temp. Class	Wave No. cm^{-1}	J_1	g_1	J_2	g_2
4644.23	50	V	21526.09	–	—	–	—
3861.18	80	V E	25891.50	–	—	–	—
3843.15	50	V E	26012.97	7?	1.439:	7?	1.367:
3815.495	80	V E	26201.51	4	1.388	3	1.554
3781.40	50	V E	26437.75	5	1.229:	4	1.343:
3760.33	50	V E	26585.88	5?	1.707	5?	1.505
3738.08	80	V E	26744.12	–	—	–	—
3717.69	80	V E	26890.80	4	1.496	4	1.709 or 1.283
3716.937	60	V E	26896.25	4	1.268:	3	1.480:
3687.78	80	V E	27108.90	–	—	–	—
3679.500	80	V E	27169.90	3	1.626	2	1.447
3621.890	50	V E	27602.05	4	.495	3	.742
3543.85	60	V E	28209.87	–	—	–	—
3453.474	50	V E	28948.09	4	1.084	3	.868
3423.09	60	V E	29205.03	–	—	–	—
3416.73	60	V E	29259.39	–	—	–	—
3412.72	60	V E	29293.77	5?	1.100::	4?	1.290::
3390.783	80	V E	29483.28	–	—	–	—
3149.88	60	V E	31738.08	5	1.914?	4	2.113?
3130.73	80	V E	31932.21	5	1.238	4	1.373
3022.148	60	V	33079.44	not on films			
2673.424	60	V E	37394.12	" " "			
2347.05	50	V	42593.61	" " "			

involve a term with $J=3\frac{1}{2}$ and $g=1.985$, which is evidently the ground term $f^7\,a^8S°_{3\frac{1}{2}}$ of Eu III. The other four patterns are consistent with origin from the same level, as shown in Table XI.

The wave-lengths are taken from the M.I.T. list,[10] the intensities estimated by King on his spark spectra. The wave number of each line evidently determines an even level of Eu III. These must arise from the configuration f^6d. Further analysis of the spectrum must await measures, which have been made only on the few lines which occur on the M.I.T. spectra, taken with lower excitation.

(17) *Classified lines of* Eu II. The final results of this investigation are found in Table XII, which lists 467 classified lines. Though only 25 percent of the known spark lines are included, they comprise much the greater part of the total intensity of emission.

A very great many additional terms and lines are to be anticipated theoretically, and might be observed, if europium were not one of the rarest of the elements. Thanks to the generosity of Dr. McCoy, Dr. King had an unusually large amount of material available. It is probable,

[10] G. R. Harrison, Massachusetts Institute of Technology *Wavelength Tables* (J. Wiley and Son, New York, 1939).

TABLE XI. *Lines of* Eu III.

λ	Int.	Patterns	J_1	g_1	J_2	g_2
2522.17	20	(**199**, 589, 990) ··· 1790, 2180, 2580, **2962**	$3\frac{1}{2}$	1.980	$2\frac{1}{2}$	1.592
2513.79	400	(**0**) **1.884**	$(3\frac{1}{2})$	(1.985)	$4\frac{1}{2}$ $2\frac{1}{2}$	1.963 2.025
2446.04	500	(**367**) **1938**	$(3\frac{1}{2})$	1.990	$3\frac{1}{2}$	1.895
2444.39	200	(**0**) **1.880**	$(3\frac{1}{2})$	(1.985)	$4\frac{1}{2}$ $2\frac{1}{2}$	1.961 2.027
2435.19	15	(**160**, 418, 732) too faint	$(3\frac{1}{2})$	(1.985)	$2\frac{1}{2}$ $2\frac{1}{2}$	1.965 2.275
2375.46	500	(**108**, 337, 561, 785) **974**, 1187, 1410, ···	$(3\frac{1}{2})$	(1.986)	$4\frac{1}{2}$	1.762
2350.53	20	(···, 625, **866**) too faint	$(3\frac{1}{2})$	(1.985)	$3\frac{1}{2}$ $3\frac{1}{2}$	1.860 2.110

TABLE X. *Lines of* Eu I.

λ	Int.	Pattern	J_1	g_1	J_2	g_2	Designation
6018.15	2500	(**98**, 297, 480) **1105**: 1390: ···	$4\frac{1}{2}$	1.783:	$3\frac{1}{2}$	1.977:	$a^8S°_{3\frac{1}{2}}-z^8P_{4\frac{1}{2}}$
4661.88	7000	(**139**, 417, 700) **1154**, 1404, 1650, 1898+···	$3\frac{1}{2}$	1.988	$2\frac{1}{2}$	2.266	$a^8S°_{3\frac{1}{2}}-y^8P_{2\frac{1}{2}}$
4627.22	8000	(···, **218**) **1.934**:	$(3\frac{1}{2})$	(1.985)	$3\frac{1}{2}$	1.924	$a^8S°_{3\frac{1}{2}}-y^8P_{3\frac{1}{2}}$
4594.03	10000	(**106**, 332, 554, 767) **999**, 1217, 1437, 1656+	$4\frac{1}{2}$	1.760	$3\frac{1}{2}$	1.982	$a^8S°_{3\frac{1}{2}}-y^8P_{4\frac{1}{2}}$
3334.33	600	(**0**) **1.837**	$4\frac{1}{2}$	1.952	$(3\frac{1}{2})$	(1.985)	$a^8S°_{3\frac{1}{2}}-106_{4\frac{1}{2}}$
3213.75	200	(**0**) **1.443**	$(3\frac{1}{2})$	(1.985)	$2\frac{1}{2}$	2.202	$a^8S°_{3\frac{1}{2}}-112_{2\frac{1}{2}}$
3111.43	500	(**124**, 365, 624) **886**, 1130, 1367, 1629+	$4\frac{1}{2}$	1.750	$3\frac{1}{2}$	1.997	$a^8S°_{3\frac{1}{2}}-115_{4\frac{1}{2}}$

TABLE XII. *Classified lines of* Eu II.

λ	Arc Int.	Temp. Class	Wave No. Vac.	Multiplet Designation
10165.61	5	V E	9834.40	$a^7D^o_4 - z^7P_4$
10142.99	2	V E	9856.33	$a^7D^o_2 - z^7P_3$
10066.03	8	V E	9931.68	$a^7D^o_1 - z^7P_2$
10034.22	12	V E	9963.17	$a^7D^o_3 - z^7P_3$
10019.58	30	V E	9977.72	$a^7D^o_3 - z^7P_4$
9988.65	15	V E	10008.62	$a^7D^o_2 - z^7P_2$
9898.30	40	V E	10099.98	$a^7D^o_4 - z^7P_5$
9883.16	10	V E	10115.45	$a^7D^o_3 - z^7P_2$
7455.52	2	V E	13409.19	$x^7P_4 - e^7F^o_5$
7426.57	1500	IV E	13461.45	$a^9D^o_4 - z^9P_3$
7370.22	2500	IV E	13564.38	$a^9D^o_5 - z^9P_4$
7301.17	2500	IV E	13692.67	$a^9D^o_3 - z^9P_3$
7217.55	1500	IV E	13851.30	$a^9D^o_2 - z^9P_2$
7194.81	1500	IV E	13895.08	$a^9D^o_4 - z^9P_4$
7077.10	3000	IV E	14126.19	$a^9D^o_3 - z^9P_4$
6645.11	8000	III E	15044.51	$a^9D^o_5 - z^9P_5$
6437.64	4000	III E	15529.36	$a^9D^o_5 - z^9P_5$
6303.41	2000	IV E	15860.05	$a^9D^o_4 - z^9P_5$
6173.05	2000	IV E	16194.98	$a^9D^o_3 - z^7P_4$
6049.51	2000	IV E	16525.70	$a^9D^o_4 - z^7P_4$
5987.5	1 —	V	16696.8	$a^7D^o_2 - 103_2$
5966.07	1200	IV E	16756.82	$a^9D^o_3 - z^7P_4$
5953.84	80*	V E	16791.24	$a^9D^o_4 - z^7P_3$
5872.98	500	IV E	17022.42	$a^9D^o_3 - z^7P_3$
5820.91	25*	V E	17174.69	$a^9D^o_2 - z^7P_2$
5818.74	1000	IV E	17181.10	$a^9D^o_2 - z^7P_3$
5794.61	6	V E	17252.64	$a^7D^o_3 - y^9P_3$
5767.61	10	V E	17333.41	$a^9D^o_2 - z^7P_2$
5749.02	3	V E	17389.46	$a^7D^o_4 - y^9P_3$
5675.9	1 —	V	17613.5	$a^7D^o_4 - 105_4$
5437.36	1	V E	18386.18	$a^7D^o_4 - y^9P_4$
5397.35	3	V E	18522.48	$a^7D^o_1 - z^7D_2$
5375.04	8	V E	18599.35	$a^7D^o_2 - z^7D_2$
5355.73	10	V E	18666.41	$a^7D^o_3 - y^9P_4$
5344.39	1	V E	18706.02	$a^7D^o_3 - z^7D_2$
5183.2	1	V E	19287.7	$a^7D^o_4 - 111_4$
5158.48	1	V E	19380.17	$a^7D^o_2 - x^9P_3$
5094.44	3	V	19623.79	$a^7D^o_4 - x^9P_3$
5060.45	1	V	19755.60	$a^7D^o_2 - 115_2$
5052.11	1	V E	19788.21	$a^7D^o_5 - y^9P_5$
5018.59	2	V	19920.38	$a^7D^o_2 - z^7D_2$
4996.91	1	V E	20006.80	$a^7D^o_4 - z^7D_4$
4995.61	6	V E	20012.01	$a^7D^o_1 - y^7P_2$
4991.89	5	V E	20026.92	$a^7D^o_3 - z^7D_3$
4976.44	6	V E	20089.10	$a^7D^o_2 - y^7P_2$
4964.06	1 —	V E	20139.20	$a^7D^o_5 - 114_5$
4961.40	3	V E	20149.99	$a^7D^o_5 - z^7D_4$
4958.00	2	V E	20163.81	$a^7D^o_4 - z^7D_5$
4950.12	3	V E	20195.91	$a^7D^o_3 - y^7P_2$
4909.49	3	V E	20363.04	$a^7D^o_3 - x^9P_4$
4885.10	3	V E	20464.71	$a^7D^o_3 - 117_3$
4852.65	1	V E	20601.56	$a^7D^o_4 - 117_3$
4824.26	4	V E	20722.80	$a^7D^o_5 - 116_6$
4783.64	1	V E	20898.76	$a^7D^o_2 - x^7P_2$
4749.64	4	V	21048.36	$a^7D^o_2 - 123_3$
4725.69	6	V E	21155.03	$a^7D^o_3 - 123_3$
4716.29	2	V E	21197.20	$a^7D^o_5 - 122_4$
4712.12	3	V E	21215.95	$a^7D^o_2 - x^7P_3$
4695.35	4	V E	21291.73	$a^7D^o_4 - 123_3$
4688.51	3	V E	21322.79	$a^7D^o_3 - x^7P_3$
4667.41	3	V E?	21419.18	$a^9D^o_3 - z^9D_3$
4658.63	15	V E	21459.55	$a^7D^o_4 - x^7P_5$
4633.07	8	V	21577.94	$a^9D^o_2 - z^9D_3$
4614.63	6	V E	21664.16	$a^7D^o_3 - y^7P_3$
4585.68	8	V E	21800.93	$a^7D^o_4 - y^7P_3$
4576.93	10	V	21842.60	$a^9D^o_5 - z^9D_4$
4575.0	2	V E	21851.8	$a^7D^o_2 - 128_2$
4545.45	3	V	21993.88	$a^7D^o_3 - y^7P_4$
4539.24	12	V E	22023.97	$z^7P_3 - e^9S^o_4$
4522.59	2000	II E	22105.05	$a^7S^o_3 - z^9P_3$
4517.36	6	V E	22130.64	$a^7D^o_4 - y^7P_4$
4508.66	10	V	22173.34	$a^9D^o_4 - z^9D_4$
4488.28	15	V E	22274.02	$a^7D^o_5 - y^7P_4$
4485.15	100	V E	22289.57	$z^7P_4 - e^9S^o_4$
4484.67	8	V	22291.95	$a^9D^o_4 - z^9D_5$
4464.97	200	V E	22390.30	$z^7P_2 - e^7S^o_3$
4462.14	5	V E	22404.50	$a^9D^o_3 - z^9D_4$
4435.58	3000	II E	22538.66	$a^7S^o_3 - z^9P_4$
4434.81	20	V E	22542.57	$z^7P_3 - e^7S^o_3$
4433.28	8	V	22550.35	$a^7D^o_4 - x^7P_4$
4405.27	20	V E	22693.73	$a^7D^o_5 - x^7P_4$
4389.2	2	V	22776.8	$a^9D^o_5 - z^9D_5$
4383.17	200	IV? E	22808.15	$z^7P_4 - e^7S^o_3$
4355.09	300	V E	22955.21	$z^9P_3 - e^9S^o_4$
4320.98	2	V E	23136.42	$a^9D^o_4 - 101_4$
4229.520	5	V E	23636.71	$a^9D^o_5 - z^9D_6$
4205.05	6000	II E	23774.26	$a^9S^o_4 - z^9P_3$
4170.0	2	V E	23974.1	$a^9D^o_5 - 105_4$
4166.05	2	V	23996.81	$a^9D^o_3 - 102_2$
4151.52	20	V E	24080.80	$a^9D^o_4 - y^9P_3$
4144.51	8	V E	24121.53	$a^9D^o_5 - z^9D_6$
4129.73	5000	II E	24207.85	$a^9S^o_4 - z^9P_4$
4124.54	10	V E	24238.31	$a^7D^o_5 - 133_6$
4112.04	30	V E	24311.99	$a^9D^o_5 - y^9P_5$
4096.804	40	V E	24402.41	$a^9D^o_5 - 107_4$
4086.423	8	V E?	24464.40	$a^9D^o_3 - 104_2$
4085.38	40	V E	24470.64	$a^9D^o_2 - y^9P_3$
4074.48	3	V	24536.10	$a^9D^o_3 - 105_4$
4042.018	15	V E	24733.15	$a^9D^o_4 - 107_4$
4024.24	4	V E	24841.80	$a^9D^o_3 - 106_3$
4017.58	100	IV E	24883.60	$a^9D^o_5 - y^9P_5$
4011.69	100	V E	24920.13	$z^9P_4 - e^9S^o_4$
4004.59	6	V E	24964.31	$a^9D^o_3 - 107_4$
3998.81	4	V E	25000.40	$a^9D^o_2 - 106_3$
3971.98	4000	II E	25169.27	$a^7S^o_3 - z^7P_4$
3964.90	60*	V E	25214.21	$a^9D^o_4 - y^9P_4$
3943.08	40	V E	25353.74	$z^9P_3 - e^9S^o_4$
3942.21	30	V E, IV?	25359.33	$a^9D^o_3 - 108_3$
3930.50	4000	II E	25434.88	$a^7S^o_3 - z^7P_3$
3929.91	6	V E	25438.70	$z^9P_4 - e^7S^o_3$
3928.87	15	V E	25445.43	$a^9D^o_3 - y^9P_4$
3917.70	10	V E	25517.98	$a^9D^o_2 - 108_3$
3917.29	60	II, V E	25520.65	$a^9D^o_5 - y^9D_5$
3907.10	3000	II E	25587.21	$a^7S^o_3 - z^7P_2$
3901.63	3	V	25623.08	$a^9D^o_4 - 110_4$
3875.10	8	V?	25798.50	$a^7D^o_3 - 140_{3,4}$
T3864.04	2		25872.34	$z^9P_3 - e^7S^o_3$
3854.64	20	V E	25935.43	$a^7D^o_4 - 140_{3,4}$
3844.23	8?	V E	26005.66	$a^9D^o_5 - y^9P_5$
3838.239	30	V E	26046.25	$z^7P_3 - e^7F^o_4$
3826.68	50	V E	26124.93	$z^7P_4 - e^7F^o_5$
3819.67	6000	II E	26172.87	$a^9S^o_4 - z^9P_5$
3810.76	3?	V E	26234.07	$z^7P_2 - e^7F^o_3$
3799.66	3	V E	26310.70	$a^9D^o_5 - 113_4$
3799.492	10	V E	26311.87	$z^7P_4 - e^7F^o_4$
3799.009	100	V E	26315.21	$a^9D^o_4 - x^9P_3$
3796.01	8	V E	26336.00	$a^9D^o_4 - y^9P_5$
3794.39	4	V E	26347.24	$a^9D^o_3 - 111_4$
3793.06	25	V E	26356.48	$a^9D^o_5 - 114_5$
3791.50	30	V E	26367.32	$a^9D^o_5 - z^7D_4$
3788.765	30	V E	26386.36	$z^7P_3 - e^7F^o_3$
3778.87	6	V E	26455.45	$a^9D^o_5 - 116_6$
3778.65	4	V?	26456.99	$a^7D^o_4 - 141_{4,5}$
3765.93	150	V E	26546.35	$a^9D^o_3 - x^9P_3$
3761.12	300	V E	26580.30	$a^9D^o_5 - x^9P_4$
3758.29	30	V	26600.31	$a^7D^o_4 - 141_{4,5}$
3757.639	30	V E	26604.92	$z^7P_2 - e^7F^o_2$
3752.83	15	V E	26639.01	$a^7D^o_4 - 142_5$
3752.51	5	V E	26641.29	$a^9D^o_4 - 113_4$
3747.21	3	V E	26678.97	$z^7P_3 - 1^o_4$
3744.54	20	V E	26697.99	$a^9D^o_4 - z^7D_4$
3743.556	100	IV E	26705.00	$a^9D^o_2 - x^9P_3$
3741.31	400	IV E	26721.04	$a^9D^o_5 - x^9P_5$
3736.26	2	V E	26757.15	$z^7P_2 - e^7F^o_2$
3732.73	8	V E	26782.45	$a^9D^o_5 - 142_5$
3729.740	20	V E	26803.92	$a^9D^o_5 - 120_5$
3724.94	4000	II E	26838.67	$a^9S^o_4 - z^7P_4$
3714.904	100	V E	26910.97	$a^9D^o_4 - x^9P_4$
3713.45	125	V E	26921.51	$a^9D^o_3 - 115_2$
3712.40	8	V E	26929.12	$a^9D^o_3 - z^7D_4$
3710.870	80	V E	26940.22	$a^9D^o_5 - 116_6$
3710.282	10	V E	26944.49	$z^7P_4 - 1^o_4$
3688.42	1500	II E	27104.19	$a^9S^o_4 - z^7P_3$
3683.267	40	V E	27142.12	$a^9D^o_3 - x^9P_4$
3678.259	100	V E	27179.06	$z^7P_3 - e^7D^o_1$
3676.64	20	V E	27191.03	$z^7P_3 - e^7D^o_4$
3674.634	50	V E	27205.88	$a^9D^o_5 - x^9P_5$
3673.19	80	V E	27216.57	$z^7P_3 - e^9D^o_3$
3670.81	12	V E	27234.22	$z^7P_2 - e^7D^o_2$
3664.29	3	V E	27282.67	$z^7P_3 - e^7D^o_3$
3663.47	12	V?	27288.78	$a^9D^o_5 - 120_5$
3662.94	30	V E	27292.73	$a^9D^o_4 - 117_3$
3660.629	12	V	27309.96	$a^9D^o_4 - 118_{3,4}$
3655.25	8	V	27350.14	$a^9D^o_5 - 121_4$
3650.38	3	V E	27386.63	$z^7P_3 - e^7D^o_2$
3646.75	35	V	27413.89	$a^9D^o_2 - y^7P_2$
3646.65	30	V E	27414.64	$a^9D^o_5 - 122_4$
3641.19	20	V E	27456.51	$z^7P_4 - e^7D^o_4$
3637.68	50	V E	27482.24	$z^7P_4 - e^9D^o_3$
3635.85	20	V E	27496.07	$z^7P_3 - 2^o_{3,4}$
3632.18	80	V E	27523.86	$a^9D^o_5 - 117_3$
3630.50	12	V E	27536.59	$a^9D^o_4 - x^9P_5$
3629.80	40	V E	27541.90	$z^7P_4 - e^9D^o_4$
3623.430	12	V E	27590.32	$z^7P_4 - e^7D^o_5$
3622.54	150	V E	27597.10	$a^9D^o_6 - 125_7$
3616.152	100	V E	27645.85	$z^7P_4 - e^9D^o_5$
3614.80	8	V E	27656.19	$a^9D^o_6 - 126_5$
3611.57	100	V E	27680.92	$a^9D^o_4 - 121_4$
3611.357	25	V E	27682.56	$a^9D^o_5 - 117_3$
3606.70	80	V E	27718.30	$a^9D^o_3 - 119_2$
3603.20	200	V E	27745.22	$a^9D^o_4 - 122_4$
3602.49	12	V E	27750.69	$z^7P_4 - e^7D^o_3$

TABLE XII.—*Continued.*

λ	Arc Int.	Temp. Class	Wave No. Vac.	Multiplet Designation
3601.08	8	V E	27761.56	$z^7P_4 - 2^6{}_{3,4}$
3583.22	3	V E	27899.92	$z^7P_2 - 3^6{}_3$
3578.49	8	V E	27936.80	$z^7P_3 - 4^6{}_4$
3572.58	20	V E	27983.02	$a^9D^6{}_4 - 123_3$
3563.79	3	V	28052.03	$z^7P_4 - 3^6{}_5$
3562.174	20	V E	28064.76	$a^9D^6{}_3 - x^7P_2$
3559.42	3	V E	28086.47	$a^7D^6{}_5 - 143_3$
3559.09	6	V?	28089.08	$z^7P_3 - 4^6{}_3$
3552.516	100	V E	28141.05	$a^9D^6{}_5 - 126_5$
3551.27	8	V E	28150.93	$a^9D^6{}_4 - x^7P_3$
3544.17	20	V E	28207.32	$z^9P_4 - e^9D^6{}_4$
3542.152	80	V E	28223.39	$a^9D^6{}_2 - x^7P_2$
3538.08	40	V E	28255.87	$z^9P_5 - e^7D^6{}_5$
3532.23	25	V E	28302.67	$z^7P_2 - 5^6{}_3$
3531.151	60	V E	28311.31	$z^9P_5 - e^9D^6{}_5$
3530.36	8	V E	28317.66	$z^7P_4 - 3^6{}_3$
3526.06	8	V	28352.19	$a^9D^6{}_5 - 127_4$
3525.78	6	V E	28354.44	$z^7P_4 - 4^6{}_3$
3523.49	30	V E	28372.87	$a^9D^6{}_2 - 123_3$
3522.37	15	V E	28381.89	$a^9D^6{}_3 - x^7P_2$
3521.09	100	V E	28392.21	$z^9P_5 - e^9D^6{}_5$
3513.326	10	V E	28454.95	$z^7P_3 - 5^6{}_3$
3511.03	60	V E	28473.56	$a^9D^6{}_5 - 129_6$
3508.852	20	V E	28491.23	$a^9D^6{}_3 - y^7P_4$
3508.731	10	V E?	28492.21	$a^9D^6{}_4 - y^7P_3$
3505.30	20	V E	28520.10	$a^7S^6{}_3 - z^9D_2$
3502.79	20	V E	28540.53	$a^9D^6{}_2 - x^7P_2$
3488.301	30	V E	28659.08	$a^9D^6{}_2 - 124_1$
3485.43	25	V E	28682.69	$a^9D^6{}_4 - 127_4$
3480.837	6	V E	28720.53	$z^7P_4 - 5^6{}_3$
3476.604	30	V E	28755.50	$z^9P_4 - e^7F^6{}_5$
3461.38	80	V E	28881.97	$a^9D^6{}_2 - y^7P_3$
3460.281	15	V E	28891.14	$a^7D^6{}_3 - 144_4$
3457.56	30	V E	28913.88	$a^9D^6{}_3 - 127_4$
3454.146	15	V E	28942.45	$z^9P_4 - e^7F^6{}_4$
3452.25	15	V E?	28958.35	$a^9D^6{}_3 - 129_6$
3445.176	30	V E	29017.81	$a^9D^6{}_3 - 128_5$
3443.97	4	V	29027.97	$a^7D^6{}_4 - 144_4$
3440.999	80	V E	29053.03	$a^9D^6{}_4 - y^7P_4$
3440.820	30	V E	29054.54	$z^7P_2 - f^7D^6{}_1$ $z^7P_3 - 6^6{}_{3,4}$
3439.59	10	V E?	29064.93	$z^7P_2 - f^7D^6{}_2$
3427.757	15	V E	29165.26	$z^7P_2 - f^7D^6{}_2$
3427.045	6	V E	29171.32	$a^7D^6{}_5 - 144_4$
3426.442	20	V E	29176.46	$a^9D^6{}_5 - 128_5$
3425.022	80	V E	29188.72	$a^9D^6{}_4 - 131_6$
3421.68	25	V E	29217.06	$z^7P_3 - f^7D^6{}_3$
3414.02	5	V E	29282.61	$z^9P_4 - e^7F^6{}_3$
3409.95	5	V E	29317.56	$z^7P_3 - f^7D^6{}_2$
3409.645	15	V E	29320.18	$z^7P_4 - 6^6{}_{3,4}$
3403.16	12	V E	29376.05	$z^7P_4 - e^7F^6{}_4$
3396.58	200	V E	29432.96	$z^7P_4 - f^7D^6{}_5$
3394.064	20	V E	29454.78	$z^7P_4 - f^7D^6{}_4$
3391.989	100	V E	29472.80	$a^9D^6{}_3 - x^7P_4$
3380.25	100	V E	29575.15	$z^9P_4 - 1^6{}_4$
3379.65	6	V E	29580.40	$a^7D^6{}_4 - 145_4$
3369.055	200	V E	29673.42	$a^9D^6{}_5 - 131_6$
3367.635	40	V E	29685.93	$a^9D^6{}_3 - 130_3$
3364.21	15	V E	29716.15	$z^9P_5 - e^7F^6{}_5$
3363.35	8	V E	29723.75	$a^7D^6{}_5 - 145_4$
3351.20	20	V	29831.51	$a^7S^6{}_3 - z^9D_3$
3349.7	3	V	29844.9	$a^9D^6{}_2 - 130_3$
3338.75	80	V E	29942.75	$z^7P_4 - 8^6{}_5$
3335.62	12	V E	29970.85	$a^9D^6{}_4 - 133_6$
3329.805	12	V E	30023.18	$z^7P_3 - 9^6{}_{3,4}$
3322.74	8	V E	30087.02	$z^9P_4 - e^7D^6{}_4$
3321.857	100	V E	30095.02	$a^9D^6{}_4 - 134_5$
3321.47	8	V E	30098.52	$z^9P_5 - f^7D^6{}_5$
3319.89	80	V E	30112.85	$z^9P_4 - e^9D^6{}_5$
3314.03	2	V E	30166.09	$z^7P_4 - 10^6{}_4$
3313.33	400	V E	30172.46	$z^9P_4 - e^9D^6{}_4$
3308.02	200	V E	30220.89	$z^9P_4 - e^7D^6{}_5$
3307.34	6	V E	30227.11	$a^9D^6{}_5 - 132_4$
3304.19	40	V E	30255.92	$z^7P_3 - 11^6{}_{3,4}$
3301.95	150	V E	30276.45	$z^9P_4 - e^9D^6{}_4$
3300.61	4	V E	30288.74	$z^7P_4 - 9^6{}_{3,4}$
T3289.38	(5)	—	30392.14	$z^9P_4 - 2^6{}_{3,4}$
3285.11	5	V E	30431.64	$z^7P_4 - 10^6{}_4$
3282.51	20	V E	30455.75	$a^9D^6{}_5 - 133_6$
3277.78	600	V E	30499.70	$z^9P_3 - e^9D^6{}_2$
3275.51	4	V E	30520.83	$z^9P_3 - e^7D^6{}_4$
3275.43	5	V E	30521.58	$z^7P_4 - 11^6{}_{3,4}$
3272.77	400	V E	30546.38	$z^9P_3 - e^9D^6{}_3$
3266.39	200	V E	30606.04	$z^9P_3 - e^9D^6{}_4$
3246.393	20	V E	30794.56	$a^9D^6{}_3 - 135_4$
3240.89	4	V E	30846.85	$a^7D^6{}_1 - 146_2$
3239.92	6	V E	30856.09	$a^7D^6{}_1 - 147_{1,2}$
3232.82	5	V E	30923.85	$a^7D^6{}_2 - 146_2$
3231.87	10	V E	30932.94	$a^7D^6{}_2 - 147_{1,2}$
3221.694	30	V E	31030.64	$a^7D^6{}_3 - 146_2$
3217.467	6	V E	31071.41	$a^9D^6{}_4 - 137_4$
3214.79	2	V E	31097.28	$z^9P_5 - 10^6{}_4$
3211.90	4	V E	31125.26	$a^9D^6{}_4 - 135_4$
3204.45	5	V E	31197.62	$a^7D^6{}_3 - 149_2$
3196.560	10	V E	31274.62	$a^7D^6{}_2 - 149_2$
3195.100	10	V E	31288.91	$a^9D^6{}_2 - 150_3$
3186.44	4	V E	31373.94	$a^7D^6{}_4 - 148_3$
3184.229	8	V E	31395.73	$a^7D^6{}_5 - 150_3$
3173.607	100	V E	31500.80	$a^9S^6{}_4 - z^9D_4$
3171.942	50	V E	31517.34	$a^7D^6{}_5 - 148_3$
3170.409	50	V E	31532.58	$a^7D^6{}_4 - 150_3$
3165.14	3	V	31585.07	$a^9D^6{}_3 - 136_4$
3160.33	10	V E	31633.14	$a^9D^6{}_5 - 137_4$
3157.313	15	V E	31663.36	$a^7D^6{}_2 - 152_3$
3151.84	6	V E	31718.34	$a^7D^6{}_1 - 154_2$
3150.484	15	V E	31732.00	$a^9D^6{}_3 - 151_4$
3146.699	6	V E	31770.16	$a^7D^6{}_2 - 152_3$
3144.82	6	V E	31789.14	$z^7P_3 - 12^6{}_3$
3144.207	15	V E	31795.34	$a^7D^6{}_3 - 154_2$
3136.964	15	V E	31868.75	$a^7D^6{}_5 - 151_4$
3133.23	8	V E	31906.73	$a^7D^6{}_4 - 152_3$
3129.83	3	V E?	31941.39	$z^7P_3 - 12^6{}_3$
3128.90	8	V E?	31950.88	$z^9P_4 - 6^6{}_{3,4}$
3124.19	12	V E	31999.05	$a^7D^6{}_4 - 153_{4,3}$
3123.42	2	V E	32006.94	$a^7D^6{}_2 - 155_2$
3122.91	6	V E	32012.16	$a^7D^6{}_5 - 151_4$
3117.603	15	V E	32066.66	$a^9D^6{}_5 - 139_4$
3115.77	5	V E?	32085.52	$z^9P_4 - f^7D^6{}_4$
3113.02	30	V E	32113.86	$a^7D^6{}_3 - 155_2$
3110.26	6	V E	32142.36	$a^7D^6{}_5 - 153_{4,3}$
3101.53	3	V	32232.83	$a^7D^6{}_2 - 156_3$
3097.45	100	V E	32275.28	$a^7S^6{}_3 - 103_2$
3094.183	6	V E	32309.36	$a^9D^6{}_3 - 138_2$
3091.292	10	V E	32339.57	$a^7D^6{}_3 - 156_2$
3089.64	3	V E	32356.86	$a^9D^6{}_3 - y^9D_2$
3087.02	2	V	32384.33	$z^9P_3 - 6^6{}_{3,4}$
3085.89	2	V E	32396.18	$a^7D^6{}_1 - 157_2$
3079.058	8	V E?	32468.06	$a^9D^6{}_3 - 138_2$
3078.57	5	V E	32473.21	$a^7D^6{}_2 - 157_2$
3078.27	1	V	32476.38	$a^7D^6{}_4 - 156_3$
3077.358	200	V E	32486.00	$a^9S^6{}_4 - z^9D_4$
3075.14	3	V E	32509.43	$z^7P_2 - 13^6{}_3$
3074.556	6	V E?	32515.60	$a^9D^6{}_2 - y^9D_2$
3071.58	5	V E	32547.11	$z^9P_4 - f^7D^6{}_5$
3069.110	50	V E	32573.30	$z^9P_4 - 8^6{}_5$
3068.47	1	V E	32580.09	$a^7D^6{}_3 - 157_2$
3060.81	4	V E	32661.62	$z^7P_2 - 13^6{}_3$
3054.94	600	V E	32724.38	$a^7S^6{}_3 - y^9P_2$
3042.53	4	V E	32857.85	$a^9D^6{}_3 - 140_{3,4}$
3040.77	40	V E	32876.87	$a^7S^6{}_3 - 104_2$
3040.429	12	V E	32880.56	$a^9D^6{}_4 - y^9D_3$
3036.84	5	V	32919.42	$z^9P_4 - 9^6{}_{3,4}$
3036.11	4	V	32927.33	$z^7P_4 - 13^6{}_4$
3015.869	6	V	33148.31	$a^9D^6{}_4 - 141_{4,3}$
3015.52	2	V	33152.15	$z^7P_4 - 11^6{}_{3,4}$
3006.26	80	V E	33254.26	$a^7S^6{}_3 - 106_2$
3004.80	20	V E	33270.42	$a^9D^6{}_2 - y^9D_2$
2999.4	1	V E	33330.3	$a^9D^6{}_4 - 142_3$
2997.36	2	V E	33353.00	$z^9P_3 - 9^6{}_{3,4}$
2995.221	50	V E	33376.81	$a^7S^6{}_3 - 107_4$
2991.33	300	V E	33420.23	$a^9S^6{}_4 - z^9D_3$
2990.26	15	V E	33432.18	$a^9D^6{}_3 - y^9D_4$
2976.58	2	V E?	33585.83	$z^9P_3 - 11^6{}_{3,4}$
2973.30	2	V	33622.88	$a^7D^6{}_3 - 158_1$
2966.52	10	V E	33699.72	$a^7D^6{}_2 - 158_1$
2960.21	300	V E	33771.55	$a^7S^6{}_3 - 108_3$
2959.47	80	V E	33779.99	$a^9S^6{}_4 - 101_4$
2956.07	2	V	33818.84	$a^9D^6{}_5 - 143_3$
2952.68	600	V E	33857.67	$a^7S^6{}_3 - y^9P_4$
2949.12	25	V E	33898.54	$a^7S^6{}_3 - 109_2$
2947.29	100	V E	33919.59	$a^9S^6{}_4 - 102_3$
2940.82	15	V E	33994.21	$a^9D^6{}_3 - y^9D_4$
2940.45	8	V E	33998.48	$a^9D^6{}_4 - y^9D_3$
2925.04	600	IV E	34177.59	$a^7S^6{}_3 - y^7D_2$
2917.439	30	V E	34266.63	$a^7S^6{}_3 - z^9F_4$
2914.29	4	V E	34303.66	$a^9D^6{}_3 - 143_3$
2906.68	1000	IV E	34393.46	$a^9S^6{}_4 - y^9P_3$
2899.10	8	V	34483.38	$a^9D^6{}_4 - y^9D_4$
2893.83	300	I, V E	34546.18	$a^9S^6{}_4 - 104_3$
2887.85	60	V E	34617.71	$a^9S^6{}_4 - 105_4$
2886.46	3	V	34634.38	$a^9D^6{}_4 - 143_3$
2876.06	60	V E	34759.62	$a^7S^6{}_3 - 111_4$
2871.57	12	V E	34813.96	$a^9D^6{}_4 - y^9D_3$
2864.42	20	V	34900.86	$a^9D^6{}_3 - y^9D_3$
2862.57	500	V E	34923.41	$a^9S^6{}_4 - 106_3$
2859.67	300	V E	34958.83	$a^7S^6{}_3 - z^9P_3$
2852.55	8	V	35046.08	$a^9S^6{}_4 - 107_4$
2843.96	60	V E	35151.93	$a^7S^6{}_3 - 112_3$
2834.34	2	V E	35271.23	$z^9P_3 - 12^6{}_3$
2833.26	125	V E	35284.67	$a^7S^6{}_3 - 113_4$
2829.30	125	V E	35334.06	$a^7S^6{}_3 - 115_2$
2828.72	500	V E	35341.30	$a^7S^6{}_3 - z^7D_4$

TABLE XII.—*Continued.*

λ	Arc Int.	Temp. Class	Wave No. Vac.	Multiplet Designation
2825.17	8	V	35385.71	$a^9D^\circ_5 - y^9D_6$
2820.78	800	IV E	35440.78	$a^9S^\circ_4 - 108_3$
2816.18	500	IV E	35498.66	$a^7S^\circ_3 - z^7D_3$
2813.94	1200	IV E	35526.92	$a^9S^\circ_4 - y^9P_4$
2811.75	200	V E	35554.59	$a^7S^\circ_3 - x^9P_4$
2810.71	15	V E?	35567.74	$a^9S^\circ_4 - 109_5$
2802.84	600	IV E	35667.61	$a^7S^\circ_3 - y^7P_2$
2781.93	400	IV E	35935.68	$a^9S^\circ_4 - 110_4$
2781.89			35936.20	$a^7S^\circ_3 - 117_3$
2780.53	20	V	35953.78	$a^7S^\circ_3 - 118_{3,4}$
2766.92	10	V E	36130.62	$a^7S^\circ_3 - 119_2$
2752.17	150	V E	36324.25	$a^7S^\circ_3 - 121_4$
2747.286	100	V E	36388.82	$a^7S^\circ_3 - 122_4$
2744.26	200	V E	36428.94	$a^9S^\circ_4 - 111_4$
2740.62	200	V E	36477.32	$a^7S^\circ_3 - x^7P_2$
2729.44	300	V E	36626.73	$a^7S^\circ_3 - 123_3$
2729.33	300	IV E	36628.20	$a^9S^\circ_4 - x^9P_3$
2727.78	800	IV E	36649.01	$a^9S^\circ_4 - y^9P_3$
2716.98	400	IV E	36794.69	$a^7S^\circ_3 - y^7P_3$
2715.02	3	V	36821.25	$a^9S^\circ_4 - 112_3$
2705.28	150	V E	36953.81	$a^9S^\circ_4 - 113_4$
2701.90	400	V E	37000.03	$a^9S^\circ_4 - 114_5$
2701.14	250	V E	37010.44	$a^9S^\circ_4 - z^7D_4$
2692.03	250	V E	37135.68	$a^7S^\circ_3 - y^7P_3$
2685.66	200	V E	37223.76	$a^9S^\circ_4 - x^9P_4$
2678.29	200	V E	37326.18	$a^7S^\circ_3 - 127_4$
2670.85	15	V	37430.15	$a^7S^\circ_3 - 128_2$
2668.34	300	V E	37465.36	$a^7S^\circ_3 - y^7P_4$
2658.41	20	V E	37605.30	$a^9S^\circ_4 - 117_3$
2657.17	10	V	37622.83	$a^9S^\circ_4 - 118_{3,4}$
2641.27	250	V E	37849.31	$a^9S^\circ_4 - x^9P_3$
2638.77	400	V E	37885.17	$a^7S^\circ_3 - y^7P_4$
2635.50	60	V	37932.17	$a^9S^\circ_4 - 120_5$
2631.23	15	V E	37993.72	$a^9S^\circ_4 - 121_4$
2626.776	25	V E	38058.14	$a^9S^\circ_4 - 122_4$
2624.01	6	V	38098.26	$a^7S^\circ_3 - 130_3$
2610.5	2	V	38295.4	$a^9S^\circ_4 - 123_3$
2605.47	4	V	38369.34	$a^7D^\circ_1 - 159_2$
2600.26	10	V	38446.21	$a^7D^\circ_2 - 159_2$
2597.81	4	V	38482.47	$a^7D^\circ_1 - 160_2$
2592.61	10	V	38559.65	$a^7D^\circ_2 - 160_2$
2585.76	12	V E?	38661.79	$a^7D^\circ_1 - x^7F_0$
2585.45	2	V	38666.42	$a^7D^\circ_3 - 160_2$
2581.86	30	V E	38720.19	$a^7D^\circ_2 - x^7F_3$
2581.2	1	V	38730.1	$a^9D^\circ_3 - 152_3$
2577.56	20	V	38784.78	$a^9S^\circ_4 - 126_5$
2577.14	150	V E	38791.10	$a^7D^\circ_3 - x^7F_4$
2576.22	10	V	38804.95	$a^9S^\circ_4 - y^7P_3$
2574.76	30	V E	38826.95	$a^7D^\circ_3 - x^7F_3$
2568.53	20	V, V E	38921.12	$a^7D^\circ_1 - x^7F_1$
2568.17	80	V E	38926.58	$a^7D^\circ_3 - x^7F_4$
2565.71	6	V E	38963.90	$a^7D^\circ_4 - x^7F_3$
2564.55	10	V E	38981.52	$a^7D^\circ_2 - 161_3$
2564.17	125	V E	38987.30	$a^7D^\circ_4 - x^7F_5$
2563.6	1	V	38996.0	$a^9S^\circ_4 - 127_4$
2563.48	10	V E	38997.78	$a^7D^\circ_2 - x^7F_1$
2559.18	80	V E	39063.31	$a^7D^\circ_4 - x^7F_4$
2557.54	25	V E	39088.36	$a^7D^\circ_3 - 161_3$
2554.781	50	V E	39130.57	$a^7D^\circ_5 - x^7F_5$
2554.50	4	V E	39134.87	$a^9S^\circ_4 - z^7P_4$
2552.01	15	V E?	39173.05	$a^9D^\circ_4 - 155_2$
2549.82	4	V	39206.69	$a^7D^\circ_5 - x^7F_4$
2548.63	4	V E?	39225.00	$a^7D^\circ_4 - 161_3$
2547.243	15	V E	39246.36	$a^7D^\circ_1 - x^7F_2$
2542.262	40	V E	39323.25	$a^7D^\circ_2 - x^7F_2$
2535.36	8	V E?	39430.29	$a^7D^\circ_3 - x^7F_2$
2527.40	5	V	39554.5	$a^9S^\circ_4 - x^7P_4$
2516.10	4	V	39732.09	$z^7P_3 - f^7S^\circ_3$
2514.36	3	V	39759.58	$z^7P_4 - f^9S^\circ_4$
2513.76	5	V	39769.07	$a^7S^\circ_3 - 135_4$
2499.391	50	V	39997.69	$a^7S^\circ_3 - 136_4$
2496.81	10	V E	40039.03	$a^7D^\circ_1 - 162_{1,2}$
2496.4	1	V	40045.6	$a^7S^\circ_3 - 137_4$
2492.02	15	V	40115.99	$a^7D^\circ_2 - 162_{1,2}$
2490.46	10	V E	40141.11	$a^7D^\circ_2 - 163_3$
2488.83	3	V E?	40167.40	$a^7D^\circ_2 - 164_{2,3}$
2483.84	8	V	40248.09	$a^7D^\circ_3 - 163_3$
2483.23	3	V	40274.19	$a^7D^\circ_3 - 164_{2,3}$
2472.96	8	V	40425.15	$z^9P^\circ_5 - f^9S^\circ_4$
2468.8	1	V	40493.26	$a^7D^\circ_3 - 165_{3,4}$
2460.50	12	V	40629.85	$a^7D^\circ_4 - 165_{3,4}$
2454.944	60	V	40721.80	$a^7S^\circ_3 - 138_2$
2452.08	40	V	40769.35	$a^7S^\circ_3 - y^9D_2$
2445.99	5	V	40870.85	$a^9S^\circ_4 - 132_4$
2435.86	2	V	41040.81	$a^7S^\circ_3 - 139_4$
2425.05	8	V	41223.23	$a^9S^\circ_4 - 134_5$
2407.492	40	V	41524.36	$a^7S^\circ_3 - y^9D_3$
2403.34	5	V	41596.09	$a^7D^\circ_1 - 166_2$
2398.916	10	V	41672.80	$a^7D^\circ_2 - 166_2$
2396.5	2	V E	41714.8	$a^9D^\circ_4 - 137_4$
2392.77	3	V	41779.83	$a^7D^\circ_3 - 166_2$
2390.43	8	V E	41820.72	$a^7D^\circ_1 - 167_1$
2386.05	40	V	41897.48	$a^7D^\circ_2 - 167_1$
2379.65	50	V	42010.16	$a^7D^\circ_1 - 168_2$
2375.31	60	V	42086.91	$a^7D^\circ_2 - 168_2$
2369.3	1	V	42193.7	$a^7D^\circ_3 - 168_2$
2361.14	30	V	42339.46	$a^7D^\circ_4 - 169_{4,5}$
2358.32	3	V E?	42390.08	$z^9P^\circ_4 - f^9S^\circ_4$
2357.39	12	V	42406.81	$a^7S^\circ_3 - y^9D_4$
2353.18	2	V	42482.67	$a^7D^\circ_3 - 169_{4,5}$
2340.64	20	V	42710.25	$a^9S^\circ_4 - 139_4$
2332.76	8	V E	42854.51	$a^7D^\circ_3 - 170_{3,4}$
2325.34	6	V	42991.24	$a^7D^\circ_4 - 170_{3,4}$

* Intensity refers to blend of arc and spark line.

therefore, that a complete analysis of this extremely complex spectrum will be long deferred.

In conclusion it is a pleasure to express our gratitude to Professor G. R. Harrison for the observations of the Zeeman effect, upon which a great part of the results of the present work depend, and to Dr. A. S. King for communicating unpublished spectroscopic data.

On the Momentum Loss of Heavy Ions

J. H. M. BRUNINGS AND J. K. KNIPP
Purdue University, Lafayette, Indiana

AND

E. TELLER
George Washington University, Washington, D. C.

(Received September 10, 1941)

In the calculation of the momentum loss of a heavy ion in its passage through matter, an estimate is needed of the charge of the ion as a function of its velocity. The process of capture and loss of electrons in collisions is characterized by the velocity within the ion of the electron or electrons participating. This velocity is roughly proportional to the ion velocity. The factor of proportionality is introduced as a convenient parameter γ. Two methods are used to estimate the charge of the ion: (1) It is supposed that the characteristic velocity is that of the energetically most easily removable electron, which is determined from the Thomas-Fermi model. Under this assumption γ tends to increase with atomic number ($\gamma=1.3$ for $Z=6$ to $\gamma=1.8$ for $Z=55$). (2) It is supposed that the characteristic velocity is that of the outermost electron, which is also calculated from the Thomas-Fermi model. γ is found to decrease with atomic number ($\gamma=0.6$ for $Z=6$ to $\gamma=0.35$ for $Z=55$). The characteristic velocity probably lies between these extremes.

AN energetic heavy particle, such as a fragment produced in nuclear fission or an atom recoiling from the impact of an alpha-particle, becomes ionized as it passes through matter. The electronic stopping cross section is proportional to the square of the particle charge. The proportionality factor is the specific stopping cross section, which is the stopping cross section for a particle of unit charge. The specific stopping cross section has been calculated for air from data on alpha-particles in an earlier paper.[1]

The average charge of the particle must be estimated from the process of capture and loss. This process is very complicated; our knowledge concerning it is limited to little more than the fact that, when an electronic state of the particle is being filled and emptied because of collisions with atoms, the probabilities for capture into that state and loss out of that state are about equal when the average velocity of an electron in that state is approximately equal to the particle velocity. At any particular velocity there are only a few electronic states for which one or the other of the probabilities is not negligible. For that velocity the process is characterized by the average velocity of electrons in those states. This characteristic velocity is roughly proportional to the particle velocity. It has been found convenient to introduce the factor of proportionality as a parameter γ. Thus

$$V_e=\gamma V,$$

where V is the particle velocity and V_e is the characteristic velocity.

In an attempt to calculate the characteristic velocity, it has been supposed that this velocity is equal to the root mean square velocity of the *energetically* most easily removable electron in the Thomas-Fermi model for the ion. This quantity is calculable from the expression

$$V_e^2=\frac{4}{5h^3\pi m^2}\left\{\int_0^{r_1} drr^2(p_0^5-p_1^5)+\int_{r_1}^{r_0} drr^2p_0^5\right\}, \quad (1)$$

where p_0 is the maximum value of the electron momentum and p_1 is its minimum value at the position considered, r_0 is the radius of the ion, and r_1 is so determined that there is one electron in an energy range measured from the top of the Thomas-Fermi distribution. If the electron is supposed limited to an infinitesimal energy range at the top of the distribution, the expression can be written

$$V_e^2=\frac{1}{m^2}\int_0^{r_0} drr^2p_0^3\Big/\int_0^{r_0} drr^2p_0. \quad (1a)$$

Results of calculations from (1) and (1a) are shown plotted in the heavier curves of Fig. 1.

[1] J. Knipp and E. Teller, Phys. Rev. **59**, 659 (1941).

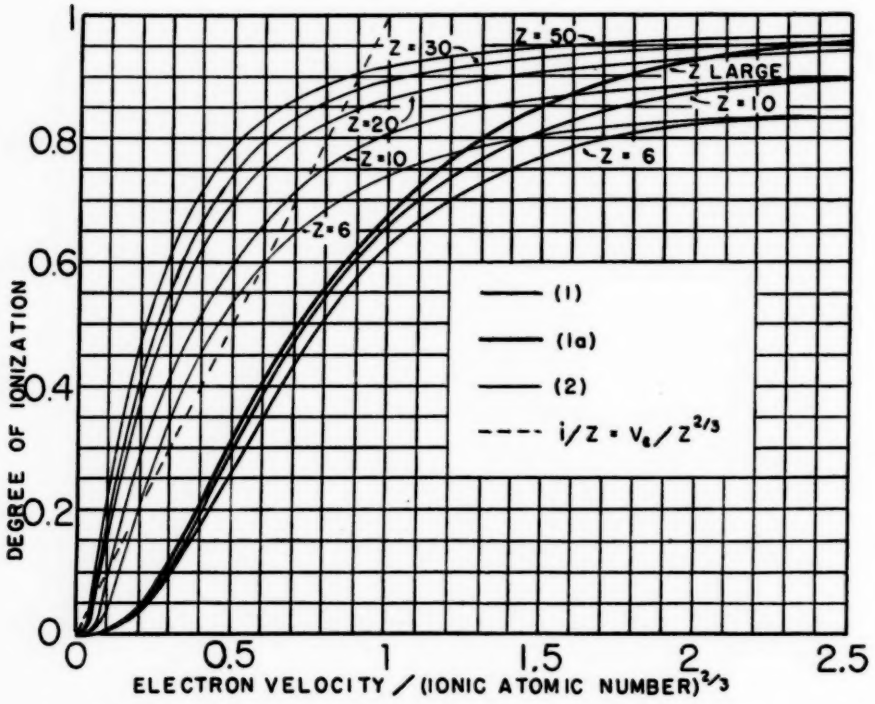

FIG. 1. Curves showing the ratio of ionic to nuclear charge i/Z plotted as a function of the velocity characteristic of the process of capture and loss (in units $Z^{\frac{1}{2}}e^2/\hbar$). The curves (1) are calculated under the assumption that the characteristic velocity is the energetically most easily removable electron of the ion. The very heavy curve (1a) is the limiting curve for very large Z. The curves (2) are calculated by assuming the characteristic velocity to be the velocity of the outermost electron of the ion. The dotted line is a relation which follows from one proposed by Bohr [Phys. Rev. 59, 270 (1941)].

It is equally instructive to make the supposition that the characteristic velocity is equal to the root mean square velocity of the *outermost* electron of the Thomas-Fermi distribution for the ion. This quantity is obtainable from the expression

$$V_e^2=\frac{4}{5h^3\pi m^2}\int_{r_2}^{r_0} drr^2p_0^5, \qquad (2)$$

where r_2 is so determined that there is one electron in the spherical shell between r_2 and r_0. Results of calculations from (2) are shown plotted in the light curves of Fig. 1.

Equations (1) and (2) represent extremes. In (1) the electron is assumed to have a definite energy as determined by the average potential of the other charges of the ion, but otherwise unaffected by them. In (2) it is supposed that electron collisions are so frequent that states of a definite energy are of little meaning for an individual electron. Then an electron participates

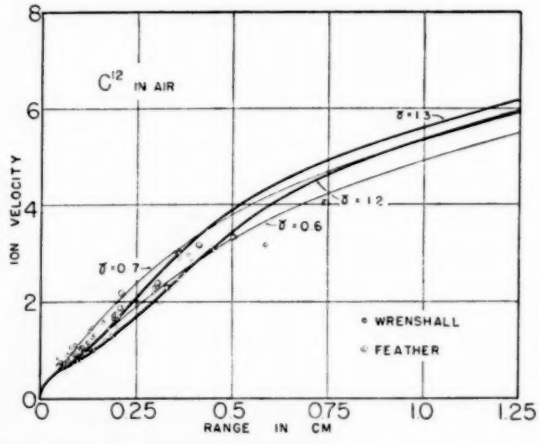

FIG. 2. Range in air of C^{12} ions plotted against the velocity (in units $e^2/\hbar$). The parameter γ, which is the ratio of the characteristic velocity to the particle velocity, is assumed to be constant throughout the range. The two heavy curves are for $\gamma=1.2$ and 1.3 and are calculated by using (1). The two light curves are for $\gamma=0.6$ and 0.7 and are calculated from (2). The points are experimental observations of Feather and of Wrenshall on individual tracks in cloud chambers containing various gases. These observations have been reduced to "equivalent air ranges" by comparison with alpha-particle behavior.

in the process of capture and loss whenever it is found near the surface of the ion. At the same time it also becomes the slowest electron in the velocity distribution. Since for the same atomic number velocities from (1) are greater than velocities from (2), the parameter γ will be greater under the first assumption than under the second.

Velocity-range relations have been calculated for C^{12}, Ne^{20}, and the light and heavy fragments of binary fission. The details of method are the same as used in reference 1. Curves are shown in Figs. 2, 3, 4, and 5. The experimental points of Fig. 2 are "reduced air ranges" from observations by Feather and by Wrenshall.[2] The experimental points of Fig. 3 are "reduced air

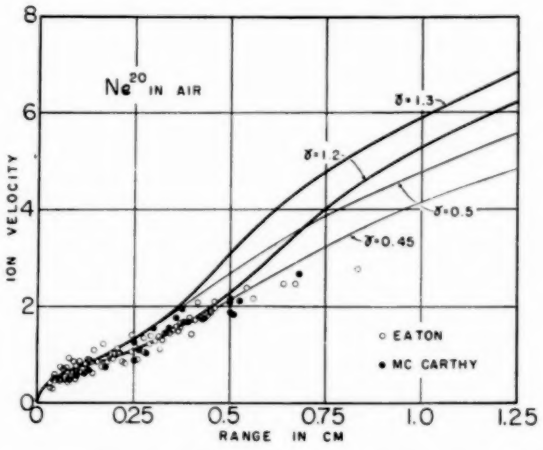

FIG. 3. Range in air of Ne^{20} ions plotted against the velocity (in units $e^2/\hbar$). The two heavy curves are for $\gamma=1.2$ and 1.3 and are calculated from (1). The two light curves are for $\gamma=0.45$ and 0.5 and are calculated from (2). The points are experimental observations of Eaton and of McCarthy.

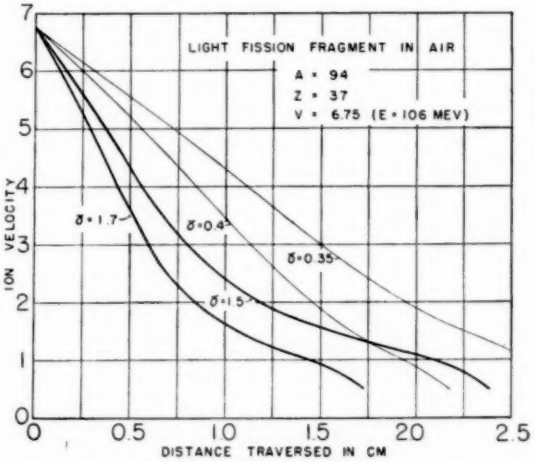

FIG. 4. Velocity (in units $e^2/\hbar$) of the light fragment produced in binary fission plotted against the distance traversed in air, measured from the point where fission took place. The two heavy curves are for $\gamma=1.5$ and 1.7 and are calculated by use of (1a). The two light curves are for $\gamma=0.35$ and 0.4 and are calculated from (2). The range of the light fission particle is observed to be about 2.5 cm.

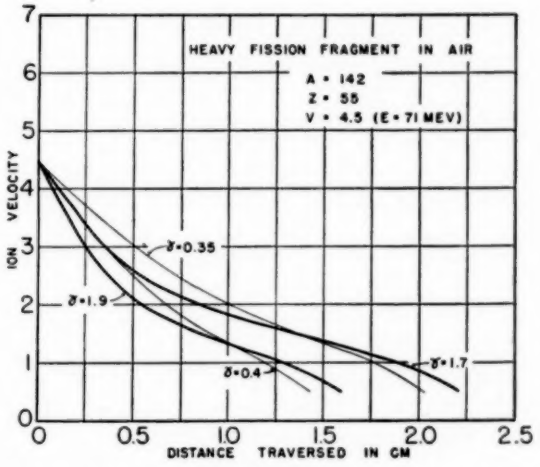

FIG. 5. Velocity (in units $e^2/\hbar$) of the heavy fragment produced in binary fission plotted against the distance traversed in air, measured from the point where fission took place. The two heavy curves are for $\gamma=1.7$ and 1.9 and are calculated by use of (1a). The two light curves are for $\gamma=0.35$ and 0.4 and are calculated by using (2). The range of the heavy fission particle is observed to be about 2 cm.

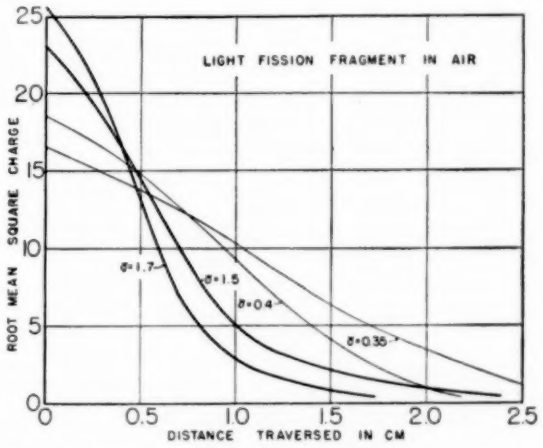

FIG. 6. Root mean square charge of the light fission fragment plotted against the distance traversed in air for the values of the parameter used in Fig. 4.

[2] N. Feather, Proc. Roy. Soc. **141**, 194 (1933); recoils from alphas in a mixture of 80 percent helium and 20 percent carbon tetrafluoride. G. A. Wrenshall, Phys. Rev. **57**, 1095 (1940); recoils from alphas in a mixture containing 52 percent methyl-chloride, 26 percent helium, 16 percent ethyl alcohol and 6 percent water vapor and also in a mixture containing 49 percent acetylene, 40 percent helium, 8 percent ethyl alcohol and 3 percent water vapor.

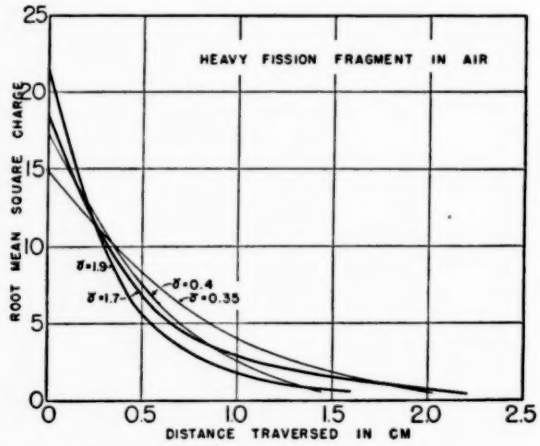

FIG. 7. Root mean square charge of the heavy fission fragment plotted against the distance traversed in air for the values of the parameter used in Fig. 5.

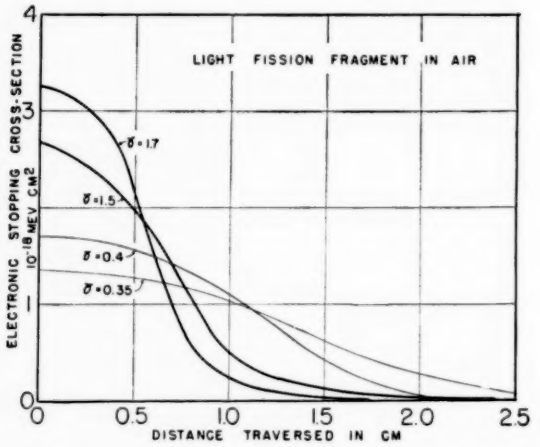

FIG. 8. Electronic stopping cross section of the light fission fragment plotted against the distance traversed in air for the values of the parameter used in Fig. 4..

ranges" from observations by Eaton and by McCarthy.[3]

If we assume (1), the best values of the parameter seem to be: C^{12}, $\gamma=1.3$ (below an ion velocity of $2e^2/h$); Ne^{20}, $\gamma=1.2$ (below an ion

[3] W. W. Eaton, Phys. Rev. **48**, 921 (1935); recoils from alphas, some in almost pure neon and others in a mixture of about 85 percent neon, 10 percent air and 5 percent hydrogen. J. T. McCarthy, Phys. Rev. **53**, 30 (1938); recoils from alphas in a mixture of about equal parts of neon and deuterium.

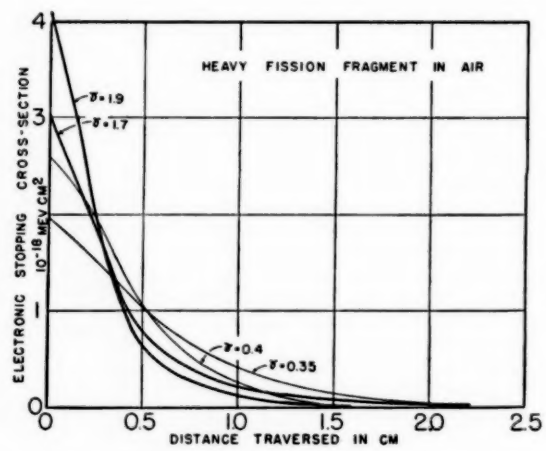

FIG. 9. Electronic stopping cross section of the heavy fission fragment plotted against the distance traversed in air for the values of the parameter used in Fig. 5.

velocity of $2e^2/h$); light fission fragment ($Z=37$), $\gamma=1.5$; heavy fission fragment ($Z=55$), $\gamma=1.8$. The experimental data for intermediate ions seem to indicate that the parameter decreases with increasing ion velocity. The parameter is smaller for more tightly bound electrons.

If we assume (2), the best values seem to be: C^{12}, $\gamma=0.6$; Ne^{20}, $\gamma=0.45$; light fission fragment, $\gamma=0.37$; heavy fission fragment, $\gamma=0.35$.

The parameter tends to increase with increasing atomic number for (1) and to decrease for (2). The fact that both extremes seem to give fairly reasonable results shows that there is in the method an uncertainty which is the uncertainty in the characteristic velocities and the parameters as calculated by the two methods.[4]

The root mean square charge of the fission fragments is plotted in Figs. 6 and 7 as a function of the distance traversed. The electronic stopping cross section, which is roughly proportional to the ionization produced, is plotted in Figs. 8 and 9. Experimental data on these quantities will tend to clear up the uncertainty in the methods of calculation used.

[4] The procedure proposed by Bohr (see Fig. 1) is, over a considerable range, intermediate between our extreme cases (1) and (2). In fact Bohr's calculations would seem to give fairly satisfactory results assuming $\gamma=1$.

Anisotropy of the Electronic Work Function of Metals

R. SMOLUCHOWSKI*
Palmer Physical Laboratory, Princeton University, Princeton, New Jersey
(Received July 24, 1941)

Work function is experimentally known to be different for different faces of a crystal by amounts ranging from one-tenth to half a volt. For tungsten the faces can be arranged according to decreasing work function as follows: 110, 211, 100 and finally 111. The explanations so far suggested for the differences of the work function are discussed and shown to give either an incorrect sequence or a wrong order of magnitude of the observed differences. The author uses the picture of Wigner and Bardeen according to which the work function is a sum of a volume contribution and a contribution due to a double layer on the surface of the metal. The origin of the latter can be described in the following manner. With every atom one can associate a polyhedron ("*s*-polyhedron") with the atom at its center, such that it contains all points nearer to the atom under consideration than to any other atom. If the distribution of the electron density within these polyhedra of the surface atoms was the same as for the inside atoms then there would be no double layer on the surface. However, this is not the case since the total energy is lowered by a redistribution of the electron cloud on the surface. There are two effects: the first is a partial spread of the charge out of the *s*-polyhedra and the second is a tendency to smooth out the surface of the polyhedra. In consequence of the second effect the surfaces of equal charge density are more nearly plane than in the original picture. The two effects have opposite influences and since they are comparable in magnitude, it is not possible to predict the sign of the total double layer without numerical computations. Some general formulae for the double layers are derived and discussed more fully in the case of a simple cubic and a body-centered cubic lattice. The minimum problem of the surface energy is solved for four faces of a body-centered crystal and the results are applied to the case of tungsten. One obtains the differences between the work functions for different directions. The results agree satisfactorily with the experimental data: assuming a reasonable density of the free electrons, one obtains the correct sequence of faces and the correct differences of the work function. The surface energies are calculated and found in agreement with the observed stability of certain crystal faces.

1.

THE intensity of thermionic electron emission of metals is well represented as a function of temperature by the formula

$$I = AT^2 e^{-\varphi/kT}, \tag{1}$$

where A and φ are constants. Many experimental investigations have shown that this emission is anisotropic. In particular the work function φ, representing the minimum energy necessary to bring an electron from the inside of the metal to the outside, is different for different crystal faces.[1] Recent photographs[2] of emission of single crystalline spheres of various metals give a nice illustration of this fact. They indicate also that the directional dependence of the work function is mainly connected with crystallographic orientation of the surfaces, and is the same for two metals if the metals have the same crystal lattice.

The purpose of this paper is to give a theoretical explanation for the observed differences of φ. A few explanations have already been suggested. One of them assumes an anisotropic Fermi surface inside the metal which would lead to different values of the work function for different directions. It will be explained below why this idea appears to us to be incorrect.

Let us consider the k space which for electrons in a metal is similar to the momentum space for free electrons. The difference is that, in general, the energy is not proportional to k^2. This k space is, as is well known, divided into regions, the so-called Brillouin zones, within which the energy varies continuously. To illustrate this we use a simple two-dimensional k lattice. We assume first (Fig. 1(a)) that the Fermi surface, A (that is the equi-energetical surface corresponding to

* Now at General Electric Company Research Laboratory, Schenectady, New York.

[1] R. P. Johnson and W. Shockley, Phys. Rev. **49**, 436 (1936); R. B. Nelson, M. I. T. Thesis 1938; S. T. Martin, Phys. Rev. **56**, 947 (1939); M. H. Nichols, Phys. Rev. **57**, 297 (1940). A probably more correct definition of work function is: the temperature independent term of the work required to remove an electron from the metal. The influence of temperature on the work function, if any, is still an unsolved problem. [See, e.g., C. Herring, Phys. Rev. **59**, 889 (1941)].

[2] M. Benjamin and R. O. Jenkins, Proc. Roy. Soc. **176**, 262 (1940).

the energy E_0 of the highest occupied electron states), lies within one zone and does not touch nor cross any zone boundary. One computes the number of electrons having momentum components in a particular direction larger than a certain minimum value p_0. The maximum energy of electrons in every direction is, by definition of the Fermi surface, the same. Thus p_0 and therefore the work function φ is isotropic. Let us consider now the other case (Fig. 1(b)) in which the Fermi surface touches or crosses the zone boundary. As we know there is a region of forbidden energy values at the zone boundary. Thus from the energy spectrum of the electrons having enough energy to leave the metal certain regions are missing and the electron emission intensity, therefore, is lower. The minimum energy necessary to bring out an electron is now no longer isotropic. In formula (1) the factor A would be multiplied by $(1-r)$ where r is the so-called reflection coefficient. (For polycrystalline material an "average" reflection coefficient $\bar{r}$ occurs.) Since the energy discontinuity occurs at, or at least near, the Fermi surface, the number of electrons missing from the emission depends upon temperature. Therefore the ratio of the number of missing electrons to the total current is not constant. This would amount to a temperature dependent reflection coefficient $r(T)$. The experimental data,[1] however, are, within the limits of error, well represented with a constant r, different for each surface. From the Richardson plots we get the work functions φ. Certain special aspects of the experimental data and the so-called "patch-effect" were discussed in this connection by Nichols.[3] If the emission were disturbed by such a boundary as discussed above, then one would not obtain a straight Richardson line. We are thus led to the conclusion that either such crossings of the Fermi surface and the zone boundary do not occur or their influence is covered up completely by electrons occupying other zones. If dr/dT is small it may not show up in the Richardson plot because of the exponential term. As we know there is a very complicated system of zones in metal lattices and electrons can originate in more than one zone. Also, if such crossings were responsible for the anisotropy, there would be no reason for metals crystallizing in the same crystal lattice to have a similar anisotropy as is true for tungsten and molybdenum.

Frequently one has to assume a certain $r \neq 0$ in order to fit the experimental data. This is probably connected with some surface phenomena, which we do not consider here. All we are interested in now is the work function and the fact that its anisotropy cannot be attributed to a volume effect. In other words, the presence of an accidental anisotropy of the Fermi surface is not supported by experiment. The anisotropy of the work function and the necessity for assuming $r \neq 0$, if A is a general constant, must have another origin.

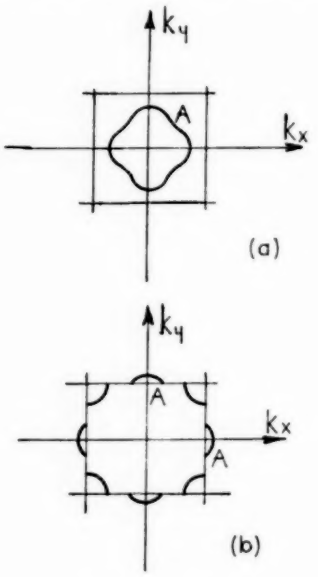

FIG. 1. k space of a two-dimensional cubic lattice with the Fermi surface (a) contained within one zone (b) crossing the boundary.

It is perhaps worth including a remark, which is, however, not an essential point in our considerations. Suppose the Fermi surface in a certain direction, say the x direction, falls just within the forbidden region. One might conclude that the electron emission in that direction is impossible. This is erroneous, since one has to consider the fact that the connection between k and E is not unique. If the zone boundary occurs at $k_x=k$, $k_y=k_z=0$ and $E(k)$ is below the necessary limit then another vector $k(k_x, k_y, k_z)$ may exist lying within the zone, such that its momentum along the x direction is large enough to bring the electron out from the metal.

[3] M. H. Nichols, Rev. Mod. Phys. (to appear shortly).

Müller[4] and Benjamin and Jenkins[2] made calculations on the hypothesis that the condition of the Bragg reflection of the electron wave is fulfilled for those electrons which have enough energy to escape across a particular crystal face. As pointed out by the last authors, this hypothesis leads to impossibly high energy values for the electrons and has some further drawbacks.

In the present paper we want to correlate the observed facts on the basis of another idea brought forward by Wigner and Bardeen.[5] According to these authors the work function is essentially a sum of two parts; the first is the volume contribution arising from the binding energy of the electron in the metal as a whole and the second is the energy necessary to penetrate the double layer at the surface. The first part is isotropic and is equal to the difference of the energy of a crystal composed out of an equal number of positive and negative charges and of the same crystal containing one electron less. It has been evaluated for a free electron model by these authors. Later Bardeen[6] made a careful study of the double layer using self-consistent solutions of the Fock equations. The model used by Bardeen consists of a charge distribution which is uniform positive inside of the crystal and zero outside. The electronic charge distribution, obtained by solving the corresponding Fock equations, is found to be uniform throughout the crystal except in the neighborhood of the surface. There it changes slowly and decreases to zero outside of the crystal within a fraction of the lattice constant from the surface. We have thus a deviation of the electronic density from the distribution characteristic for the inside of the metal and a spread of the charge beyond the surface of the crystal. From the point of view of the work function this is equivalent to the presence of a double layer which the electrons have to penetrate on their way to the outside.

The model in which the positive charge has a uniform distribution is of course isotropic and it is only if the atomic structure of the positive charges is taken into account that any anisotropy can be expected. Even in this latter model the volume contribution will remain isotropic and it is the double layer which must be made responsible for the observed differences in the work function or the potential differences[7] between different crystal faces.

The moment of the double layer on the surface of a metal is defined as the electrostatic potential difference between the outside of the metal and a point inside. Every atom in the lattice can be surrounded by a polyhedron of which each point is nearer to the atom under consideration than to any other one. These polyhedra are called usually *s*-polyhedra and the spheres of equal volume surrounding the atoms *s*-spheres. The inside point, in the definition of the double layer, is chosen at the surface of the *s*-sphere surrounding some atom. The point outside is taken as usual at a distance large compared with the lattice parameter and small compared with the size of the crystal surface. If all the atoms including those at the surface had the same radial electronic distribution inside the *s*-spheres, there would be no double layer since the dipole moment of an *s*-sphere is zero. However, because in the neighborhood of the surface atom the charge distribution is appreciably disturbed, a double layer may result.[8] If the double layer has a moment M normal to the surface and if we define its sign as positive if the positive charge is on the outside and the negative on the inside of the surface then the work function is given by

$$A-4\pi eM,$$

where A is the volume contribution mentioned before.

For a continuous positive charge distribution the double layer is zero if the negative charge density is constant within the metal and zero outside.

2.

We wish to carry out first a general qualitative, and later on a quantitative investigation of the conditions which occur on the surface of the metal and to see how they depend upon the

[4] E. Müller, Naturwiss. **27**, 820 (1939).
[5] E. Wigner and J. Bardeen, Phys. Rev. **48**, 84 (1935).
[6] J. Bardeen, Phys. Rev. **49**, 653 (1936).
[7] H. E. Farnsworth and B. A. Rose, Proc. Nat. Acad. Sci. **19**, 777 (1933); B. A. Rose, Phys. Rev. **44**, 585 (1933).
[8] See F. Seitz *Modern Theory of Solids* (McGraw-Hill Book Company, New York, 1940), p. 396.

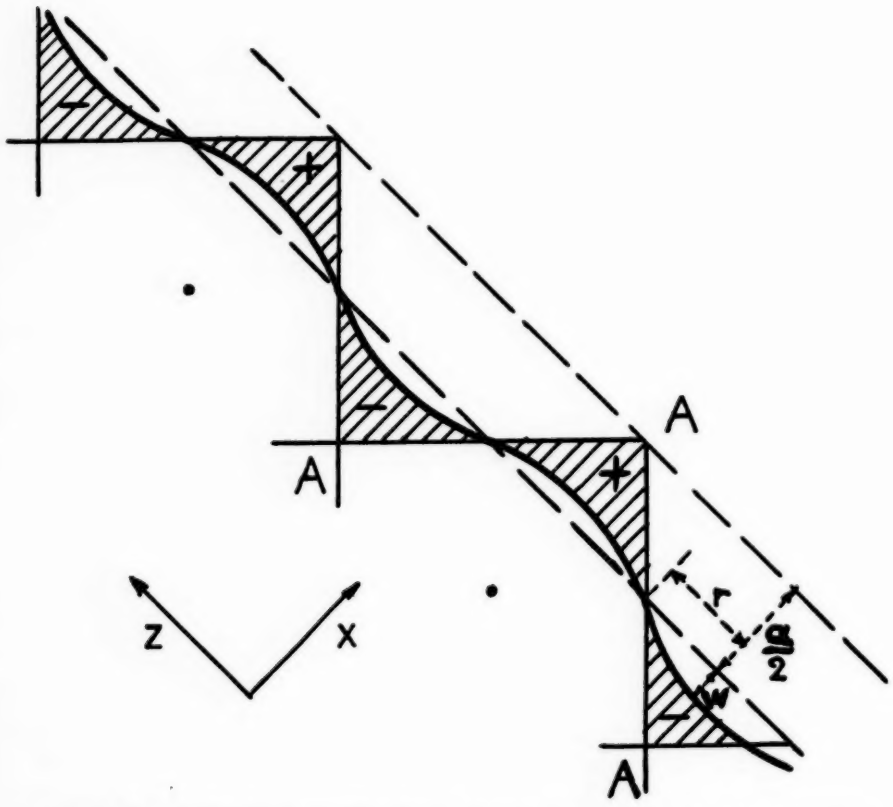

FIG. 2. Positive double layer resulting from the smoothing effect. Thick line represents the equilibrium charge distribution.

orientation of this surface with respect to the crystal lattice. Let us imagine a crystal surface which has just been exposed by splitting the crystal into two. If no changes of the charge distribution of the surface atoms occur then according to our definition there would be no double layer. However, we might expect two effects. First, as a result of the absence of the next atomic layer the potential field acting on the electrons binds them less than the potential in the inside of the metal. Thus the wave functions of these electrons are less concentrated within the original *s*-polyhedra; their expansion into the free space is accompanied by a decrease of the energy. This spread should be comparable with the difference of atomic diameter in crystal and vapor state. Because of this spreading of the negative charge there arises a corresponding positive charge within the *s*-polyhedra. We have thus a negative double layer which increases the work function since it is an additional potential preventing the electrons from leaving the crystal. We shall consider this effect later more in detail.

The other effect occurring on the surface is the smoothing of the surface of the electronic cloud of the metal. This smoothing is due to the fact that the energy of electrons when enclosed in a volume bounded by large flat planes is lower than when surrounded by the complicated walls of the surface polyhedra (Fig. 2). It means that the charge "flows" from the "hills" into the "valleys" formed by the surface atoms. In this way there arises a net positive charge on the "hills" and a negative charge in the "valleys." This is a positive double layer. The potential drop here decreases the work function. Thus the less smooth the final surface the more difficult it is for the electrons to leave the metal. The electrostatic energy accompanying the smoothing-out limits this process. The final shape of the surface of the electron cloud will be something like the thick curve in Fig. 2. It corresponds to

the balance between the different processes. The first effect mentioned above we shall call "spreading," the second "smoothing." They are both associated with the decrease of energy and are really not independent. However, since they have opposite influence on the work function it is convenient in a qualitative discussion to consider them separately.

We shall derive now some general formulas governing both effects making use of a very simple model. Let us consider first the spreading effect in the case of a uniform distribution of negative and positive charges in s-polyhedra throughout the whole crystal. In Fig. 3 the ordinate is the charge density σ (both $+$ and $-$) per unit volume, the line $P-P$ is the surface of the metal and at the same time the surface of the uniform charge distribution in the original crystal. We assume now that the electronic charge spreads so that its density decreases linearly to zero. One can see that this approximation is justified by comparing it with the exact distribution as calculated by Bardeen for a particular case. Thus up to the point S the negative and positive charges compensate each other. From S to P we have positive charge increasing up to the density $\frac{1}{2}\sigma$ on the inner side of the surface and then a negative charge decreasing from P to N in a symmetric distribution. If the spread of the electronic charge is small so that the disturbance does not reach the centers of the s-polyhedra then the potential difference is given by

$$D=-2\pi\sigma\frac{y^2}{3}\text{e}.$$

We introduce n, the number of electrons in a unit cell, and put for the lattice constant d its value b expressed in atomic units:

$$D=-\frac{n}{b}\left(\frac{y}{d}\right)^2\cdot 56.8 \text{ ev}. \qquad (2)$$

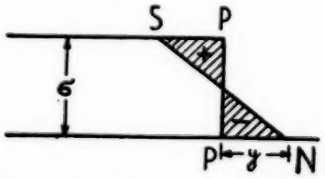

FIG. 3. Spreading of the electron density and the resulting negative double layer.

If however the disturbance of the negative charge in the metal extends beyond the center of the surface polyhedra then the positive charges in these polyhedra will be displaced towards the surface, by the amount $\frac{1}{2}d+y-(2dy)^{\frac{1}{2}}$. Then the potential drop is given by

$$D=-\frac{2\pi}{3}\frac{ne^2}{d}\left[\left(\frac{y}{d}\right)^2-\frac{3}{d^2}[d-(2dy)^{\frac{1}{2}}]^2\right]. \qquad (3)$$

Both formulas give the value of the double layer on a flat surface for a uniform charge distribution within the metal.

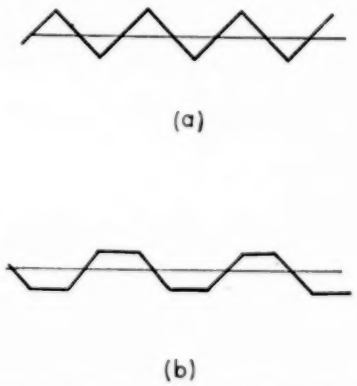

FIG. 4. Cross section of a "pyramidal" and "truncated" charge distribution on the surface.

Let us consider next the smoothing effect on crystal surfaces. In most cases one finds that the profile of the original, "rough," crystal face is either like Fig. 4(a) or 4(b). The plane P parallel to the crystal face and equally distant from the "hills" and from the "valleys" is the ideal plane surface which would be obtained if the smoothing were complete. The amount of negative charge "cut off" by this plane is equal to the charge needed to fill up the "valleys." This is a general statement true for all faces. The density of both $+$ and $-$ charges at this plane is $\frac{1}{2}\sigma$, half the value of the density inside of the crystal. A coordinate system is chosen so that the axis x is normal to the plane P and the charge density per unit volume is plotted as a function of x. Averages over the whole crystal face are taken parallel to the plane P. If the face is made out of prisms parallel to the crystal face (as all $hk0$ faces in simple cubic lattices are) the charge is a linear function of x. For pyramids it is a quadratic function. Figure 4(b) corresponds to trun-

cated pyramids typical for many faces of body-centered lattices. Typical charge distributions are shown in Fig. 5.

Let $\frac{1}{2}a$ be the distance from the plane P to the top of the "hill." We can calculate the potential differences obtained if the face is smoothed out completely, i.e., for all negative charge from the "hills" moved into the "valleys." In the general case of a truncated pyramid the

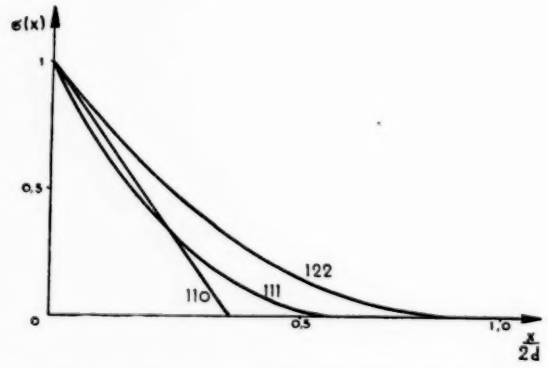

FIG. 5. Average charge density as a function of the distance from the ideal smooth surface for a simple cubic lattice.

charge distribution in the direction perpendicular to the plane P is given by

$$\sigma(x)=\frac{\sigma}{2a^2}(px^2-qa|x|+a^2)$$

for which the charge density at $x=\pm\frac{1}{2}a$ is equal to

$$\sigma'=\left(\frac{p}{4}-\frac{q}{2}+1\right)\frac{\sigma}{2}=m\frac{\sigma}{2}.$$

The corresponding potential difference is given by

$$V=\frac{\pi a^2}{2}e\sigma\left(\frac{p}{8}-\frac{q}{3}+1\right)$$

$$=\frac{\pi n}{2}\left(\frac{a}{d}\right)^2\frac{e^2}{d}\left(\frac{p}{8}-\frac{q}{3}+1\right). \quad (4)$$

For a quadratic decrease of charge density to zero at $x=\pm\frac{1}{2}a$: $m=0$, $p=2q-4$ or for a pyramid $p=q=4$; for a linear decrease to σ' at $x=\pm\frac{1}{2}a$: $p=0$, $q=2(1-m)$ and finally for linear decrease to zero at $x=\pm\frac{1}{2}a$: $m=p=0$, $q=2$. We shall make frequent use of these formulas for particular cases.

3.

In the former paragraph the effects occurring on the surface were discussed qualitatively and some general formulas were derived. Some particular cases will be considered here in more detail. Although the few metals for which data are available crystallize in a body-centered lattice we shall begin with a brief discussion of the simple cubic lattice. This case provides a good illustration of our model and of the method of approach.

In the simple cubic lattice the 100 face is smooth (Fig. 6). Thus there occurs only the spreading effect; the resulting double layer increases the work function. Next let us consider a $hk0$ plane (Fig. 6) for which $a=dhk/(h^2+k^2)^{\frac{1}{2}}$ and, in formula (4), $p=m=0$. We have thus

$$V=\frac{\pi e\sigma}{6}d^2\frac{h^2k^2}{h^2+k^2} \quad (5)$$

for the potential difference which is obtained for complete smoothing. Similarly for a hkl plane for which

$$a=2dhkl/(h^2k^2+k^2l^2+l^2h^2)^{\frac{1}{2}}$$

and $m=0$ we get

$$V=\frac{\pi e\sigma}{3}d^2\frac{h^2k^2l^2}{h^2k^2+k^2l^2+l^2h^2}. \quad (6)$$

If the smoothing is not complete, there remains

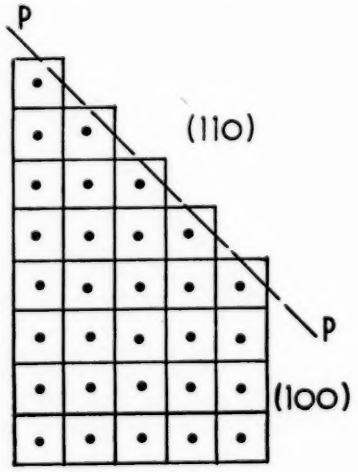

FIG. 6. Simple cubic lattice. Smoothing occurs on the 110 plane, none on the 100 plane.

a certain wave-like surface of the negative charge distribution and a correction should be made. This corrective term has to be subtracted from the values obtained from (5) or (6). We shall give an estimate for this correction below for the body-centered lattice. It is evident, however, that the number n of electrons per unit cell will enter into the result. Since it occurs as a linear factor it changes only the absolute values and not the relative magnitudes of the double layers for different faces. This is fortunate since n is unknown for most metals.

Let us consider the body-centered lattice. The polyhedron surrounding each atom in a body-centered crystal lattice is a truncated octahedron (Fig. 7) made out of eight 111 hexagons and six 100 squares. Since there are two atoms per unit cell the volume of the polyhedron is $\frac{1}{2}d^3$. We shall consider only a few particular faces which are actually observed on single crystals of tungsten, molybdenum etc. for which experimental data are known. These are the 100, 110, 111 and 211 faces. The structure of these surfaces can be seen in Fig. 8. The most densely packed surface is the 110 face, for which $a=\sqrt{2}d/4$; then comes the 100 face with $a=\frac{1}{2}d$ and 111 with $a=\sqrt{3}d/3$. The 211 face differs greatly from the other three faces which have a (truncated) pyramidal structure. On these faces each atom has at least four nearest neighbors; in the 211 face, on the other hand, an atom has only three nearest neighbors: and out of these two are in the surface layer. Thus there exists a long row of closely packed atoms separated by deep and long depressions.[9] If we consider the atoms on the 211 plane individually then $a=\sqrt{6}\,d/4\leqq 0.61d$. However, if we treat rather the rows of atoms as elements of that surface and average the charge distribution in the $\bar{1}11$ direction then $a\leqq 0.42d$. On the 211 plane, the ideal smooth surface, i.e., the plane P, cuts off certain volumes which fit into the remaining depressions. The charge distributions along the axis x, perpendicular to the plane P, are represented in Fig. 9 by continuous lines. For the 100, 110 and 111 faces the charge is a quadratic function of x, for the 211 face it is linear up to $x=\frac{1}{6}a$ then quadratic till $x=\frac{1}{3}a$ and finally again quadratic, with other constants, till $x=\frac{1}{2}a$.

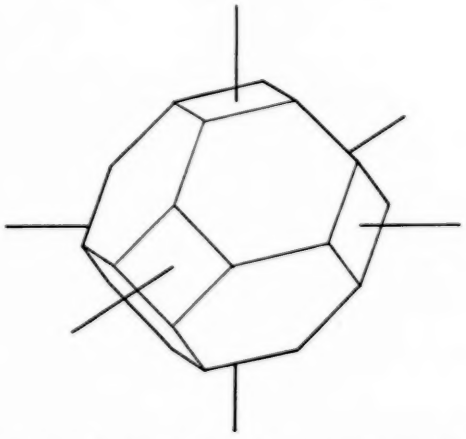

FIG. 7. s-polyhedron for a body-centered cubic lattice.

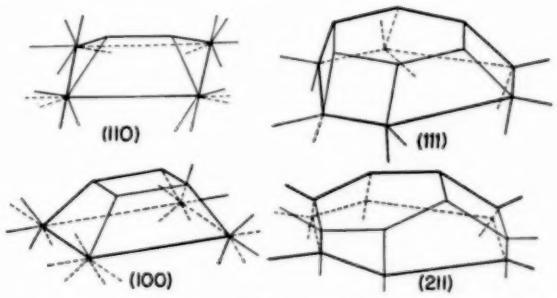

FIG. 8. Charge distribution on different faces of a body-centered cubic lattice.

We apply now formula (4) and obtain the values of the potential differences as if the smoothing were complete. We express the lattice constant in atomic units $d=ba_0$. For the 110 plane we have $m=0$, $q=3$, and thus

$$V^{110}=\frac{\pi n}{b}\frac{1}{64}\frac{e^2}{a_0}=\frac{n}{b}-1.33 \text{ ev} \tag{7}$$

for the 100 plane $p=1$, $q=2$ and

$$V^{100}=\frac{\pi n}{b}\frac{11}{192}\frac{e^2}{a_0}=\frac{n}{b}-4.88 \text{ ev} \tag{8}$$

for the 111 plane $p=\frac{4}{13}$, and $q=\frac{16}{13}$ and

$$V^{111}=\frac{\pi n}{b}\frac{19}{156}\frac{e^2}{a_0}=\frac{n}{b}-10.38 \text{ ev}. \tag{9}$$

The 211 plane has a rather complicated charge

[9] See S. T. Martin (reference 1), p. 957 or D. Langmuir and R. B. Nelson, Rev. Sci. Inst. **11**, 295 (1940).

distribution and the potential difference can be calculated by applying formula (4) separately to each interval within which the charge variation is expressed by a simple formula. The result is

$$V^{211}=\frac{\pi n}{b}\frac{41}{64\times 9}\frac{e^2}{a_0}\frac{n}{b}=-6.06 \text{ ev.} \qquad (10)$$

If we assume the charge distribution on the 211 face averaged in the $\bar{1}11$ direction, then we have

$$V^{211'}=\frac{n}{b}-5.80 \text{ ev.} \qquad (11)$$

All these values correspond to an ideal smooth charge distribution. Since, as mentioned before, some of the original structure of the surface will be left over we must correct for this fact. As it will appear later, these corrections are very essential, the surface charge distribution being far from smooth.

4.

So far we have considered the double layers arising on the crystal surfaces as if the smoothing were complete. Now we want to evaluate the actual electron distribution at the surface and the remaining "roughness" of the charge density. In the qualitative discussion it was pointed out that both spreading and smoothing are due to the decrease of kinetic energy of the electron gas, and are limited by the increasing potential energy of the resulting double layers. We shall treat now this question as a variational problem. The kinetic and the potential energy has to be expressed as a function of two parameters, one correlated with the spreading, the other with the smoothing effect. The total energy per unit surface has to be minimized with respect to each of these two parameters for each surface of the crystal. The calculations are rather involved and we shall consider more in detail only the 211 face which is the easiest to treat.

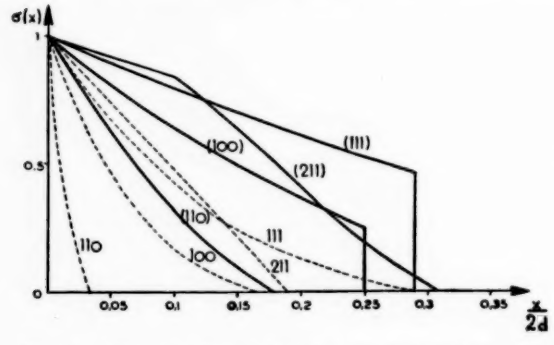

FIG. 9. Average charge density as a function of the distance from the ideal smooth surface for a body-centered cubic lattice.

The charge distribution on the 211 face is rather complicated (see Figs. 8 and 9) and we shall simplify it somewhat. It was said before that on that face the atoms form closely packed rows divided by relatively wide gaps. The approximation we want to use is that of a prismoidal charge distribution similar to that on the 110 face of a simple cubic lattice. However, the angle of the prism is here not a right angle. The width, $2r$, of the base of a prism cut off by the P plane is equal to half the distance between the rows of atoms. The height $\frac{1}{2}a_{\text{eff}}$ is such that the prism contains the same amount of charge as the part of the s-polyhedron cut off by the plane P. The charge density depends thus only upon two coordinates: x—perpendicular to the surface and z—lying in the surface and perpendicular to the rows of atoms. In Fig. 10 we have the density plotted against the two coordinates. In the original distribution both charges fill up the prism AAA with uniform density. The electrons tend to form a more smooth surface along the BBB line and finally spread along the x axis. The final charge density is given by the surface CCC. We put the origin of the coordinates at the point B and express the electron density in the region $0<z<1$ by

$$\rho=\tfrac{1}{2}\sigma e^{-\alpha(x-\beta z)} \quad \text{for } x>0 \text{ and by} \qquad (12a)$$

$$\rho=\tfrac{1}{2}\sigma(2-e^{\alpha(x-\beta z)}) \quad \text{for } x<0. \qquad (12b)$$

σ is here the number of electrons per unit volume inside the crystal, obviously α is the parameter associated with the spreading effect and β with the smoothing effect. For the original distribution we have $\beta=a_{\text{eff}}/2r$ and $\alpha\to\infty$. If the smoothing is complete we have $\beta=0$. The charge distribution as given by (12) is convenient for the computation of the kinetic energy. For mathematical reasons a slightly different, essentially equivalent form will be used for the calculation of the potential energy of the double layer. In calculating the kinetic energy it is useful to employ an expression which depends upon the

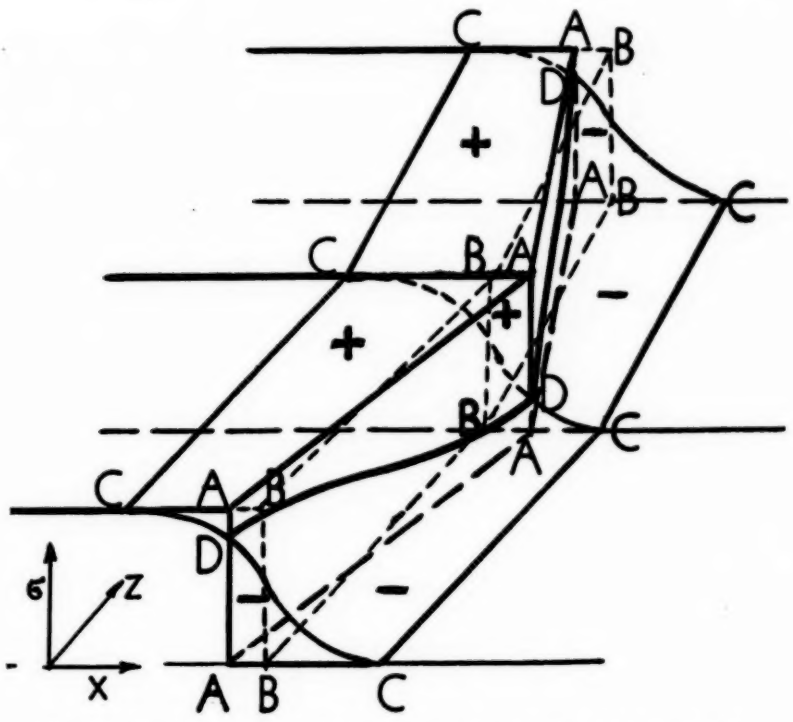

FIG. 10. Spreading and smoothing effect on the 211 face. *AAA*—original distribution of electron density, *CCC*—final distribution.

gradient of the density since this is an important magnitude in our considerations. Such an expression was given by Weizsäcker.[10]

$$\text{K.E.}=A\rho^{5/3}+B\frac{(\text{grad}\rho)^2}{\rho} \tag{13}$$

with

$$A=\frac{4\pi h^2}{5m}\left(\frac{3}{8\pi}\right)^{5/3} \quad \text{and} \quad B=\frac{h^2}{32\pi^2 m}.$$

The first term is the usual Fermi energy per unit volume, the second term is the important term depending upon the gradient of charge density. One has to calculate separately for $x<0$ and for $x>0$, integrate and add both energies. Integrating from $x=0$ to $-\infty$ with (12b) would give infinity but since we need only the differences of the kinetic energy it is enough to calculate the kinetic energy of the charge which is missing from the continuous distribution for $x<0$. We have thus

$$-\sigma^{5/3}\int_{-\infty}^{0}\{(1-\tfrac{1}{2}e^{\alpha(x-\beta z)})^{5/3}-1\}dx,$$

which is the decrease of kinetic energy as compared with the original distribution. We can represent the integrand as a series

$$\int_{-\infty}^{0}\sum_{k=1}^{\infty}\binom{5/3}{k}\frac{(-1)^k}{2^k}e^{k\alpha x}dx$$

and obtain

$$\frac{1}{\alpha}\sum_{k=1}^{\infty}\binom{5/3}{k}\frac{(-1)^k}{k2^k}=\frac{1}{\alpha}\int_0^{1/2}\frac{(1-u)^{5/3}-1}{u}du,$$

which can be evaluated. The total kinetic energy per unit length is

$$\sigma^{5/3}A\frac{6r}{2^{5/3}5\alpha}-\sigma^{5/3}A\frac{1.5852r}{\alpha}+\sigma B\alpha(1+\beta^2)2rln2. \tag{14}$$

[10] C. F. von Weizsäcker, Zeits. f. Physik **96**, 431 (1935).

The first term is the Fermi energy for $x>0$, the second the same for $x<0$ and the third "the Weizsäcker energy" due to the gradient of density.

To calculate the potential energy we make a small change in the expression for density so that the potential for the given charge is easy to obtain. We must compute the potential energy of the negative charge outside of the original s-polyhedron and the same amount of the positive charge inside of the polyhedron. This is shown by the thickly drawn lines in Fig. 10. The charge density along the surface of the polyhedron is given by the line DDD. Our new distribution differs by replacing this line by a cosine curve and plotting it in a plane perpendicular to the x axis. We put the origin of the coordinates at the point A, which is more convenient than point B for this computation. The charge for $x>0$ is now negative, for $x<0$ positive. We put

$$\rho = M\cos(\pi z)\int_{-\infty}^{+\infty}\frac{\cos\alpha x\omega}{1+\omega^2}d\omega + N\int_{-\infty}^{+\infty}\frac{\alpha\omega\sin\alpha x\omega}{1+\omega^2}d\omega$$

$$= M\cos(\pi z)\pi e^{-\alpha|x|} + N\pi\alpha e^{-\alpha|x|}\operatorname{sgn}x \tag{15}$$

(sgn x stands for "signum x," the sign $+$ or $-$ of x) which is shown in Fig. 11. The charge has a pattern, in the P plane, as given in Fig. 12(a). High negative and low positive charge density is indicated by full lines and the opposite by dotted lines. Formula (15) represents well our charge distribution (Fig. 10) and from it the potential can be obtained easily:

$$-\frac{V}{4\pi} = M\cos(\pi z)\int_{-\infty}^{+\infty}\frac{\cos\alpha x\omega}{(1+\omega^2)(\pi^2+\alpha^2\omega^2)}d\omega + N\int_{-\infty}^{+\infty}\frac{\sin\alpha x\omega}{(1+\omega^2)\alpha\omega}d\omega$$

$$= M\cos(\pi z)\frac{1}{\alpha^2-\pi^2}(\alpha e^{-\pi|x|}-\pi e^{-\alpha|x|}) + N\frac{\pi}{\alpha}(1-e^{-\alpha|x|})\operatorname{sgn}x. \tag{16}$$

The coefficients M and N must be adjusted so as to correlate the charge distribution given by (12) with that given by (15). It turns out that we must put

$$M=\frac{e\sigma}{2\pi}(e^{\alpha c}-1) \quad \text{and} \quad N=\frac{e\sigma}{2\pi\alpha}$$

with $c=\frac{1}{2}a_{\text{eff}}-r\beta$. The product $r\beta=W$ determines the remaining roughness of the surface measured perpendicular to the plane P. Equation (15) has also the advantage as compared with (12) that the subsequent integration is easy. We have

$$-\int_0^1 dz\int_{-\infty}^{+\infty}dx\frac{V\rho}{4\pi} = M^2\frac{\pi(2\alpha+\pi)}{2\alpha(\pi+\alpha)^2}+N^2\frac{\pi^2}{\alpha}$$

and the potential energy per unit length, in proper units has the form

$$\text{P.E.}=\frac{e^2\sigma^2}{\alpha}\frac{2\alpha+k}{(k+\alpha)^2}r^2[1+e^{\alpha c}(e^{\alpha c}-2)]+\frac{e^2\sigma^2}{\alpha^3}2r^2k \tag{17}$$

with $k=\pi/2r$.

The equations of the minimum problem are obtained by differentiating the total energy with respect to α and β (or W). One gets

$$e^m e^{2y}-e^y+\gamma e^{-m}y=0 \tag{18}$$

with

$$\gamma=\frac{B(\alpha+k)^2 2ln2}{\sigma e^2 r^3(2\alpha+k)}, \quad m=\frac{\alpha a_{\text{eff}}}{2} \quad \text{and} \quad y=-\alpha\beta r$$

and

$$a_2x^7+3ka_2x^6+(a_1+3k^2a_2)x^5+(3ka_1+k^3a_2-4a_3)x^4+(3k^2a_1-9ka_3)x^3+(a_1k^3-19a_3k^2)x^2$$
$$-18k^3a_3x-6k^4a_3+4a_3ce^{xc}(e^{xc}-1)x^5+2a_3[(3kc-2)e^{2xc}-(3kc-4)e^{xc}]x^4$$
$$-ka_3[(2kc+3)e^{2xc}-(2kc+6)e^{xc}]x^3-k^2a_3e^{xc}(e^{xc}-2)x^2=0 \quad (19)$$

with $x=\alpha$ and $a_1=\sigma^{\frac{1}{3}}A1.147$; $a_2=B(1+\beta^2)2\ln 2$ and $a_3=\sigma e^2r$.

No analytic form of the solution of these equations can be given but a solution is easily obtained by a trial and error method. We get thus α and β (or $W=r\beta$).

Next we give a brief summary of the conditions on other faces. On the 110 face the original charge distribution is approximated by a pyramid with a rectangular base, $2r_1\times 2r_2$, the same that is formed on the s-polyhedron, Fig. 8. Its height is again such that the pyramid has the same volume as the segment cut off from the polyhedron. The charge distribution used for calculation of the kinetic energy is essentially the same as (12). For computing the potential energy we have now

$$\rho=M\cos\frac{\pi z}{2r_1}\cos\frac{\pi y}{2r_2}\pi e^{-\alpha|x|}+N\pi\alpha e^{-\alpha|x|}\operatorname{sgn}x \quad (20)$$

and

$$-\frac{V}{4\pi}=M\cos\frac{\pi z}{2r_1}\cos\frac{\pi y}{2r_2}\frac{1/\lambda}{\alpha^2-\pi^2\lambda^2}(\alpha e^{-\pi\lambda|x|}-\pi\lambda e^{-\alpha|x|})+N\frac{\pi}{\alpha}(1-e^{-\alpha|x|})\operatorname{sgn}x \quad (21)$$

with $\lambda=(r_1^2+r_2^2)^{\frac{1}{2}}/2r_1r_2$, which can be also expressed in an integral form like (15). The charge has the pattern shown in Fig. 12(b) where the dots represent high negative charge for $x>0$ and low positive for $x<0$ and the circles indicate just the opposite. We have the kinetic energy

$$\text{K.E.}=-\sigma^{5/3}\frac{A}{\alpha}r_1r_2 2.994+\sigma B\alpha r_1r_2(1+2\lambda^2W^2)4\ln 2 \quad (22)$$

with $W=r_1\beta_1=r_2\beta_2$ and the potential energy

$$\text{P.E.}=\frac{e^2\sigma^2}{\alpha}\frac{2\alpha+k}{(\alpha+k)^2}\frac{r_1r_2}{2\lambda}[1+e^{\alpha c}(e^{\alpha c}-2)]+\frac{e^2\sigma^2}{\alpha^3}\frac{2r_1r_2k}{\lambda}. \quad (23)$$

Differentiation gives again two equations for the minimum problem from which one obtains α and W.

On the 100 face we have a pyramid with a square base. Thus all the formulas for the 110 face are valid if we put $r=r_1=r_2$. The most complicated case is that of the 111 face. Here the charge distribution is symmetrical around a threefold axis. The actual shape of the segment of the s-polyhedron cannot be approximated as well as in the other cases. A pyramid with the triangular base seems to be the best choice. The edge of the base has the length $d\sqrt{2}$ where d is the lattice constant. We have

$$\rho=M(\sin 2\pi z+2\sin\pi z\cos\pi y\sqrt{3})\pi e^{-\alpha|x|}+N\pi\alpha e^{-\alpha|x|}\operatorname{sgn}x \quad (24)$$

and

$$-\frac{V}{4\pi}=M(\sin 2\pi z+2\sin\pi z\cos\pi y\sqrt{3})\frac{1}{2(\alpha^2-4\pi^2)}(\alpha e^{-2\pi|x|}-2\pi e^{-\alpha|x|})+N\frac{\pi}{\alpha}(1-e^{-\alpha|x|})\operatorname{sgn}x, \quad (25)$$

which can also be expressed in integral form. The charge pattern in the plane P is given in Fig. 12(c). We have the kinetic energy

$$\text{K.E.}=-\sigma^{5/3}\frac{A}{\alpha}h^2\sqrt{3}\,0.765+\sigma B\alpha(h^2+9W^2)\frac{4}{3}\sqrt{3}\ln 2 \quad (26)$$

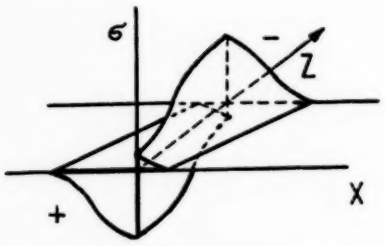

FIG. 11. Positive and negative charge distribution on the 211 face as used in the evaluation of the potential energy.

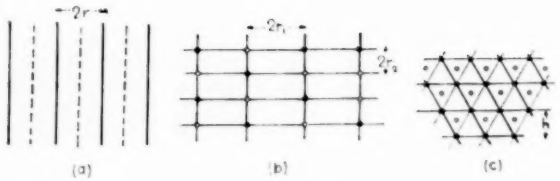

FIG. 12. Charge patterns on different faces of a body-centered lattice. Thick lines (or dots) indicate high negative or low positive charge density; dotted lines (or circles) indicate the opposite.

and the potential energy

$$\text{P.E.}=\frac{e^2\sigma^2}{\alpha}\frac{\alpha+k}{(\alpha+2k)^2}\frac{4\sqrt{3}}{27}h^3[1+e^{\alpha c}(e^{\alpha c}-2)]+\frac{e^2\sigma^2}{\alpha^3}\frac{2\sqrt{3}}{3}h^3k \tag{27}$$

with $k=\pi\sqrt{6}/3d$ and $h=d\sqrt{6}/2$. Differentiation of the total energy with respect to W and α leads to the equations of the minimum problem.

The solution of the minimum problem for each of the faces of a crystal gives the final charge distribution. From this we know the values of the effective double layers and thus also the differences between the work functions for different crystal faces. Finally having the expressions for the total energy for each surface we can calculate the energy of formation of a certain surface. Or rather, since we have only the relative values, we get the differences between the surface energies of a crystal. The following is an application of all these considerations in a particular case.

5.

The first thing one has to know in order to apply the formulas developed above is the average density of electrons (n or σ) which are involved in the formation of the double layer. In most cases this task is not easy. Among the metals for which data on work function are pretty well known only for sodium is this density accurately known. For other metals its estimate is more difficult. We are most interested in tungsten since the anisotropy for this metal is well measured. According to the calculations of Manning and Chodorow[11] there is much less than one electron per atom in the s band in metallic tungsten. On the other hand some of the d electrons might contribute to the effective density.

With the lattice constant of tungsten $d=3.16$A we get for the different magnitudes appearing in our formulas the values, in angtrom units given in Table I. As mentioned above, the only magnitude which is not known is the electron density σ. For the minimum problem we assume one electron per atom. This value has not much justification for tungsten but is probably true for most of the monovalent metals. The equations of the minimum problem were solved for each surface separately by the trial and error method. In most cases it was sufficient to try a few neighboring values in the full equation and to interpolate. The results are given in Table II. We see first of all that α, which is the parameter of the spreading of the charge in the direction normal to the surface, is almost constant. This is an interesting result and it justifies the point of view expressed in Part 1 that the positive contribution to the work function caused by the spreading is isotropic. Its value depends to a certain extent upon the analytical form of the charge distribution assumed in Eq. (12). It follows thus that all anisotropy is due to the smoothing of the charge distribution and formation of the new equilibrium surface. The magnitude W, given in Table II is the deviation of the surfaces of equal charge density, in the final distribution from the ideal plane P, see Fig. 2. We see that the conditions are very different on different surfaces; the 110 is smoothest, the 111

[11] M. F. Manning and M. I. Chodorow, Phys. Rev. **56**, 787 (1939).

is the most rough. This result was qualitatively to be expected on the basis of comparison of the number of close-packed atoms in these surfaces. The last column shows what fraction of the charge Q_0 which originally was outside of the plane P still remains outside in the form of the roughness Q_f of the surface and is not "smoothed out." Here we see again a great difference between the surfaces. In particular the difference between 211 and 100 should be noted since it is an essential point in the comparison with experiment, as made below.

Knowing the final charge distribution we can calculate the contributions to the double layers caused by spreading and smoothing of the charge. The first as we saw is almost isotropic and its value does not play a role in our comparison with experiment. However, we can use Bardeen's calculations, discussed in reference 1 and apply his result that the spread is about half the radius of the s-sphere. This result, obtained by more rigorous quantum-mechanical methods for a particular case is probably more correct than ours. This gives, with the help of formula (2), $D \leqq 1.2$ ev as the positive contribution to the work function under the assumption of one electron per atom.

The negative contributions to the work functions caused by smoothing are calculated first for the case of a perfectly smooth charge distribution, i.e., for $\beta=0$. Formulas (7)–(10) give with $n=2$ and $b=6a_0$ the values in the second column of Table III. These values are undoubtedly too high since the total work function for tungsten is about 4.5 ev. This is a result of our assumption of one electron per atom and $\beta=0$. It may be pointed out that $\beta=0$ gives us the sequence of crystal faces in the order of decreasing work function: 110, 100, 211, 111. This is not in accord with experiment. We shall see that it is the correction due to $\beta \neq 0$ which brings about the right sequence. The values of the second column must be decreased by the contribution of charge which did not take part in the smoothing process. In Fig. 9 the dotted lines indicate how much charge is left over after the equilibrium distribution is established. The particularly simple dependence of ρ on distance from the plane P is of course the result of our approximations. It has no appreciable influence however on the results. In an actual crystal the contours are more smooth, the amount of displaced charge being practically the same.

TABLE I. *Values of various constants for tungsten.*

	110	211	100	111
r	$r_1=0.79$ $r_2=1.116$	1.116	1.116	$h=3.87$
a	1.116	1.935	1.580	1.824
a_{eff}	1.396	2.185	2.765	3.19

TABLE II. *Parameters of the final charge distribution for tungsten.*

SURFACE	α	W	Q_f/Q_0
110	$1.10A^{-1}$	0.106A	0.15
211	1.08	0.600	0.55
100	1.10	0.518	0.37
111	1.14	0.910	0.46

From Table II we have the necessary data and with the help of formula (4) we can calculate the corrections. These corrected values in which the remaining unevenness of the charge distribution is taken into account are given in the third column of Table III. We see that the sequence of the faces is: 110, 211, 100, and 111. This is in accord with the experimental results of Nichols.[1] It may be mentioned here that there were attempts to explain the anisotropy of the work function relating it directly to the surface density of the atoms. This density relation however gives the same in correct sequence of faces, which was obtained for $\beta=0$. It appears thus that it is necessary to take into account the relative position of the atoms and the equilibrium distribution of charge in order to explain the observed facts.

Another comparison with experiment is the actual numerical value of the differences between the work function in different directions. Using $V_{\beta\neq 0}$ from Table III and comparing with the last column in which the experimental data of Nichols are given, we see that the theoretical values are about six times too large. This is, in the first place, a result of the arbitrarily assumed density of one electron per atom, which is certainly too high. The only indication is the quoted result[11] that the density in the $s-p$ band is of the order 0.1 electron per atom. We take here one-sixth of an electron per atom so as to

TABLE III. *Contributions to work functions.*

SURFACE	$V_{\beta=0}$	$V_{\beta\neq0}$	ΔV_{calc}	ΔV_{obs}
110	0.44 ev	0.43 ev	0.38 ev	>0.30 ev
211	2.04	1.35	0.22	0.30
100	1.64	1.40	0.21	0.17
111	3.48	2.70	0.0	0.0

fit the experimental data. The values ΔV_{calc} given in the column before last in Table III are obtained by making use of the fact that the electron density is a linear factor in our expressions of the double layer. This statement is not quite true, however, for the minimum problem which depends on the charge density in a non-linear manner. It was checked, however, that the dependence of W upon electron density justifies this approximation. Both W and α decrease slowly with decreasing σ. We see that the agreement between the computed and observed values is satisfactory in view of the simple model on which our theory is based.[12]

One important fact must be pointed out. All these computations were done as if the electronic charge density were uniform throughout the crystal, i.e., as if the ion cores were small. This may be a good approximation in the case of sodium but is less good for tungsten. Studies of the structure of the electron bands in metallic tungsten indicate that the 6*s* and 5*d* bands are broad and overlap considerably. About one-third of the four *d* electrons in an atom lie outside of the metallic *s*-sphere. Thus the ionic core is large and even the lower energy states are perturbed. It follows that a deformation of the original spherically symmetric charge distribution involves an additional potential energy. This is true especially for deep-penetrating disturbances. One might expect thus that the smoothing is less complete than would follow from our theory. As a result the negative contributions to the work function would be somewhat smaller than those in Table III.

[12] The ΔV are calculated with respect to the 111 rather than to the 110 plane. This is more satisfactory since the observed work function on the 110 plane is probably too low by 0.1 ev or more (see M. Nichols reference 1).

TABLE IV. *Energy per unit area; ergs/cm².*

Surface	110	211	100	111
Energy	30	334	362	952

Finally as indicated before, we can calculate the total energy per unit area for each of the four surfaces. From formulas (13), (17), (22), (23), (26), (27), we obtain the energy in ergs per cm² as given in Table IV. This is not the actual surface energy since in tungsten we might expect most of the binding energy to be due to the 5*d* electrons[13] which as mentioned above extend near to the surface of the *s*-spheres. However, these figures give the relative expenditure of energy in formation of these surfaces. We see that the most stable is the 110 face and the least stable the 111 face. These results agree with the observations on single crystals of tungsten. In particular the stability and development of the 110 and 211 faces is in accord with experimental data. Since the values in Table IV are differences of numbers of the order of about 2500 the relative error for the 110 face is large. On the other hand for the 111 face the approximation of the uniform charge distribution is least satisfactory since here the deeper layers around the atom are disturbed. Therefore these two extreme cases are less certain.

The author takes the opportunity to express his sincere thanks to Professor E. Wigner for advice and helpful criticism, and to Dr. C. Herring and Dr. M. Nichols for valuable discussion and remarks.

[13] See F. Seitz, reference 8, p. 432.

Magnetic Moments at High Frequencies

LEIGH PAGE
Sloane Physics Laboratory, Yale University, New Haven, Connecticut
(Received September 15, 1941)

The magnetic moments of conducting, permeable spheres and cylinders in an oscillating magnetic field are calculated as functions of the conductivity, permeability, radius of cross section and wave-length. Also the electric moment of a conducting sphere in an oscillating electric field is obtained. The results are applied to the determination of the effect of particle size on the effective permeability of magnetic powders.

(1) INTRODUCTION

FERROMAGNETIC materials, such as iron and nickel, are generally good conductors of electricity. In an oscillating magnetic field a perfectly conducting sphere or cylinder will acquire no magnetic moment however great its true permeability may be, for the electromagnetic waves impinging on it will be completely reflected from its surface. On the other hand, if the conductivity of the magnetic sphere or cylinder is large but finite, electromagnetic waves striking it will penetrate a short distance into the interior, and give rise to a magnetic moment which will be smaller, the higher the frequency. A theoretical investigation of the dependence of the magnetic moment of a sphere on its conductivity, permeability and radius at a given frequency of the magnetizing field, is of importance in view of the increasing use[1] of cores of magnetic powder. Obviously the effective permeability of such a core at a given frequency is larger the smaller the grains of the powder.

The chief objects of this paper are to calculate the magnetic moments of (a) a sphere, (b) a cylinder, of permeability μ and of large but finite conductivity σ, when placed in an axially symmetrical oscillating magnetic field, with the primary purpose, in the case of the sphere, of finding how small the particles of a powdered core need be in order to obtain any desired fraction of the maximum available magnetic moment. In addition the electric moment of a conducting, permeable sphere in the oscillating electric field which must accompany any oscillating magnetic field is determined. Finally calculations are made of both the effective permeability μ_e and the effective permittivity or dielectric constant κ_e of a magnetic powder consisting of spherical particles. It will be assumed throughout that the true permittivity of the sphere or cylinder is negligible compared with $\sigma/\omega[\omega=2\pi\nu=$angular frequency$]$, and therefore the symbol κ representing the permittivity will always be interpreted as $i\sigma/\omega$. Furthermore the calculations will be limited to wave-lengths λ in free space which are very large compared with the radius a of cross section of the sphere or cylinder. Specifically we are interested in the range of wave-lengths from $\lambda=1$ cm up, with $a/\lambda<(10)^{-3}$. Both the conductivity σ and the true or intrinsic permeability μ will be treated as constants. However much these quantities may vary with frequency in actuality, our results will nevertheless be significant in judging the dependence of the magnetic moment on the size of the sphere or cylinder at a given frequency, provided the conductivity and the intrinsic permeability do not depend upon size. Heaviside-Lorentz symmetrical units are used except where otherwise indicated.

[1] V. E. Legg and F. J. Given, Bell Sys. Tech. J. **19**, 385 (1940).

(2) EXCITING MAGNETIC FIELD

We may imagine the axially symmetrical oscillating magnetic field to be produced by a very long straight circular solenoid carrying a current which varies sinusoidally with the time. Employing right-handed cylindrical coordinates r, ϕ, z with the Z axis along the axis of the solenoid, it follows from symmetry that the magnetic vector has the form

$$\mathbf{H}=\mathbf{k}H_0(r)e^{-i\omega t}, \qquad (1)$$

where $\mathbf{k}$ is a unit vector along the Z axis. The

wave equation

$$\nabla\cdot\nabla\mathbf{H}=(1/c^2)\partial^2\mathbf{H}/\partial t^2$$

where c is the velocity of light, reduces, for the case under consideration, to the single scalar equation

$$\frac{d^2H}{dr^2}+\frac{1}{r}\frac{dH}{dr}+\frac{\omega^2}{c^2}H=0,$$

which assumes the simpler form

$$\frac{d^2H}{dp^2}+\frac{1}{p}\frac{dH}{dp}+H=0, \tag{2}$$

if we put $p\equiv(\omega/c)r=2\pi r/\lambda$.

Without loss of generality we may take the amplitude of H on the axis to be unity. Then the only solution of the wave equation (2) which is finite on the axis is

$$\mathbf{H}=\mathbf{k}J_0(p)e^{-i\omega t}, \tag{3}$$

where $J_0(p)$ is the Bessel function of zero order.

From the circuital equations we find for the associated electric field

$$\mathbf{E}=\boldsymbol{\phi}_1 iJ_1(p)e^{-i\omega t}, \tag{4}$$

where $\boldsymbol{\phi}_1$ is a unit vector in the direction of increasing azimuth ϕ, and $J_1(p)$ is the Bessel function of first order. Evidently $\mathbf{H}$ and $\mathbf{E}$ are both solenoidal.

(3) Magnetic Moment of Sphere

We may imagine the sphere of radius a to be placed inside the solenoid with its center on the axis. In order to apply the necessary boundary conditions at its surface we must find solutions of the field equations both inside and outside the sphere in spherical coordinates. Taking origin at the center of the sphere and polar axis along the axis of the solenoid, we introduce the right-handed spherical coordinates r, θ, ϕ, where r is the radius vector, θ the polar angle and ϕ the azimuth. We can infer from symmetry that the only non-vanishing field components are H_r, H_θ, E_ϕ, and that these are functions of r and θ only. Put $\psi\equiv(\omega/c)\kappa$, $\chi\equiv(\omega/c)\mu$. Then the circuital equations take the form

$$\nabla\times\mathbf{H}=-i\psi\mathbf{E}, \qquad \nabla\times\mathbf{E}=i\chi\mathbf{H},$$

which yields the scalar equations

$$\frac{1}{r}\left\{\frac{\partial}{\partial r}(rH_\theta)-\frac{\partial}{\partial\theta}(H_r)\right\}=-i\psi E_\phi,$$

$$\frac{1}{r^2\sin\theta}\frac{\partial}{\partial\theta}(r\sin\theta E_\phi)=i\chi H_r,$$

$$-\frac{1}{r\sin\theta}\frac{\partial}{\partial r}(r\sin\theta E_\phi)=i\chi H_\theta.$$

If we put $W'(r,\theta)\equiv r\sin\theta E_\phi$ and eliminate H_r and H_θ we get the wave equation

$$\frac{\partial^2W'}{\partial r^2}+\frac{\sin\theta}{r^2}\frac{\partial}{\partial\theta}\left(\frac{1}{\sin\theta}\frac{\partial W'}{\partial\theta}\right)+\psi\chi W'=0.$$

On making the substitutions $\rho\equiv(\psi\chi)^{\frac{1}{2}}r$, $x\equiv\cos\theta$, $W\equiv(\psi\chi)^{\frac{1}{2}}W'$, this equation assumes the simpler form

$$\rho^2\{\partial^2W/\partial\rho^2+W\}+(1-x^2)\partial^2W/\partial x^2=0. \tag{5}$$

We introduce the functions:

$$u_0 \equiv \sin\rho/\rho, \qquad v_0 \equiv \cos\rho/\rho,$$

$$u_1 \equiv \sin\rho/\rho^2 - \cos\rho/\rho, \qquad v_1 \equiv \cos\rho/\rho^2 + \sin\rho/\rho,$$

$$u_2 \equiv \left(\frac{3}{\rho^3} - \frac{1}{\rho}\right)\sin\rho - \frac{3}{\rho^2}\cos\rho, \qquad v_2 \equiv \left(\frac{3}{\rho^3} - \frac{1}{\rho}\right)\cos\rho + \frac{3}{\rho^2}\sin\rho,$$

$$u_3 \equiv \left(\frac{15}{\rho^4} - \frac{6}{\rho^2}\right)\sin\rho - \left(\frac{15}{\rho^3} - \frac{1}{\rho}\right)\cos\rho, \qquad v_3 \equiv \left(\frac{15}{\rho^4} - \frac{6}{\rho^2}\right)\cos\rho + \left(\frac{15}{\rho^3} - \frac{1}{\rho}\right)\sin\rho,$$

. . . . . .

$$u_l = (\pi/2\rho)^{\frac{1}{2}} J_{l+\frac{1}{2}}(\rho), \qquad v_l = (-1)^l (\pi/2\rho)^{\frac{1}{2}} J_{-(l+\frac{1}{2})}(\rho).$$

Evidently the u_l's are finite at the origin, whereas the v_l's are infinite. We note that

$$\frac{u_l}{\rho} = \frac{u_{l-1} + u_{l+1}}{2l+1}, \quad \frac{du_l}{d\rho} = \frac{l u_{l-1} - (l+1)u_{l+1}}{2l+1}, \tag{6}$$

and likewise for the v_l's.

If, now, we put

$$U \equiv \{A_1 u_1(\rho) + B_1 v_1(\rho)\} P_{11}(x) + \{A_2 u_2(\rho) + B_2 v_2(\rho)\} P_{21}(x) + \cdots,$$

where the $P_{l1}(x)$'s are associated Legendrian polynomials, the solution of (5) is

$$W = U\rho(1-x^2)^{\frac{1}{2}}, \tag{7}$$

and the solenoidal field components are

$$E_\phi = U, \quad H_r = i\left(\frac{\psi}{\chi}\right)^{\frac{1}{2}} \frac{1}{\rho}\frac{\partial}{\partial x}[U(1-x^2)^{\frac{1}{2}}], \quad H_\theta = i\left(\frac{\psi}{\chi}\right)^{\frac{1}{2}} \frac{1}{\rho}\frac{\partial}{\partial \rho}[\rho U]. \tag{8}$$

Next we must expand the field vectors of the exciting wave in terms of the u_l's and the P_{l1}'s. Noting that p in (3) and (4) is equal to $\rho(1-x^2)^{\frac{1}{2}}$, we find that the field components of the exciting wave are given by (8) with

$$U = i\left[\frac{3}{2}u_1(\rho)P_{11}(x) + \frac{7}{8}u_3(\rho)P_{31}(x) + \frac{11}{16}u_5(\rho)P_{51}(x) + \frac{75}{128}u_7(\rho)P_{71}(x) + \cdots\right]. \tag{9}$$

The reflected wave must be propaged *away* from the center of the sphere. Hence each u_l and v_l must appear in the combination

$$w_l = v_l + iu_l. \tag{10}$$

We shall distinguish the region inside the sphere from that outside by primes. Thus

$$\rho' = (\psi'\chi')^{\frac{1}{2}} r = \frac{2\pi r}{\lambda}(\kappa\mu)^{\frac{1}{2}},$$

where $\kappa = i\sigma/\omega$ is the permittivity and μ the permeability of the sphere, and

$$\rho = (\psi\chi)^{\frac{1}{2}} r = 2\pi r/\lambda.$$

In both expressions, and everywhere else in this paper, λ represents the wave-length in free space outside the sphere.

Since the field remains finite at the origin the function U' inside the sphere is limited to

$$U'=A_1'u_1(\rho')P_{11}(x)+A_3'u_3(\rho')P_{31}(x)+A_5'u_5(\rho')P_{51}(x)+A_7'u_7(\rho')P_{71}(x)+\cdots, \tag{11}$$

and since the reflected wave is divergent the complete function U outside the sphere must have the form

$$U=A_1w_1(\rho)P_{11}(x)+A_3w_3(\rho)P_{31}(x)+A_5w_5(\rho)P_{51}(x)+A_7w_7(\rho)P_{71}(x)+\cdots$$
$$+i\left[\frac{3}{2}u_1(\rho)P_{11}(x)+\frac{7}{8}u_3(\rho)P_{31}(x)+\frac{11}{16}u_5(\rho)P_{51}(x)+\frac{75}{128}u_7(\rho)P_{71}(x)+\cdots\right] \tag{12}$$

to account for both the reflected and the exciting waves.

The boundary conditions at the surface of the sphere demand the continuity of E_ϕ, μH_r and H_θ. Hence

$$U=U', \tag{13}$$

$$\frac{\partial}{\partial x}[U(1-x^2)^{\frac{1}{2}}]=\frac{\partial}{\partial x}[U'(1-x^2)^{\frac{1}{2}}], \tag{14}$$

$$\frac{1}{\rho}\frac{\partial}{\partial\rho}[\rho U]=\left(\frac{\psi'}{\chi'}\right)^{\frac{1}{2}}\frac{1}{\rho'}\frac{\partial}{\partial\rho'}[\rho'U']. \tag{15}$$

If (13) is satisfied for the coefficient of each $P_{l1}(x)$, then (14) is satisfied automatically. We need use, then, only (13) and (15). From (13) we find

$$A_1w_1(\rho)+\tfrac{3}{2}iu_1(\rho)=A_1'u_1(\rho'),$$
$$A_3w_3(\rho)+\tfrac{7}{8}iu_3(\rho)=A_3'u_3(\rho'),$$
$$\cdots\cdots\cdots\cdots$$

and from (15), with the aid of (6),

$$A_1[2w_0(\rho)-w_2(\rho)]+\tfrac{3}{2}i[2u_0(\rho)-u_2(\rho)]=\gamma A_1'[2u_0(\rho')-u_2(\rho')],$$
$$A_3[4w_2(\rho)-3w_4(\rho)]+\tfrac{7}{8}i[4u_2(\rho)-3u_4(\rho)]=\gamma A_3'[4u_2(\rho')-3u_4(\rho')],$$
$$\cdots\cdots\cdots\cdots\cdots\cdots\cdots\cdots\cdots$$

where

$$\gamma\equiv(\psi'/\chi')^{\frac{1}{2}}=(i\sigma/\omega\mu)^{\frac{1}{2}}.$$

Solving for A_1' we have

$$A_1'=\frac{9}{2}\frac{i}{\rho^2}\frac{1}{\gamma w_1(\rho)[2u_0(\rho')-u_2(\rho')]-[2w_0(\rho)-w_2(\rho)]u_1(\rho')}$$

with $r=a$. Since, however, we are interested only in waves of length great compared with a, we may replace $w_1(\rho)$ by $1/\rho^2$ and $2w_0(\rho)-w_2(\rho)$ by $-3/\rho^3$. Hence, if

$$\alpha\equiv\frac{2\pi a}{\lambda},\quad \alpha'\equiv\frac{2\pi a}{\lambda}\left(\frac{i\sigma\mu}{\omega}\right)^{\frac{1}{2}}=a\left(\frac{2\pi i\sigma\mu}{\lambda c}\right)^{\frac{1}{2}},$$

$$A_1'=\frac{9}{2}i\frac{1}{\gamma[2u_0(\alpha')-u_2(\alpha')]+(3/\alpha)u_1(\alpha')} \tag{16}$$

to the required degree of approximation. We shall not require the coefficients of higher index.

Now we are ready to calculate the magnetic moment of the sphere. For the component H_z' of the magnetic field inside the sphere in the direction of the exciting field we find from (8) and (11)

$$H_z' = H_r' x - H_\theta'(1-x^2)^{\frac{1}{2}}$$

$$= -i\gamma\left[\frac{2}{3}A_1' u_0(\rho')P_0(x) + \left\{\frac{2}{3}A_1' + \frac{12}{7}A_3'\right\}u_2(\rho')P_2(x) + \left\{\frac{12}{7}A_3' + \frac{30}{11}A_5'\right\}u_4(\rho')P_4(x)\right.$$

$$\left. + \left\{\frac{30}{11}A_5' + \frac{56}{15}A_7'\right\}u_6(\rho')P_6(x) + \cdots\right], \quad (17)$$

where the $P_l(x)$'s are Legendrian polynomials. The amplitude of the magnetic moment of the sphere in a unit magnetic field is, then,

$$p_H = 2\pi(\mu-1)\int_{-1}^{1}\int_{0}^{a} H_z' r^2 dr dx.$$

Every term of (17) except the first vanishes on integration with respect to x, and we get, on substituting (16),

$$p_H = \frac{4\pi a^3}{1+[k(\alpha')/(\mu-1)]}, \quad (18)$$

where

$$k(\alpha') \equiv \frac{\alpha'^2 \sin\alpha'}{\sin\alpha' - \alpha'\cos\alpha'}. \quad (19)$$

Since $\sqrt{i}$ appears in the expression for α' it is convenient to write

$$\alpha' \equiv \tfrac{1}{2}\pi\epsilon(1+i), \quad \epsilon = 2a(\sigma\mu/\pi\lambda c)^{\frac{1}{2}}.$$

For small α' we can calculate $k(\alpha')$ from the series

$$k(\alpha') = 3\left[1 - \frac{1}{15}\alpha'^2 - \frac{1}{525}\alpha'^4 - \frac{2}{23{,}625}\alpha'^6 - \cdots\right], \quad (20)$$

whereas for large α' we find

$$k(\alpha') = \frac{(\frac{1}{2}\pi\epsilon)^3 - i\{(\frac{1}{2}\pi\epsilon)^3 - (\frac{1}{2}\pi\epsilon)^2\}}{(\frac{1}{2}\pi\epsilon)^2 - (\frac{1}{2}\pi\epsilon) + \frac{1}{2}}. \quad (21)$$

For intermediate values of α' for which (19) must be used we note that

$$\sin\alpha' = \sin\tfrac{1}{2}\pi\epsilon\cosh\tfrac{1}{2}\pi\epsilon + i\cos\tfrac{1}{2}\pi\epsilon\sinh\tfrac{1}{2}\pi\epsilon,$$

$$\cos\alpha' = \cos\tfrac{1}{2}\pi\epsilon\cosh\tfrac{1}{2}\pi\epsilon - i\sin\tfrac{1}{2}\pi\epsilon\sinh\tfrac{1}{2}\pi\epsilon.$$

If $p_{H\infty}$ is the magnetic moment of a sphere of the same radius and intrinsic permeability in a unit static field, we find by putting $\alpha' = 0$ in (18) that

$$p_{H\infty} = 4\pi a^3[(\mu-1)/(\mu+2)], \quad (22)$$

in agreement with magnetostatic theory. The significant quantity we wish to calculate is the ratio

$$\frac{p_H}{p_{H\infty}} = 1\Big/\left(1 + \frac{k(\alpha')-3}{\mu+2}\right). \quad (23)$$

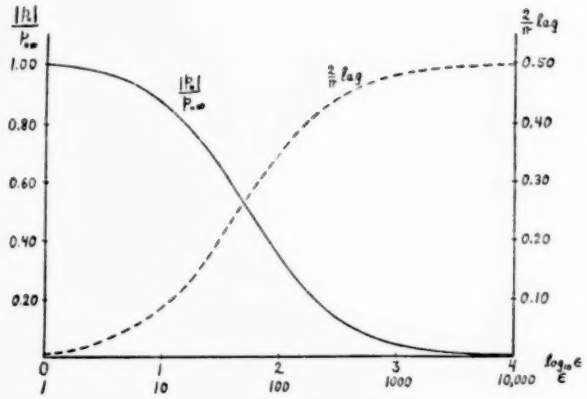

FIG. 1. Values for sphere.

It is very satisfactory that, with the exception of the divisor $\mu+2$, the conductivity, permeability, wave-length and radius enter only in the single parameter α'. In Table I we give computed values of $k(\alpha')$ over a considerable range of ϵ. Also, in the last two columns, is given the ratio of the modulus of p_H to $p_{H\infty}$ and the ratio of the lag of p_H behind the exciting magnetic field to $\pi/2$, for a sphere with an intrinsic permeability $\mu=100$. The latter quantities are plotted in Fig. 1 against the logarithm of ϵ, the solid curve representing $|p_H|/p_{H\infty}$ and the broken curve $(2/\pi)$ lag.

From Table I we can calculate the radius of the particles of a magnetic powder, having an intrinsic permeability $\mu=100$ at the wave-length specified, necessary for these particles to acquire, at that wave-length, magnetic moments equal to any given fraction of the magnetic moments acquired by a like powder of the same intrinsic permeability in a static field. For example, the resistivity of iron is approximately $(10)^4$ e.m.u. This gives a conductivity $\sigma=4\pi c^2(10)^{-4}$ in h.l.u., for which

$$\epsilon/a=6.93(10)^3(\mu/\lambda)^{\frac{1}{2}}.$$

For an iron powder for which the intrinsic permeability is 100 at the specified wave-length,

$$\epsilon/a=6.93(10)^4(1/\sqrt{\lambda}).$$

If, now, we desire 99.9 percent of the maximum available magnetic moment, we see from the table that ϵ must equal unity. Hence, for a wave-length of 100 cm the radius of the particles must not be greater than $1.44(10)^{-4}$ cm, although for a wave-length of 10 meters they need not have a radius less than $1.44(10)^{-3}$ cm. On the other hand, if we are satisfied with 90 percent of the maximum moment, ϵ may be as large as eight. This requires particles of radius not greater than $1.15(10)^{-3}$ cm for $\lambda=100$ cm or radius not greater than $1.15(10)^{-2}$ cm for $\lambda=10$ meters.

The ratio $|p_H|/p_{H\infty}$ is given in the table only for an intrinsic permeability of 100, but this ratio can be computed without much labor for other intrinsic permeabilities from the tabulated values of $k(\alpha')$ by means of (23).

(4) Electric Moment of Sphere

Since every oscillating magnetic field is accompanied by an oscillating electric field, it is important to calculate the electric moment p_E acquired by the sphere of permeability μ and of large conductivity σ treated in the last section when placed in an oscillating electric field. Taking the electric field to be an axially symmetrical field of unit amplitude, the analysis is so nearly identical with that developed in calculating the

TABLE I. *Computed values of $k(\alpha')$ and of $|p_H|/p_{H\infty}$ and ratio to $\frac{1}{2}\pi$ of the lag of p_H behind the exciting field for a sphere with $\mu=100$.*

ϵ	$k(\alpha')$	$\mu=100$ $\lvert p_H\rvert/p_{H\infty}$	$\mu=100$ $(2/\pi)$ lag
0.2	3.000–*i*0.039	1.000	0.0000
0.4	3.004–*i*0.158	1.000	0.0009
0.6	3.018–*i*0.354	1.000	0.0022
0.8	3.056–*i*0.624	0.999	0.0039
1.0	3.132–*i*0.958	0.999	0.0059
1.2	3.261–*i*1.340	0.997	0.0083
1.4	3.447–*i*1.746	0.995	0.0107
1.6	3.688–*i*2.153	0.993	0.0133
1.8	3.967–*i*2.544	0.990	0.0157
2.0	4.282–*i*2.921	0.987	0.0180
3.0	5.815–*i*4.581	0.972	0.0278
4.0	7.362–*i*6.190	0.957	0.0371
5.0	8.917–*i*7.782	0.943	0.0459
6.0	10.478–*i*9.366	0.928	0.0543
7.0	12.04–*i*10.95	0.914	0.0626
8.0	13.61–*i*12.52	0.900	0.0706
9.0	15.17–*i*14.09	0.887	0.0781
10.0	16.74–*i*15.67	0.873	0.0857
20.0	32.43–*i*31.40	0.755	0.1493
30.0	48.13–*i*47.11	0.660	0.1972
40.0	63.84–*i*62.82	0.584	0.234
50.0	79.55–*i*78.53	0.523	0.264
60.0	95.25–*i*94.24	0.472	0.288
70.0	111.0–*i*110.0	0.430	0.307
80.0	126.7–*i*125.7	0.395	0.324
90.0	142.4–*i*141.4	0.365	0.337
100.0	158.1–*i*157.1	0.338	0.349
500.0	786.3–*i*785.4	0.086	0.462
1000.0	1572–*i*1571	0.044	0.480
5000.0	7854–*i*7854	0.009	0.496
10,000.0	15710–*i*15710	0.005	0.498

magnetic moment that it is unnecessary to reproduce it here. In place of (18) we find

$$p_E=\frac{4\pi a^3}{1+[k(\alpha')/(\kappa-1)]}, \tag{24}$$

where $\kappa=i\sigma/\omega$. Now for iron σ/ω is approximately $6(10)^6\lambda$, so it is clear from Table I that $k(\alpha')/\kappa$ is negligible compared with unity for all $\epsilon<100$. For $\epsilon>100$ we may use for $k(\alpha')$ the approximate expression

$$k(\alpha')=\tfrac{1}{2}\pi\epsilon(1-i)=a(2\pi\sigma\mu/\lambda c)^{\frac{1}{2}}\exp(-i\tfrac{1}{4}\pi)$$

from (21). Hence

$$\frac{k(\alpha')}{\kappa}=\frac{2\pi a}{\lambda}\left(\frac{\mu}{6(10)^6\lambda}\right)^{\frac{1}{2}},$$

which is negligible compared with unity for $\lambda>1$ cm, $a/\lambda<(10)^{-3}$, and any conceivable value of μ. We may conclude, therefore, that the amplitude of the electric moment in a unit electric field is given by the same expression

$$p_E=4\pi a^3 \tag{25}$$

as for a sphere of infinite conductivity in a static field, for all wave-lengths greater than 1 cm, provided a/λ is small.

(5) Effective Permeability and Permittivity of Magnetic Powder Composed of Spheres

In calculating the effective permeability μ_e and the effective permittivity κ_e of a magnetic powder we must use statistical methods and therefore are on much less sure grounds than in the straight-forward analysis of the previous sections. Although the Clausius-Mosotti formula holds well for gases, it gives permeabilities of magnetic powders at low frequencies much smaller than those found experimentally by Legg and Given.[1] It would seem that the large permeabilities of these powders must be due to the arrangement of the particles. Hence we shall attempt to derive a modification of the Clausius-Mosotti formula which will accord with the experimental findings of Legg and Given. In so doing we shall treat the magnetic field as static.

Table II. *Comparison of experimental and calculated values of μ_e for seven packing factors.*

p	μ^e(exp)	μ^e(calc)	220^p
0.18	3.1	2.4	2.6
0.30	5.4	4.4	5.0
0.47	11	10.5	13
0.66	22	30	35
0.76	54	54	60
0.85	80	94	98
0.89	130	122	122

If H_1 is the uniform impressed field responsible for the magnetization of an elementary sphere,

Table III.

ϵ	$\lvert\mu_e-1\rvert$	$(2/\pi)$ lag
0	71.8	0.000
1	68.0	0.150
3	33.3	0.388
6	18.3	0.445
10	11.4	0.465
30	3.9	0.489
100	1.2	0.496
300	0.4	0.499
1000	0.1	0.500

it follows from (18) that H_1 is related to the magnetic moment p_H of the sphere by the formula

$$H_1=\frac{p_H}{3\tau}\frac{\mu+2}{\mu-1},$$

where $\tau\equiv(4/3)\pi a^3$ is the volume of the sphere. Also, the field H_2 inside the sphere due to its own magnetization is

$$H_2=-p_H/3\tau.$$

If I is the intensity of magnetization of the powder, and p is the packing factor, that is, the ratio of the volume filled by the magnetic material to the total volume, it is clear that $p_H/\tau=I/p$. Hence the total field inside a sphere is

$$H^i=H_1+H_2=\frac{I}{3p}\left[\frac{\mu+2}{\mu-1}-1\right].$$

In the gaps between spheres we would expect the total field to be represented by H_1 if the spheres were distributed chaotically. This assumption would lead to the Clausius-Mosotti formula. But, if the spheres are arranged in an ordered manner, we might expect their magnetization to contribute to the outer field H^0, giving

$$H^0=H_1-\eta\frac{p_H}{3\tau}=\frac{I}{3p}\left[\frac{\mu+2}{\mu-1}-\eta\right],$$

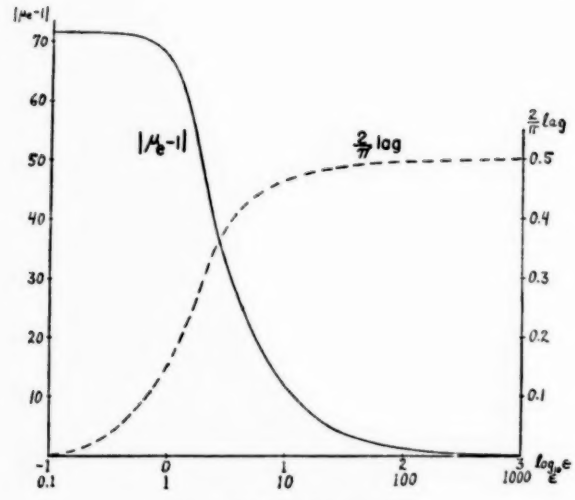

FIG. 2. Values for powder.

where η is a function of p (and possibly of μ) which vanishes for $p=0$.

The mean total field is evidently

$$H=pH^{i}+(1-p)H^{0},$$

which leads to the expression

$$\mu_e-1=\frac{3p(\mu-1)}{3+(1-p)(1-\eta)(\mu-1)} \qquad (26)$$

for the effective permeability μ_e.

If we calculate η from the data obtained by Legg and Given we find that η decreases with p as expected, indicating that the Clausius-Mosotti law is approached as the dilution increases. Now the linear dimensions of the filled region are proportional to $p^{\frac{1}{3}}$, so we should expect η to be a function of $p^{\frac{1}{3}}$. We find that if we take $\eta=0.96\,p^{\frac{1}{3}}$ we get as good agreement with the measured values of Legg and Given as is given by their purely empirical formula $\mu_e=\mu^p$. This is shown in Table II for the series of seven packing factors covering the greatest range among their measurements. As they give no table of values, the values of p and $(\mu_e)_{\text{exp}}$ have been estimated from their figure. The intrinsic permeability of the molybdenum Permalloy used by them was 220. It is seen that the values of μ_e in the third column, calculated from (26), lie as close to the experimental values as those in the fourth column calculated from Legg and Given's empirical formula.

This agreement justifies us in extending the method employed in this section to high frequencies. If $1/z$ represents the ratio $p_H/p_{H\infty}$ given by (23), we must replace the expression for H_1 used above by

$$H_1=z\frac{p_H}{3\tau}\frac{\mu+2}{\mu-1}.$$

This gives

$$\mu_e-1=\frac{3p[(\mu-1)/(\mu+2)]}{z-[(\mu-1)/(\mu+2)]\{1-(1-p)(1-\eta)\}}. \qquad (27)$$

Although p is only 0.74 for close packed spheres all of the same radius, Legg and Given obtain packing factors as high as 0.89, due, no doubt, to the presence of smaller particles in the interstices between the larger ones. Hence we have calculated μ_e from (27) for $p=0.9$ and $\mu=100$, taking $\eta=0.96\,p^{\frac{1}{3}}$. The results are shown in Table III, the second column containing the modulus of μ_e-1 and the third column the ratio of the lag of μ_e-1 to $\pi/2$. In Fig. 2 these quantities are plotted against $\log_{10}\epsilon$, the solid curve representing $|\mu_e-1|$ and the broken curve $(2/\pi)$ lag.

It is seen that $|\mu_e-1|$ falls off with increasing ϵ much more rapidly than $|p_H|/p_{H\infty}$ as given in Table I and Fig. 1. For $\epsilon=1$ the former is only 95 percent of its value for $\epsilon=0$, whereas the latter has the value 99.9 percent. Hence, for a wave-length of 100 cm, the radius of the particles must not be greater than $1.44(10)^{-4}$ cm to obtain 95 percent of the maximum available permeability, for a packing factor of 0.9.

The effective permittivity κ_e of the powder, calculated from the Clausius-Mosotti formula, is 28 for a packing factor of 0.9. It is independent of wave-length. If, however, the same causes

TABLE IV. *Ratio of moduli and ratio to $\frac{1}{2}\pi$ of lag of p_H behind exciting field.*

δ	$\frac{\lvert p_H\rvert}{p_{H\infty}}=\frac{\lvert\mu_m-1\rvert}{\mu-1}$	$\frac{2}{\pi}$ lag
0.2	1.000	0.0032
0.4	1.000	0.0126
0.6	0.998	0.0285
0.8	0.995	0.0506
1.0	0.987	0.0787
1.5	0.941	0.1682
2.0	0.847	0.267
2.5	0.727	0.347
3.0	0.615	0.398
3.5	0.527	0.424
4.0	0.461	0.437
4.5	0.412	0.444
5.0	0.373	0.449
5.5	0.341	0.453

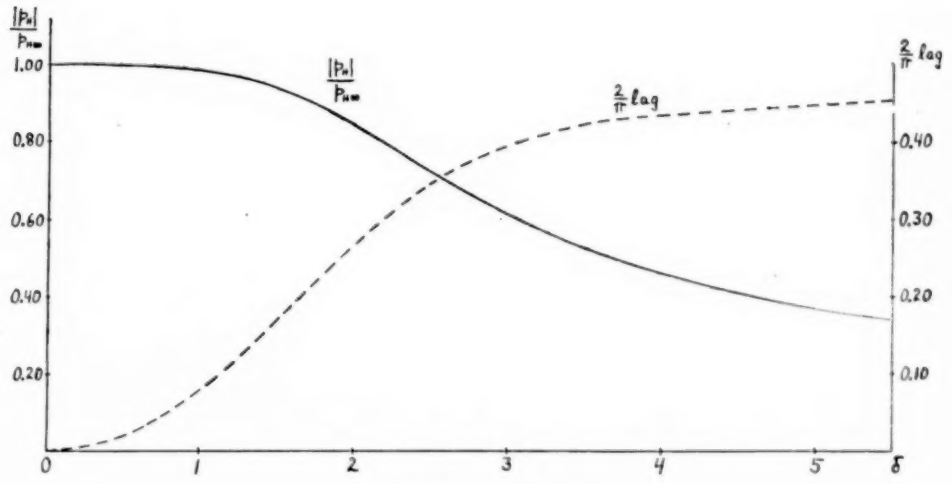

FIG. 3. Values for cylinder.

operate here as in the calculation of the effective permeability to make the Clausius-Mosotti formula give values which are too low, we may expect the actual permittivity to be considerably higher.

(6) MAGNETIC MOMENT OF CYLINDER

In this last section we shall calculate the magnetic moment per unit length of a cylinder of radius a and infinite length placed in an axially symmetrical oscillating magnetic field of unit amplitude parallel to the axis of symmetry of the cylinder. As in the case of the sphere already investigated, the cylinder will be supposed to have a permeability μ and a large but finite conductivity σ.

The exciting field has already been found, $\mathbf{H}$ and $\mathbf{E}$ being given by (3) and (4), respectively. Using cylindrical coordinates as specified in Section 2, we find for the field inside the cylinder

$$\left.\begin{aligned}\mathbf{H}'&=\mathbf{k}A'J_0(p')e^{-i\omega t},\\ \mathbf{E}'&=\boldsymbol{\phi}_1 i\beta A'J_1(p')e^{-i\omega t},\end{aligned}\right\} \tag{28}$$

where

$$p'\equiv(2\pi r/\lambda)(\kappa\mu)^{\frac{1}{2}},\quad \beta\equiv(\mu/\kappa)^{\frac{1}{2}}=(\omega\mu/i\sigma)^{\frac{1}{2}},$$

and for the reflected wave outside the cylinder

$$\left.\begin{aligned}\mathbf{H}&=\mathbf{k}A\{J_0(p)+iN_0(p)\}e^{-i\omega t},\\ \mathbf{E}&=\boldsymbol{\phi}_1 iA\{J_1(p)+iN_1(p)\}e^{-i\omega t},\end{aligned}\right\} \tag{29}$$

where $p=2\pi r/\lambda$ and $N_0(p)$ and $N_1(p)$ are the Neumann functions of zero and first order, respectively.

The boundary conditions at the surface of the cylinder require the continuity of both $\mathbf{H}$ and $\mathbf{E}$. Consequently

$$A'=\frac{2i}{\pi\alpha}\frac{1}{\beta J_1(\alpha')[J_0(\alpha)+iN_0(\alpha)]-J_0(\alpha')[J_1(\alpha)+iN_1(\alpha)]}, \tag{30}$$

where

$$\alpha\equiv\frac{2\pi a}{\lambda},\quad \alpha'\equiv\frac{2\pi a}{\lambda}\left(\frac{i\sigma\mu}{\omega}\right)^{\frac{1}{2}}=a\left(\frac{2\pi i\sigma\mu}{\lambda c}\right)^{\frac{1}{2}}.$$

We are interested only in small values of α. Hence the terms in $J_0(\alpha)$, $J_1(\alpha)$, $N_0(\alpha)$ in the denominator of A' are negligible compared with the term in $N_1(\alpha)=-2/\pi\alpha$. Therefore

$$A'=1/J_0(\alpha'). \tag{31}$$

The amplitude of the magnetic moment per unit length of the cylinder in a unit magnetic field is, then,

$$\begin{aligned}p_H&=2\pi(\mu-1)A'\int_0^a J_0(p')rdr\\ &=\pi a^2(\mu-1)\frac{1}{J_0(\alpha')}\left[\frac{2J_1(\alpha')}{\alpha'}\right].\end{aligned} \tag{32}$$

For a static field ($\alpha'\to 0$) this reduces to

$$p_{H\infty}=\pi a^2(\mu-1) \tag{33}$$

in accord with magnetostatic theory. Therefore the ratio of the magnetic moment at any wave-length to that at infinite wave-length for the same intrinsic permeability is

$$\frac{p_H}{p_{H\infty}}=\frac{1}{J_0(\alpha')}\left[\frac{2J_1(\alpha')}{\alpha'}\right], \tag{34}$$

which is a function of the single complex parameter α'. It is convenient to put

$$\alpha'\equiv\delta\sqrt{i}, \quad \delta=a(2\pi\sigma\mu/\lambda c)^{\frac{1}{2}}.$$

Then (34) may be written

$$\frac{p_H}{p_{H\infty}}=\frac{2}{\delta}\frac{(1/\sqrt{i})J_1(\delta\sqrt{i})}{J_0(\delta\sqrt{i})}. \tag{35}$$

The measured permeability μ_m of the cylinder at any frequency is evidently given by

$$\mu_m-1=(p_H/p_{H\infty})(\mu-1) \tag{36}$$

in terms of the true or intrinsic permeability μ.

In Table IV we have listed the ratio of the modulus of p_H to $p_{H\infty}$ and the ratio of the lag of p_H behind the exciting magnetic field to $\pi/2$. The solid curve in Fig. 3 represents the first of these quantities, and the broken curve the second, plotted against δ. By virtue of (36) these curves also represent the modulus and lag of $(\mu_m-1)/(\mu-1)$.

Since the intrinsic permeability μ is assumed to be a constant independent of frequency in these calculations, measurements of the permeability of a sample of iron or other conducting permeable material in the form of a long rod or ring indicate a change of intrinsic permeability with frequency only insofar as the experimental curves differ from those of Fig. 3.

The author takes pleasure in acknowledging several helpful conversations with his colleague, Captain N. I. Adams, Jr., during the course of this investigation.

NOVEMBER 1, 1941 PHYSICAL REVIEW VOLUME 60

Some Measurements on the Validity of the Principle of Superposition in Solid Dielectrics

H. SILVA* AND B. GROSS
Instituto Nacional de Tecnologia, Rio de Janeiro, Brazil

(Received August 21, 1941)

Alternating-current measurements in carnauba wax in the frequency range between 20 c/sec. and 20 Mc/sec. are reported and the correlation of the experimental data in terms of the principle of superposition is given.

THE principle of superposition plays a very important role in most theories concerning the anomalous behavior of solid dielectrics. It is the underlying principle of all calculations of the dielectric losses based on Schweidler's phenomenological theory.[1] It is a necessary consequence for such theories as those of Wagner[2] and Debye,[3] which are expressed by linear differential equations with constant coefficients. Nevertheless, there are few exact experimental confirmations of its validity at least within the range of audio- and higher frequencies, where it is mostly used for interpretation of the a.c. behavior of technical dielectrics and insulators. Tank[4] has measured directly the absorption current and the dielectric loss of some capacitors and has shown that the relation between them is given by Schweidler's formula derived under the assumption of the validity of the principle of superposition. Yaeger[5] has shown that the a.c. behavior of many dielectrics is in good agreement

* Now at the Escola de Engenharia da Universidade do Brasil.

[1] E. v. Schweidler, Ann. d. Physik **24**, 711, 1907.
[2] K. W. Wagner, Archiv f. Elektrotechnik **3**, 83 (1914).
[3] P. Debye, *Polar Molecules* (Chemical Catalog Company, 1929).
[4] F. Tank, Ann. d. Physik **48**, 307 (1915).
[5] W. Yaeger, Physics **7**, 434 (1936).

with Wagner's theory. This can be interpreted, too, as a confirmation of the principle of superposition.

In this paper we report some measurements of a.c. conductance and capacitance of condensers containing carnauba wax, and the correlation of the experimental data in terms of the principle of superposition.

I

Let $G(\beta)$ be the conductance and $C(\beta)$ the capacitance of a condenser containing a solid dielectric, to which is applied a sinusoidal voltage of frequency $f=\beta/2\pi$. It has been shown by one of us,[6] that *with the aid of the principle of superposition* there can be obtained the direct relations between G and C, which for the case of optical dispersion have been announced by Kronig[7] and Kramers.[8] These are the Eqs. (10) of the paper of Gross, if one takes into account (6) and (11).

$$G(\beta)-G_0=\frac{2}{\pi}\int_0^\infty \frac{\beta^2 C(\alpha)}{\beta^2-\alpha^2}d\alpha, \tag{1a}$$

$$C(\beta)-C_0=\frac{2}{\pi}\int_0^\infty \frac{G(\alpha)}{\alpha^2-\beta^2}d\alpha. \tag{1b}$$

The integrals are principal values. C_0 is the geometric capacitance $[C_0=C(\infty)]$ and G_0 the d.c. (leakage) conductance $[G_0=G(0)]$. The relations are independent of the form of the absorption current and follow immediately from the principle of superposition. Their deduction has been recently given also by R. H. Cole.[9]

These relations are suitable for any numerical calculations and may be used conveniently for the sake of confirmation of the validity of the principle of superposition. One measures simultaneously G and C as a function of the frequency. This can be done with great accuracy at least within the range of technical frequencies, and one finds whether or not the relations (1) are satisfied.

The evaluation seems at first sight to be difficult, because the interval of integration goes from 0 to ∞, whereas G and C are known only in a limited interval of frequencies. Yet this difficulty is easily overcome.

We shall use Eq. (1b); so we may restrict our considerations to this equation. Let us suppose that we know G between the 2 frequencies $\beta_1 \ll \beta_2$. We write the equation in the form

$$C(\beta)-C_0=\int_0^{\beta_1}+\int_{\beta_1}^{\beta-\delta}+\int_{\beta-\delta}^{\beta+\delta}+\int_{\beta+\delta}^{\beta_2}+\int_{\beta_2}^{\infty}\frac{2}{\pi}\frac{G(\alpha)}{\alpha^2-\beta^2}d\alpha. \tag{2}$$

$G(\beta)$ is an experimentally given curve. So if one chooses δ sufficiently small, one can in the interval $(\beta-\delta)<\alpha<(\beta+\delta)$ substitute the tangent for the curve.

$$(\beta-\delta)<\alpha<(\beta+\delta): G(\alpha)=G(\beta)+(\alpha-\beta)G'(\beta). \tag{3}$$

This expression enables us to evaluate analytically the integral $\int_{\beta-\delta}^{\beta+\delta}$. Hence

$$\frac{2}{\pi}\int_{\beta-\delta}^{\beta+\delta}\frac{G(\alpha)}{\alpha^2-\beta^2}d\alpha=\frac{0.734}{\beta}\log\frac{2\beta+\delta}{2\beta-\delta}\times[2\beta G'(\beta)-G(\beta)]. \tag{4}$$

Now let us suppose that the *highest* value of β, for which we shall calculate $C(\beta)$, satisfies the condition $\beta^2 \ll \beta_2^2$. Then one may neglect β^2 in the integral $\int_{\beta_2}^{\infty}$, because evidently $\alpha^2 \geq \beta_2^2 \gg \beta^2$. Therefore

$$\frac{2}{\pi}\int_{\beta_2}^{\infty}\frac{G(\alpha)}{\alpha^2-\beta^2}d\alpha \backsimeq \frac{2}{\pi}\int_{\beta_2}^{\infty}\frac{G(\alpha)}{\alpha^2}d\alpha=\text{const.} \tag{5}$$

Let us furthermore suppose, that the *smallest* value of β, for which we shall calculate $C(\beta)$, satisfies the condition $\beta^2 \gg \beta_1^2$. It is known that at least in the environment of 0, $G(\beta)$ increases nearly linearly with β. So, one sees, that the contribution of the integral $\int_0^{\beta_1}$ is very small

[6] B. Gross, Ann. Acad. Bras. Sci. **12**, 203 (1940); Phys. Rev. **59**, 748 (1941).
[7] R. de L. Kronig, J. Opt. Soc. Am. **12**, 547, 1926.
[8] H. A. Kramers, *Atti congr. dei Fisici* (Como 1927), p. 545.
[9] Abstract submitted for the Providence Meeting of the American Physical Society, 1941. We are greatly indebted to Dr. Cole for the private communication of his results before the publication of a full account of his researches.

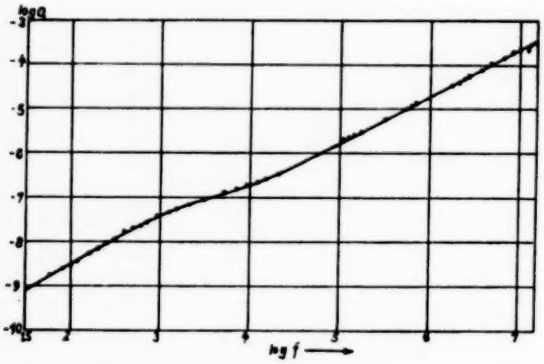

FIG. 1. Frequency dependence of the conductance.

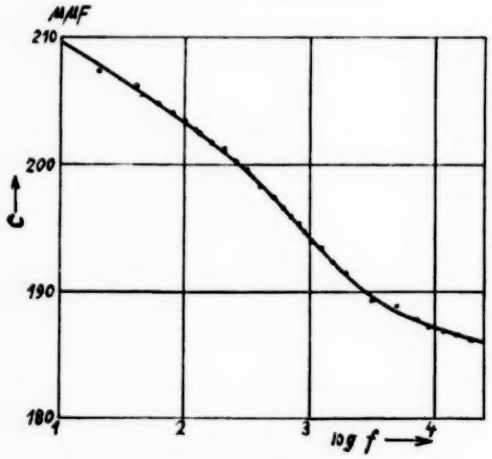

FIG. 2. Frequency dependence of the capacitance.

and may be neglected. There remain the two integrals $\int_{\beta_1}^{\beta-\delta}$ and $\int_{\beta+\delta}^{\beta_2}$. Since $G(\beta)$ is supposed to be known in the interval $\beta_1-\beta_2$, the integrals can be evaluated numerically or graphically without difficulty.

We can therefore conclude: *If the principle of superposition is valid, the difference between the experimentally given curve $C(\beta)$ and the numerically evaluated integral* $\frac{2}{\pi}\int_{\beta_1}^{\beta_2}\frac{G(\alpha)}{\alpha^2-\beta^2}d\alpha$ *must be constant.*

II

The dielectric employed in our work was carnauba wax. This substance can be considered typical of many technical dielectrics. It has been used in our earlier work.[10]

[10] B. Gross, Phys. Rev. **57**, 57 (1940). H. Silva, Ann. Acad. Bras. Sci. **13**, 21 (1941).

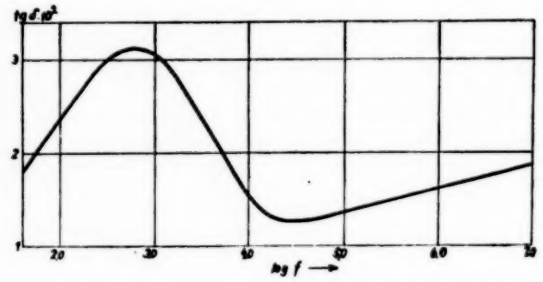

FIG. 3. Frequency dependence of the dielectric loss.

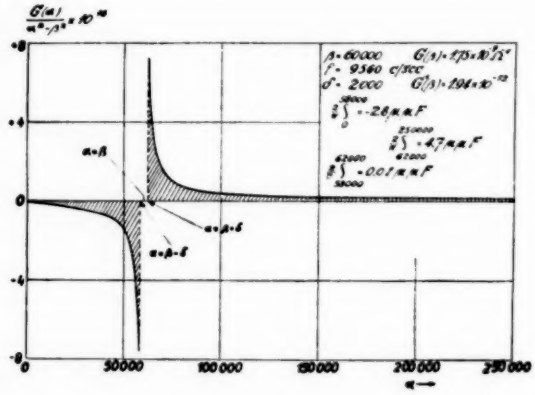

FIG. 4. Calculation of a point of the capacitance function.

Measurements in the audiofrequency range between 20 c/sec. and 20,000 c/sec., have been made with the Schering bridge (General Radio Type 716A). As this bridge has been found to work correctly only near 1000 c/sec., a substitution method had to be used. Equilibrium was established at first with the test condenser connected to the bridge. Then, without modifying the position of the bridge controls, for the test condenser were substituted an adjustable air condenser and a resistance box connected in series. Capacitance and resistance of these elements were then adjusted so that equilibrium was re-established at the bridge. The *series* conductance and capacitance of the sample under test are thus obtained directly; its *parallel* conductance and capacitance are calculated easily by well-known formulae. As detector we used an amplifier and an a.c. milliammeter and as source an audiofrequency oscillator and amplifier. The sensitivity was such, that in the neighborhood of the equilibrium point a variation of the capacitance as small as 1/50 μμf produced a clearly detectable deflection of the detector meter. The

precision of the measurement was naturally considerably less than this and dependent to some extent on the frequency. It was smallest for low frequencies.

The measurements in the radiofrequency range between 100,000 c/sec. and 20 Mc/sec. have been made with a Siemens instrument, which works on the "resonant substitution method." Details about its construction and working conditions are given by Zinke.[11] The precision and sensitivity of this method is much less than those of the Schering bridge. The measured values may be in error by as much as 3 or 4 percent. This made it impossible to obtain useful values of the difference $C(\beta)-C_0$, because in the frequency range concerned here the capacitance had already decreased nearly to its infinite frequency value C_0. So 4 percent error in $C(\beta)$ means perhaps 50 percent error in the difference $C(\beta)$-const. Yet, the values of the conductance $G(\beta)$ have been obtained fairly well. In this case, indeed, the constant component G_0 is such a small part of G that it can be neglected.

III

The experimental results are given in Figs. 1, 2 and 3. The most striking feature is that the conductance G rises nearly linearly with β over the whole range of frequencies up to 20 Mc/sec. This means that the dielectric relaxation function $\varphi(t)$ does not reach a constant initial value in the corresponding time interval 10^{-1} to 10^{-7} sec., but follows approximately the well-known t^{-n}-law. Yet, one observes clearly an irregularity in the neighborhood of 1000 c/sec. The capacitance decreases considerably, the slope of the curve reaches a maximum near 1000 c/sec. The dielectric loss factor, given by the tangent of the loss angle, shows a pronounced maximum at nearly the same frequency.

$C(\beta)$ has been calculated in the manner indicated above for 7 values of β between 500 and 60,000, with $\beta_1=100$ and $\beta_2=250{,}000$. An example of the calculations is given in Fig. 4 and its results are represented in Table I. One sees that the difference $C(\beta)-\int_{\beta_1}^{\beta_2}=\Delta$ is as constant as one may expect when the approximate character of the calculations is considered. There seems to be no systematic error. The validity of the principle of superposition is therefore completely established.

TABLE I. *Test of constancy of* Δ.

β	f (c/sec.)	$C_{meas}(\mu\mu f)$	$\int_{\beta_1}^{\beta_2}(\mu\mu f)$	$\Delta(\mu\mu f)$
60,000	9560	187.0	1.9	185.1
30,000	4780	188.4	3.4	185.0
10,000	1592	191.9	6.3	185.6
5,000	796	195.1	10.8	184.3
2,000	318	199.1	13.4	185.7
1,000	159	201.6	17.0	184.6
500	80	203.8	19.1	184.7
			mean value:	185.0

The authors are greatly indebted to the Director of the Instituto Nacional de Technologia, Professor E. L. da Fonseca Costa, who made this study possible.

[11] O. Zinke, *Hochfrequenzmesstechnik* (S. Hirzel, Leipzig, 1938), p. 193.

Letters to the Editor

PROMPT publication of brief reports of important discoveries in physics may be secured by addressing them to this department. Closing dates for this department are, for the first issue of the month, the eighteenth of the preceding month, for the second issue, the third of the month. Because of the late closing dates for the section no proof can be shown to authors. The Board of Editors does not hold itself responsible for the opinions expressed by the correspondents.

Communications should not in general exceed 600 words in length.

Autoradiography of Ores

CLARK GOODMAN AND DEAN C. PICTON
Massachusetts Institute of Technology, Cambridge, Massachusetts
October 16, 1941

THE photographic action of radiations from radioactive substances has served as a research tool since Becquerel's initial discovery. Mügge[1] made the first autoradiographs of naturally occurring radioactive minerals. Numerous investigators subsequently have used this technique to determine the distribution of uranium and thorium in terrestrial materials. Recently autoradiography has been of value in tracer studies of biological substances. The β- and γ-radiations from introduced, artificially radioactive elements reveal the locus of the active atoms and their associated stable isotopes.

Many ores, some of considerable economic value, contain sufficient concentrations of elements with large nuclear cross sections for slow neutrons to allow activation *in situ* within samples of the ore. If in addition the product nuclei have convenient half periods (one hour to twenty-four hours), autoradiographs can be made by direct contact of a previously lapped surface with photographic film.

Manganese seemed particularly suitable for a preliminary investigation. Five ores were placed in a 15 cm diameter×25 cm long paraffin cylinder and activated with stray neutrons from the M. I. T. cyclotron. Prints of the autoradiographs thus obtained are shown in the lower row of Fig. 1, while immediately above are photographs of the corresponding ore surfaces. The relative concentrations of manganese in the individual minerals of a sample are revealed by their brightness in the prints prepared from the autoradiographs. Samples a, b, and c from Franklin, New Jersey (5 to 10 percent Mn) received the same bombardment (65 minutes), were in contact with the same film for the same length of time (60 minutes), and their prints were prepared simultaneously. Consequently, intercomparisons between these samples are possible. However, samples d[2] and e from Norwegian magnetite mines (1 to 5 percent Mn) required longer bombardment and exposure. The printing of these autoradiographs was adjusted to provide good contrast. Hence, the resulting prints are only of value in showing the relative distribution of manganese within each of samples d and e.

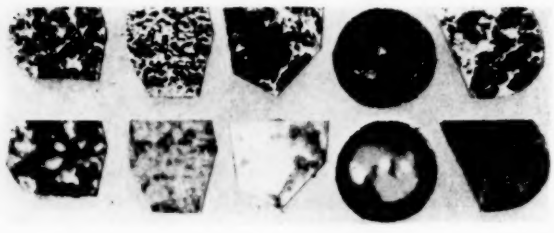

FIG. 1. Prints of autoradiographs of manganese ores are presented in the lower row. The brightness is proportional to the manganese content of the constituent minerals. Photographs of the corresponding ore surfaces are shown immediately above.

The uniformity of distribution of manganese within the separate minerals is of particular interest. For example, in the lower print of a the light areas, representing the highest manganese content, correspond to willemite, the light grains of the upper print. Similarly, grey in lower a representing intermediate manganese content, corresponds to black (franklinite) in upper a, and black in lower a representing lowest manganese content, corresponds to grey (zincite), really red in the original ore, in upper a. In each case, however, the density of brightness is uniform throughout the mineral grain. The resolution of the method is indicated by the sharpness of the mineral boundaries in the autoradiographs.

The source of the activity was checked by counter measurements. In each case the 2.6-hour period of manganese was predominant. The effects of phosphorescence and pressure were determined from exposures of the inactive ores and found to be entirely negligible.

Further investigations are in progress with the purpose of extending the method to other elements, of making the method quantitative and of applying the method to thin sections. We wish to express our appreciation to Professors R. D. Evans and W. H. Newhouse, and to Dr. A. F. Kip for their generous assistance in this investigation.

[1] O. Mügge, "Radioaktivitat und pleochroitische Höfe," Zentralbl. Mineralogie 71, 144–147 (1909).
[2] Sample d is mounted in Bakelite.

On the Resonance Level of Hg at Negative Energy

M. KIMURA
The Institute of Physical and Chemical Research, Tokyo, Japan
June 30, 1941

THE scattering cross sections of Hg and other substances for slow neutrons were measured by the method of back scattering.[1] The scattering cross sections of strong C neutron absorbers such as Hg can be measured conveniently with these geometrical arrangements. Later, the measurements were extended for the I group neutrons; the results are summarized in Table I. These values were calculated with reference to Ni and Fe on the assumption that the cross sections of the latter two are independent of neutron energy. This will be allowed from the theoretical point of view and also the experimental comparison between C and D neutrons proves to be the fact.[2,3] As will be seen from the table, Hg has a large scattering cross

TABLE I. *Scattering for various resonance levels.*

Neutron Energy*	Scattering Cross Sections $E_r=-0.3$ ev	$E_r=-0.1$ ev	$E_r=-0.05$ ev	Measured Values
C 0.026 ev	14×10^{-24} cm²	26×10^{-24} cm²	37×10^{-24} cm²	28×10^{-24} cm²
D 0.84 ev	12.8	12.9	13.0	12
I 27 ev	11.05	11.05	11.05	11

* W. J. Horvath and E. O. Salant, Phys. Rev. **59**, 154 (1941).

section for thermal neutrons which decreases rapidly as the neutron energy increases to 0.84 ev, and becomes almost constant for neutrons with ev in the order of tens. This behavior will be expected if we assume a resonance level at negative energy not far from zero. The scattering cross sections were calculated as a function of neutron energy after the formulation of Bethe.[4] We assumed that the resonance level is at -0.3 ev, -0.1 ev and -0.05 ev, respectively. The results are shown in the table. The following three assumptions are made in the process of calculation: (1) almost all of $\sigma_N{}^N$ for the I group are due to potential scattering; (2) although $\lambda_r\Gamma_N$ loses its meaning in the present case and we must come back to $\lambda\gamma$ Eq. (265a), (reference 4) the former quantity is roughly constant for various nuclei and positions of levels. Thus $\lambda_r\Gamma_N$ was put equal to $0.2_8\times10^{-12}$ on averaging the values for the levels of Rh, In, and Ag; and (3) Γ was put equal to 0.1 ev. (Small variation in this value does not influence the results greatly.) A resonance level at -0.1 ev fits the experimental results the best. A level at negative energy has already been suggested by Bethe[4] from the absorption ratio for the C and D neutrons and from the temperature effect. Moreover, Hg has another level at 9 ± 7 ev after the investigation of Nonaka.[5] It will no doubt be expected that the hump in the scattering curve due to this level is negligibly small; the absorption curve, however, will be greatly changed and the experimental absorption ratio for the C and D neutrons is more naturally understood by assuming two levels, one at -0.1 ev and another at 9 ± 7 ev rather than a single level at -0.3 ev (presumably -2.2 ev) as assumed by Bethe.

In conclusion, I express my sincere thanks to Professor S. Nishikawa and to Professor S. Tomonaga for their valuable suggestions and discussions.

[1] M. Kimura, Proc. Phys. Math. Soc. Japan **22**, 391 (1940).
[2] M. Kimura, Sci. Papers Inst. Phys. Chem. Res. **39**, 153 (1939).
[3] H. B. Hanstein, Phys. Rev. **59**, 489 (1941).
[4] H. A. Bethe, Rev. Mod. Phys. **9**, 152 (1937).
[5] I. Nonaka, Proc. Phys. Math. Soc. Japan **21**, 594 (1939).

The Limiting Form of Poisson's Distribution

E. J. GUMBEL
The New School for Social Research, New York, New York
October 13, 1941

IN a recent article E. Rodgers[1] has shown for Poisson's distribution (The law of rare events) that the probability of a deviation not exceeding the standard deviation converges to the corresponding probability for a Gaussian (normal) distribution. This theorem, the proof of which is rather complicated, is a special case of the following relation:

The Poisson distribution (x) of a variable x

$$w(x)=m^x e^{-m}:x! \tag{1}$$

converges with increasing values of m, where m stands for the mean value, towards the normal distribution. Since the Poisson law plays an important role in radioactivity, the proof, which is very simple, may be of interest for the physicists.

Defining the variable z by

$$x=m(1+z) \tag{2}$$

we obtain for large values of m which implies large x, from Stirling's formula

$$w(x)=\frac{m^{m(1+z)}e^{-m}}{[2\pi m(1+z)]^{\frac{1}{2}}m^{m(1+z)}(1+z)^{m+mz}e^{-m-mz}}$$

$$=e^{mz}(1+z)^{-m-mz-\frac{1}{2}}:(2\pi m)^{\frac{1}{2}}.$$

If

$$m\gg\tfrac{1}{2}$$

the factor $\frac{1}{2}$ which appears in the exponent may be neglected. The usual expansion gives

$$w(x)=\frac{1}{(2\pi m)^{\frac{1}{2}}}e^{mz-(x+mz)(z-\frac{1}{2}z^2\cdots)}$$

$$=\frac{e^{-mz^2/2}}{(2\pi m)^{\frac{1}{2}}}.$$

Substituting x for z, according to (2), we obtain

$$w(x)=\frac{e^{-(x-m)^2/2m}}{(2\pi m)^{\frac{1}{2}}}, \tag{3}$$

a Gaussian distribution with standard deviation $\sigma=m^{\frac{1}{2}}$. Rodgers' theorem follows at once from this general property. The convergence, established by L. von Bortkiewicz,[2] is well known in statistics. Our method does not enable one to calculate the probability of a deviation falling in the interval $m\mp\sigma$ as a function of m, as was done by Rodgers.

[1] Eric Rodgers, Phys. Rev. **57**, 735 (1940).
[2] L. von Bortkiewicz, *Das Gesetz der kleinen Zahlen* (Leipzig, 1898).

Long-Lived Activity of Rhodium

O. MINAKAWA
Nuclear Research Laboratory, Institute of Physical and Chemical Research, Tokyo, Japan
July 25, 1941

ON bombarding rhodium with slow neutrons, Fermi and his co-workers[1] found two β-activities decaying with half-lives of 44 sec. and 4 min., respectively, and Pontecorvo[2] concluded that these two activities are due to nuclear isomers of Rh^{104}. This conclusion was confirmed by some other investigators.[3,4]

Pool, Cork and Thornton[5] showed that the bombardment of rhodium with fast neutrons gives rise to an activity of 1.1-hour period. We repeated the experiments by bombarding powdered metallic rhodium (Kahlbaum) with slow neutrons (through paraffin) from Be+D, and fast neutrons from Li+D produced in our cyclotron under similar conditions previously reported.[6] A Lauritsen type electroscope was used to observe the activity. In both cases the 1.1-hour period of Pool *et al.* could not be ob-

served at all; the irradiated samples, however, showed the existence of very long periods. Then the samples were irradiated intermittently for a long time and their long-lived activities examined. The results are as follows.

1. Slow neutron bombardment. Beside the well-known two periods (44 sec. and 4 min.) two-week activities were found, their periods being about 20 hours and 70 days, respectively. But chemical separation showed that these activities were to be attributed to iridium impurity, which have very large capture cross sections for slow neutrons.

2. Fast neutron bombardment. A long-lived activity decaying with a period of 210 ± 6 days was found. Chemical separation showed that the carrier of this activity is rhodium and is neither ruthenium nor masurium.

With a thin walled G-M counter and magnetic field it was found that the emitted particles were both negative and positive electrons and that the intensity ratio of these particles was $e^-/e^+=1.2$. These particles were accompanied by a considerable amount of γ-rays. With the Al absorption and the range energy relation[7] the upper limit of the energy of these mixed β-rays was found to be 1.1 ± 0.1 Mev.

From the above observations it can be concluded that the corresponding isotope of this long-lived activity is Rh^{102}, produced from the abundant stable isotope Rh^{103} by the reaction $(n, 2n)$, and this Rh^{102} can emit either positive or negative electrons and goes over to Pd^{102} or Ru^{102}, respectively. A more detailed report will be published shortly in the Scientific Papers of the Institute of Physical and Chemical Research.

In conclusion the writer wishes to express his best thanks to Professor H. Nagaoka for his interest and kind encouragement throughout this work, and to Dr. Y. Nishina for his kind suggestions and discussions, and to Mr. T. Shirai for chemical separations of the samples.

[1] E. Fermi *et al.*, Proc. Roy. Soc. **149**, 522 (1935).
[2] B. Pontecorvo, Phys. Rev. **54**, 542 (1938); Nature **141**, 785 (1936).
[3] H. Reddemann, Naturwiss. **26**, 125 (1938).
[4] E. C. Crittenden, Jr., Phys. Rev. **56**, 709 (1939).
[5] M. L. Pool, J. M. Cork and R. L. Thornton, Phys. Rev. **52**, 239 (1937).
[6] O. Minakawa, Phys. Rev. **57**, 1189 (1940).
[7] N. Feather, Proc. Camb. Phil. Soc. **34**, 599 (1938).

Isotopic Weights of Sulphur and Titanium

T. Okuda and K. Ogata
Department of Physics, Faculty of Science, Osaka Imperial University, Osaka, Japan
July 20, 1941

WITH the mass-spectrograph of Bainbridge-Jordan type, the isotopic weights of S^{32}, S^{34}, Ti^{46}, Ti^{47}, Ti^{48}, Ti^{49} and Ti^{50} were measured by the doublet method.

1. Sulphur. (a) S^{32}: By the electric discharge through the mixture of oxygen and a trace of ethylmercaptane (C_2H_5SH) vapor, we obtained well-matched doublets $O^{16}{}_2-S^{32}$ and $C^{12}O^{16}{}_2-C^{12}S^{32}$. These mass differences are given in Table I. These two mass differences being quite in good agreement with each other within the experimental error, we take the weighted mean of these results for the mass difference $O^{16}{}_2-S^{32}$ as follows: $O^{16}{}_2-S^{32}=191.1\pm0.7$. From this difference, the following isotopic weight as well as packing fraction of S^{32} can be obtained:

$$S^{32}=31.98089\pm0.7\times10^{-4}$$

packing fraction of $S^{32}=-5.98\pm0.02$.

Table I.

Doublet	Number of Doublets Measured	Difference in Mass ($\Delta M\times10^4$)
$O^{16}{}_2-S^{32}$	11	191.5 ± 1.1
$C^{12}O^{16}{}_2-C^{12}S^{32}$	4	189.4 ± 2.3

Although this value does not agree with that of Aston, i.e., $31.9823\pm3\times10^{-4}$,[1] the Brasefield and Pollard's data[2] of $S^{32}(\alpha, p)\,Cl^{35}$ reaction as well as our recalculated chlorine mass (34.97881) enable us to obtain the following value for S^{32},

$$S^{32}=31.98054\pm3.9\times10^{-4},$$

which agrees well with our present value.

(b) S^{34}: The $SH^{32}{}_2-S^{34}$ doublet is obtained by the ordinary discharge through the vapor of ethylmercaptane, and the mass difference obtained is as follows:

Doublet	Number of Doublets Measured	Difference in Mass ($\Delta M\times10^4$)
$SH^{32}{}_2-S^{34}$	11	200.4 ± 3.2

From the results thus obtained and also from the values $S^{32}=31.98089\pm0.7\times10^{-4}$ and $H^1=1.008131\pm0.033\times10^{-4}$,[3] the following isotopic weight and packing fraction of S^{34} can be obtained,

$$S^{34}=33.97711\pm3.3\times10^{-4}$$

packing fraction of $S^{34}=-6.73\pm0.10$.

2. Titanium. In the determinations of all five isotopic weights of Ti, we obtained by the discharge through the vapor mixture of titantetrabromide, normal peptane and ethylmercaptane the doublets given in Table II. By using these results, together with $H^1=1.008131\pm0.033\times10^{-4}$,

$$C^{12}=12.003871\pm0.33\times10^{-4},^3$$

and

$$S^{32}=31.98089\pm0.7\times10^{-4},$$

Table II.

Doublet	Number of Doublets Measured	Difference in Mass ($\Delta M\times10^4$)
$C^{12}SH^{32}{}_2-Ti^{46}$	4	349.0 ± 9.5
$C^{12}SH^{32}{}_2-Ti^{47}$	6	444.2 ± 9.4
$C^{12}{}_4-Ti^{48}$	9	521.6 ± 4.6
$C^{12}{}_4H-Ti^{49}$	19	588.3 ± 5.1
$C^{12}{}_4H_2-Ti^{50}$	19	694.6 ± 3.6

Table III.

Isotopic Weight	Packing Fraction	Relative Abundance*
$Ti^{46}=45.96612\pm9.5\times10^{-4}$	-7.36 ± 0.21	7.95
$Ti^{47}=46.96473\pm9.5$	-7.50 ± 0.20	7.75
$Ti^{48}=47.96332\pm4.8$	-7.64 ± 0.10	73.45
$Ti^{49}=48.96479\pm5.3$	-7.19 ± 0.11	5.51
$Ti^{50}=49.96229\pm3.8$	-7.54 ± 0.08	5.34

* O. Hahn, S. Flügge, and J. Mattauch, Physik. Zeits. **41**, 1 (1941).

the titanium masses determined are given in Table III. These results and the oxygen ratio 1.000275[4] lead us to determine the value for the chemical atomic weight of Ti, which is found to be 47.88 ± 0.04, in good agreement within the experimental error with the international chemical atomic weight 47.90.

[1] F. W. Aston, Proc. Roy. Soc. **A163**, 403 (1937).
[2] C. J. Brasefield and E. Pollard, Phys. Rev. **50**, 296 (1936).
[3] K. Ogata, Proc. Phys. Math. Soc. Japan **22**, 486 (1940).
[4] W. R. Smythe, Phys. Rev. **45**, 299 (1934); B. F. Murphey, Phys. Rev. **59**, 320 (1941).

On the Theory of Temperature Diffuse Scattering

W. H. ZACHARIASEN
Ryerson Physical Laboratory, University of Chicago, Chicago, Illinois[5]
October 13, 1941

IN a current publication M. Born and K. Sarginson[1] derive an intensity formula for the temperature diffuse scattering. Their treatment is more general than the recent one due to the present writer[2] since it is not limited to monatomic lattices. The authors characterize my earlier work on the subject as unsatisfactory without comparing their intensity formula with that obtained by me. It may therefore be of some interest to show that our results—apart from the greater generality of their treatment—actually are identical.

In passing from Eq. (I. 7) to Eq. (I. 8), (Roman numerals I or II refer to the two articles of reference 2), the approximation $\exp(P_{ll'}) \approx 1 + P_{ll'}$ was used. Born and Sarginson object to this procedure, but they do not seem to be aware of the fact that their general intensity formula Eq. (2.41) is based upon the equivalent approximation [see their Eq. (2.36)]. The intensity expression obtained by Born and Sarginson, Eq. (2.41), when restricted to a monatomic lattice, may be written in the form

$$j_z = \frac{NI_a h}{8\pi^2 m_a \tau_0} \sum_j \frac{(\mathbf{s}\cdot\mathbf{A}_j)^2}{v_j} \coth(x_j/2),$$

where the notation of article II is used. Because of the identity $\coth(x_j/2) \equiv 2\theta_j/h\nu_j\tau_0$ it is seen that this equation is identical with Eq. (II. 1) and also with Eq. (I. 17) when the immediate neighborhood of a Laue direction is excluded.

In Section 3 of their article Born and Sarginson give detailed intensity formulae for cubic monatomic lattices and in Section 4 they use these intensity expressions to study the intensity distribution near a maximum. These discussions are based upon their Eq. (3.2) which is identical with my Eq. (I. 18) (again excluding the immediate neighborhood of a Laue direction) except for the fact that this writer neglects the dispersion of the elastic waves (which is permissible when τ_0/τ_m is small compared to unity). This writer has pointed out, however, that Eq. (I. 18) [and hence also Eq. (3.2) of Born and Sarginson] is based upon so crude approximations as to be useless for the interpretation of all but qualitative experimental data. The results given in Sections 3 and 4 of the article by Born and Sarginson are therefore of quite limited value and their conclusions regarding the position of the diffraction maximum and the intensity distribution must be heavily discounted. (For a detailed discussion see article II.)

This writer agrees with Born and Sarginson in their criticism of the explanations for the diffuse spots suggested by Preston and W. H. Bragg and by Raman, Nilakantan, and Nath.

[1] M. Born and K. Sarginson, Proc. Roy. Soc. **179**, 69 (1941).
[2] W. H. Zachariasen, I: Phys. Rev. **57**, 597 (1940); II: Phys. Rev. **59**, 860 (1941).